

SYNTHESIS AND CHARACTERIZATION OF POLYMERIC MAGNETIC
NANOPARTICLES LOADED BY GEMCITABINE

A THESIS SUBMITTED TO
THE GRADUATE SCHOOL OF NATURAL AND APPLIED SCIENCES
OF
MIDDLE EAST TECHNICAL UNIVERSITY

BY

MARYAM PARSIAN

IN PARTIAL FULFILLMENT OF THE REQUIREMENTS
FOR
THE DEGREE OF MASTER OF SCIENCE
IN
BIOTECHNOLOGY

SEPTEMBER 2014

Approval of the thesis:

**SYNTHESIS AND CHARACTERIZATION OF POLYMERIC MAGNETIC
NANOPARTICLES LOADED BY GEMCITABINE**

submitted by **MARYAM PARSIAN** in partial fulfillment of the requirements for the
degree of **Master of Science in Biotechnology Department, Middle East
Technical University** by,

Prof. Dr. Canan Özgen
Dean, Graduate School of **Natural and Applied Sciences** _____

Prof. Dr. Filiz Bengü Dilek
Head of Department, **Biotechnology** _____

Prof. Dr. Ufuk Gündüz
Supervisor, **Biology Department, METU** _____

Assoc. Prof. Aysen Tezcaner
Co-Supervisor, **Engineering Sciences Department, METU** _____

Examining Committee Members:

Assoc. Prof. Dr. Mayda Gürsel
Biology Department, METU _____

Prof. Dr. Ufuk Gündüz
Biology Department, METU _____

Assoc. Prof. Dr. Dilek Keskin
Engineering Sciences Department, METU _____

Assist. Prof. Dr. Serap Yalcin Azarkan
Food Engineering Department, Ahi Evran University _____

Dr. Pelin Mutlu
Central Laboratory, Bio and Biotech R&D Center, METU _____

Date: 03.September.2014

I hereby declare that all information in this document has been obtained and presented in accordance with academic rules and ethical conduct. I also declare that, as required by these rules and conduct, I have fully cited and referenced all material and results that are not original to this work.

Name, Last name: Maryam Parsian

Signature:

ABSTRACT

SYNTHESIS AND CHARACTERIZATION OF POLYMERIC MAGNETIC NANOPARTICLES LOADED BY GEMCITABINE

Parsian, Maryam

M.S., Department of Biotechnology

Supervisor: Prof. Dr. Ufuk Gündüz

Co-Supervisor: Assoc. Prof. Dr. Ayşen Tezcaner

September 2014, 110 pages

In this study, different types of magnetic nanoparticles were synthesized for treatment of breast cancer by targeted drug delivery. Polyamidoamine (PAMAM) dendrimer, Chitosan (CS) and Polyhydroxybutyrate (PHB) coated magnetic nanoparticles were prepared and loaded with Gemcitabine.

The loading efficiency of drug for various half generations of dendrimer coated magnetic nanoparticles (DcMNPs), Chitosan coated magnetic nanoparticles (CSMNPs) and Polyhydroxybutyrate magnetic nanoparticles (PHB-MNPs) were investigated in different solvents. The results were confirmed by spectrophotometric, FT-IR, XPS, Zeta-potential and TEM analyses.

The release and stability of Gemcitabine from the nanoparticles at various pH were investigated. The release studies were shown Gemcitabine release was higher at pH 4.2 compared to pH 5.2. The stability results indicated that Gemcitabine conjugated nanoparticles were highly stable.

The cytotoxicities of drug free nanoparticles and Gemcitabine loaded nanoparticles were determined with proliferation assays (XTT) using SKBR-3 and MCF-7 cell lines. DcMNPs, CSMNPs and PHB-MNPs were not cytotoxic by themselves. When the drug was loaded on DCMNPs, CSMNPs and PHB-MNPs, the antiproliferative effect of the drug increased. IC₅₀ values of drugs remarkably decreased 6, 1.4 and 2 folds on SKBR-3 and 3, 2.6 and 2 folds on MCF-7 cell lines, when conjugated to DcMNPs, CSMNPs and PHB-MNPs, respectively.

Considering the fact that the synthesized bare magnetic nanoparticles were not cytotoxic and Gemcitabine loaded nanoparticles exhibited higher antiproliferative activity than free drug *in vitro*, we suggested that these nanoparticles can be a promising candidate for the development of novel targeted drug delivery systems.

Keywords: Magnetic Nanoparticle, Targeted Drug Delivery, Gemcitabine, Half generation PAMAM Dendrimer, Chitosan, Polyhydroxybutyrate.

ÖZ

GEMSİTABİN YÜKLÜ POLİMERİK MANYETİK NANOPARÇACIKLARIN SENTEZİ VE KARAKTERİZASYONU

Parsian, Maryam

Yüksek Lisans, Biyoteknoloji Bölümü

Tez Yöneticisi: Prof. Dr. Ufuk Gündüz

Ortak Tez Yöneticisi: Doç. Dr. Ayşen Tezcaner

Eylül 2014, 110 sayfa

Bu çalışmada, ilaç hedefleme yolu ile meme kanseri tedavisi amaçlanmış ve farklı türlerde manyetik nanoparçacıklar sentezlenmiştir. Poliamidoamin (PAMAM) dendrimer, Kitosan (CS), ve Polihidroksibutirat (PHB) kaplı manyetik nanoparçacıklar Gemsitabin ile yüklenmiştir.

Farklı tampon çözeltilerde farklı yarı jenerasyonlarda sentezlenen dendrimer manyetik nanoparçacık (DcMNPs), kitosan manyetik nanoparçacık (CSMNPs) ve PHB manyetik nanoparçacıkların (PHB-MNP) etkili ilaç yüklenme miktarı araştırılmıştır. Sonuçlar spektrofotometrik, FT-IR, XPS, Zeta-potansiyel ve TEM analizleri ile doğrulanmıştır. Manyetik nanoparçacıklardan Gemsitabin salımı, farklı pH larda ve nanoparçacıkların kararlılıkları incelenmiştir.

İlaç yüklü olmayan nanoparçacıkların ve ilaç yüklü nanoparçacıkların sitotoksiteleri SKBR-3 ve MCF-7 hücre hatlarında hücre çoğalma analizi (XTT) ile belirlenmiştir. DcMNP, CSMNP ve PHB-MNP'lerin hücreler üzerinde kendi

başlarına toksik etkilerinin bulunmadığı, ilaç yüklü DcMNP, CSMNP ve PHB-MNP'lerin hücre üremesini önemli ölçüde azalttığı belirlenmiştir. İlaç yüklü DcMNP, CSMNP ve PHB-MNP'lerin IC₅₀ değerlerini serbest ilaca göre SKBR-3 hücre hattında sırasıyla 6, 1.4 and 2 kat ve MCF-7 hücre hattında sırasıyla 3, 2.6 and 2 kat azalttığı görülmüştür.

Sentezlenen boş manyetik nanoparçacıkların sitotoksik olmaması ve Gempitabin yüklü nanoparçacıkların serbest ilaca göre daha fazla antiproliferatif etki göstermesi göz önüne alındığında, bu nanoparçacıklar kanser tedavisinde yeni ilaç hedefleme sistemleri için uygun birer aday olabilirler.

Anahtar Kelimeler: Manyetik nanoparçacık, İlaç hedefleme, Gempitabin, PAMAM Dendrimer, Kitosan, PHB

To my valuable parents, my sister and brother.

ACKNOWLEDGEMENTS

First of all, I would like to express my deepest gratitude to my supervisor Prof. Dr. Ufuk Gündüz for her great academic guidance, advices, support and encouragement throughout this study. I also thank to my co-supervisor Assoc. Prof. Dr. Aysen Tezcaner for her support and encouragement in this research.

I would like to thank Prof. Dr. Inci Eroglu, Assoc. Prof. Dr. Bora Maviş and Gokce Avcioglu for endless support at their Laboratory. Examining committee members Assoc. Prof. Dr. Çağdaş Son, Assoc. Prof. Dr. Dilek Keskin are also greatly acknowledged for their kind participation and valuable comments during this research.

I am grateful to Assist. Prof. Dr. Serap Yalçın, Dr. Pelin Mutlu and Aktan Alpsoy for their advices, encouragement, kind and pleasant collaboration in this study.

I am deeply thankful to Negar Taghavi, Gozde Unsoy, Çağrı Urfalı, Murat Erdem, Ayca Nabioglu,, and other members of Lab 206 for their help, friendship and contributions throughout my study.

My time in Ankara became meaningful by my good friends and several invaluable friendships. Special thanks to my good friends Aslan Masahi, Kevser Betul Burun, Serhat Ozdemir and Hikmet Taner Teker for their invaluable friendship and helps during my study and living in Turkey.

I would like to express my great appreciation to my mother Mansoreh Zargar Salehi my father Mohammad Parsian, my sister Farzaneh Parsian and my brother Amir Parsian for their endless love, trust and support in every step of my life. Also special thanks for my Great nephew Ata Jodeyri Rad for his persuasion and encourage.

TABLE OF CONTENTS

ABSTRACT	v
ÖZ.....	vi
ACKNOWLEDGEMENTS.....	viii
TABLE OF CONTENTS.....	ix
LIST OF FIGURES.....	xiii
LIST OF TABLES.....	xviii

CHAPTERS

1 INTRODUCTION	1
1.1 Biology of Cancer	1
1.1.1 Breast Cancer	2
1.1.2 Physiopathological Characteristics of Tumor Tissues.....	4
1.1.2.1 Leaky Vasculature	4
1.1.2.2 Enhanced Permeability and Retention Effect.....	5
1.1.2.3 Acidic Tumor Microenvironment.....	6
1.2 Treatment of Breast Cancer.....	7
1.2.1 Surgery.....	8
1.2.2 Hormone Therapy	8
1.2.3 Radiation Therapy.....	9
1.2.4 Chemotherapy	9
1.2.4.1 Gemcitabine (Gemzar)	10
1.2.4.2 Side Effects of Chemotherapy and Gemcitabine.....	13
1.2.5 Targeted Therapy	14
1.2.5.1 Tumor Specific Targeting	14
1.2.5.2 Targeting by Drug Delivery Systems	15
1.3 Nanoparticles in Drug Delivery Systems.....	16
1.3.1 Principal Mechanisms of Drug Targeting to Tumors	17
1.3.2 Magnetic Nanoparticles	18

1.4	Coating of Magnetic Nanoparticles for Drug Delivery.....	21
1.4.1	Dendrimers for Surface Coating of Magnetic Nanoparticles	22
1.4.1.1	PAMAM Dendrimer.....	24
1.4.1.2	Dendrimers in Biomedical Applications	25
1.4.1.3	Interaction Between Dendrimer and Drugs.....	26
1.4.2	Chitosan for Surface Coating of Magnetic Nanoparticles	27
1.4.3	Polyhydroxybutyrate (PHB) for Surface Coating of Magnetic Nanoparticles.....	29
1.5	Aim of the Study.....	30
2	MATERIALS AND METHODS	31
2.1	Materials	31
2.2	Methods.....	32
2.2.1	Synthesis of PAMAM Coated Magnetic Nano Particles (DcMNPs)	32
2.2.1.1	Preparation of Bare Magnetic Nano Particles (MNP).....	32
2.2.1.2	Coating of Bare Magnetic Nanoparticles by APTS	34
2.2.1.3	Surface Coating of MNPs with PAMAM Dendrimer	35
2.2.2	Synthesis of Chitosan Coated Magnetic Nano Particles.....	36
2.2.3	Synthesis of PHB Coated Magnetic Nano Particles	36
2.2.4	Gemcitabine Loading, Release and Stability on DcMNPs	37
2.2.4.1	Loading of Gemcitabine on Different Half-Generation of DcMNPs.....	37
2.2.4.2	Release of Gemcitabine from DcMNPs	39
2.2.4.3	Stability of Gemcitabine on DcMNPs.....	39
2.2.5	Gemcitabine Loading, Release property and Stability of CSMNPs.....	40
2.2.5.1	Loading of Gemcitabine on CSMNPs.....	40
2.2.5.2	Release of Gemcitabine from CSMNPs	40
2.2.5.3	Stability of Gemcitabine on CSMNPs.....	40
2.2.6	Gemcitabine Loading, Release and Stability on PHB-MNPs	41
2.2.6.1	Loading of Gemcitabine on PHB	41
2.2.6.2	Release of Gemcitabine from PHB-MNPs.....	41
2.2.6.3	Stability of Gemcitabine on PHB-MNPs	41
2.2.7	Chemical Characterizations	42
2.2.8	Cell Culture.....	43
2.2.8.1	Cell Lines and Culture Conditions	43
2.2.8.2	Cell Proliferation Assay with XTT Reagent	43
3	RESULTS AND DISCUSSION	45

3.1	Characterization of Half Generation of PAMAM Magnetic Nano Particles (DcMNPs)	45
3.1.1	Analysis of PAMAM DcMNPs	47
3.1.1.1	TEM Analyses	47
3.1.1.2	Zeta (ζ) Potential Analyses.....	48
3.1.1.3	Fourier Transform-Infrared Spectroscopy (FT-IR)	50
3.2	Gemcitabine Loading Efficiencies on various half generation of DcMNPs	51
3.2.1	Characterization of Gemcitabine Loaded G5.5 PAMAM DcMNPs	53
3.2.1.1	TEM Analyses	53
3.2.1.2	X-Ray Photoelectron (XPS) Analyses	54
3.2.1.3	Fourier Transform-Infrared spectroscopy (FT-IR).....	56
3.2.1.4	Zeta (ζ) Potential Analyses.....	58
3.2.2	Release and Stability Efficiencies of Gemcitabine from G5.5 PAMAM DcMNPs	59
3.2.2.1	Release Profiles	59
3.2.2.2	Stability Efficiencies	60
3.2.3	<i>In vitro</i> Cytotoxicity Studies of Bare and Gemcitabine Conjugated G5.5 PAMAM DcMNPs on SKBR-3 and MCF-7 Cell Lines	61
3.3	Gemcitabine Loading Efficiencies on Chitosan Coated Magnetic Nanoparticles (CSMNPs)	65
3.3.1	Characterization of Gemcitabine Loaded CSMNPs	66
3.3.1.1	TEM Analyses	66
3.3.1.2	X-ray Photoelectron (XPS) Analyses.....	67
3.3.1.3	Fourier transform-infrared spectroscopy (FT-IR)	69
3.3.1.4	Zeta (ζ) Potential Analyses.....	70
3.3.2	Release and Stability Efficiencies of Gemcitabine from CSMNPs.....	71
3.3.2.1	Release Profile.....	71
3.3.2.2	Stability Profile.....	73
3.3.3	<i>In Vitro</i> Cytotoxicity Studies of CSMNPs and Gemcitabine Loaded CSMNPs on SKBR-3 and MCF-7 Cell Lines	74
3.4	Gemcitabine Loading Efficiencies on PHB Magnetic Nanoparticles (PHB_MNPs)	78
3.4.1	Characterization of Gemcitabine Loaded PHB-MNPs.....	79
3.4.1.1	TEM Analyses	79
3.4.1.2	X-ray Photoelectron (XPS) Analyses.....	80
3.4.1.3	Fourier Transform-Infrared Spectroscopy (FT-IR)	82
3.4.1.4	Zeta (ζ) Potential Analysis	83

3.4.2	Release and Stability Efficiencies of Gemcitabine from PHB-MNPs.....	84
3.4.2.1	Release Profile.....	84
3.4.2.2	Stability Profile.....	85
3.4.3	<i>In Vitro</i> Cytotoxicity Studies of Bare and Gemcitabine Loaded PHB-MNPs.....	86
3.5	Summary.....	90
4	CONCLUSION.....	91
	REFERENCES.....	93
APPENDIXS		
	ADDITIONAL ANALYSIS OF PAMAM DCMNPS.....	103
A.1.	Loading of Gemcitabine on Generation 4 and 7 of DcMNPs.....	103
A.2.	PAMAM Dendrimer Synthesized with Mechanical Stirrer.....	104
A.3.	Zeta (ζ) Potential Analysis.....	105
A.4.	Fourier Transform-Infrared spectroscopy (FT-IR).....	106
A.5.	Standard curves of Gemcitabine.....	107
A.6.	XTT Cell Proliferation Assay.....	108
A.7.	Light Microscopy Images of MCF-7 Cells.....	109
	ADDITIONAL ANALYSIS OF CSMNPS.....	110
B.1.	Loading of Gemcitabine on CSMNPs.....	110

LIST OF FIGURES

FIGURES

Figure 1.1. New cases of breast cancer in the USA	2
Figure 1.2. Differences between normal (A) and tumor tissues (B)	5
Figure 1.3. Differences between healthy (A) and tumor tissues (B).....	6
Figure 1.4. Treatment modalities of early stage and metastatic breast cancer.....	7
Figure 1.5. Chemical structure of Gemcitabine	10
Figure 1.6. Gemcitabine metabolism, self-potential and mechanisms of actions	12
Figure 1.7. HER2 Targeted Therapy	14
Figure 1.8. Time line of clinical stage for nanomedicine.....	15
Figure 1.9. NPs and their physicochemical characteristics which affect their performance both <i>in vitro</i> and <i>in vivo</i>	16
Figure 1.10. Therapeutic strategy using magnetic particles.....	18
Figure 1.11. Surface coating of magnetic nanoparticles.	21
Figure 1.12. Schematic overview of the sub-classes of dendritic polymers family..	22
Figure 1.13. Graphical presentation of PAMAM dendrimers from core to G7	24
Figure 1.14. Chemical structure of G2 PAMAM dendrimer.	25
Figure 1.15. The interaction between Chitosan and TPP	28
Figure 1.16. Polyhydroxybutyrate (PHB) structure	29
Figure 2.1. The bare MNP experimental synthesis setup.....	33
Figure 2.2. (a) G5.5 PAMAM dendrimer magnetic nanoparticle (G5.5 DcMNPs), (b) Gemcitabine (dfdc), (c) G5.5 DcMNPs conjugated by dfdc.....	38
Figure 3.1. (A) Full generation PAMAM dendrimer, (B) Half generation PAMAM dendrimer	46
Figure 3.2. (A) TEM images of G5DcMNPs, (B) G5.5 DcMNPs.....	47
Figure 3.3. Zeta (ζ) Potential of G5 DcMNPs (A) and G5.5 DcMNPs (B)	48
Figure 3.4. FT-IR spectra of the G5 DcMNPs and G5.5 DcMNPs	50
Figure 3.5. Loading efficiencies of Gemcitabine conjugated to different half- generations for DcMNPs.....	51
Figure 3.6. TEM images of G5.5 DcMNPs (A) and Gemcitabine conjugated G5.5 DcMNPs (B)	53
Figure 3.7. XPS spectra of G5.5 DcMNPs, and Gemcitabine conjugated G5.5 DcMNPs.....	54
Figure 3.8. XPS particular Fluorine analyses of Gemcitabine conjugated DcMNPs.	55
Figure 3.9. Gemcitabine FT-IR spectra.....	56

Figure 3.10. FT-IR spectra of (A) Gemcitabine conjugated G5.5 dendrimer coated magnetic nanoparticles, (B) G5.5 dendrimer-modified magnetic nanoparticles.	57
Figure 3.11. Zeta (ζ) potential graphs of Gemcitabine conjugated to G5.5 DcMNPs.	58
Figure 3.12. Gemcitabine release profile of DcMNPs at pH 4.2 and pH 5.2.	59
Figure 3.13. Gemcitabine release of G5.5 DcMNPs in PBS (pH 7.2) results for stability test.	60
Figure 3.14. Cytotoxicity of G5.5 DcMNPs on MCF-7 and SKBR-3 cell lines.....	61
Figure 3.15. XTT cell proliferation assay of (A) Gemcitabine, (B) Gemcitabine conjugated DcMNPs on SKBR-3 cells.	63
Figure 3.16. XTT cell proliferation assay of (A) Gemcitabine, (B) Gemcitabine conjugated DcMNPs on MCF-7 cells.	64
Figure 3.17. Loading efficiencies of Gemcitabine conjugated to CSMNPs	65
Figure 3.18. TEM images of CSMNPs (A) and Gem-CSMNPs (B)	66
Figure 3.19. XPS scanning spectra of CSMNPs, and Gemcitabine loaded CSMNPs.	67
Figure 3.20. XPS particular fluorine analyses of Gemcitabine conjugated CSMNPs.	68
Figure 3.21. FT-IR spectra of CSMNPs and Gem-CSMNPs	69
Figure 3.22. Zeta potential measurements of CSMNPs (A) and Gem-CSMNPs (B).	70
Figure 3.23. Gemcitabine release profile of CSMNPs in acetate buffer at pH4.2 and pH 5.2.....	71
Figure 3.24. Stability of Gemcitabine conjugated CSMNPs in PBS buffer (pH 7.2)..	73
Figure 3.25. Cytotoxicity of CSMNPs on MCF-7 and SKBR-3 cell lines.	74
Figure 3.26. XTT cell proliferation assay of Gemcitabine and Gemcitabine conjugated CSMNPs on SKBR-3 cells.....	76
Figure 3.27. XTT cell proliferation assay of Gemcitabine and Gemcitabine conjugated CSMNPs on MCF-7 cells.	77
Figure 3.28. Loading efficiencies of Gemcitabine conjugated to PHB-MNPs.....	78
Figure 3.29. TEM images of PHB-MNPs (A) and Gemcitabine conjugated PHB-MNPs (B)	79
Figure 3.30. XPS scanning spectrum of PHB-MNPs, and Gemcitabine conjugated PHB-MNPs	80
Figure 3.31. XPS results for Fluorine analysis of Gemcitabine conjugated PHB-MNPs.	81
Figure 3.32. FT-IR results related to PHB-MNPs and Gemcitabine conjugated PHB-MNPs	82

Figure 3.33. Zeta (ζ) Potential graphs of PHB-MNPs (A), and Gemcitabine conjugated PHB-MNPS (B).....	83
Figure 3.34. Gemcitabine release profile of PHB-MNPs at pH 4.2.....	84
Figure 3.35. Stability of Gemcitabine loading PHB-MNPs in PBS buffer (pH 7.2).85	
Figure 3.36. Cytotoxicity of PHB-MNPs on MCF-7 and SKBR-3 cell lines	86
Figure 3.37. XTT cell proliferation assay results (A) Gemcitabine, (B) Gemcitabine loaded PHB-MNPs on SKBR-3 cells.....	88
Figure 3.38. XTT cell proliferation assay results (A) Gemcitabine, (B) Gemcitabine loaded PHB-MNPs on MCF-7 cells.....	89
Figure A. 1. Gemcitabine conjugation efficiency of various half – generation of PAMAM dendrimer synthesized with mechanical stirrer.....	104
Figure A. 2. FT-IR spectra of Gemcitabine, G4.5MNP and G4.5MNPs conjugated by 7.5, 15 and 22.5 $\mu\text{g/ml}$ Gemcitabine.....	106
Figure A. 3. FT-IR spectra for GEM-G7.5 DcMNP. Difference between Gemcitabine, DcMNPs and Gem-DcMNPs.....	106
Figure A. 4. Standard curves of Gemcitabine in (A) PBS (pH 7.2), and acetate buffer at (B) pH 4.2 and (C) pH 5.2.....	107
Figure A. 5. Schematic representation of MCF-7 (6×10^3 cells/well) cells seeded to 96 well plates and treated by bare DcMNPs, 4h after XTT reagent addition to plate....	108
Figure A. 6. Schematic representation of MCF-7 (6×10^3 cells/well) cells seeded to 96 well plates and treated by Gemcitabine conjugated DcMNPs, 4h after XTT reagent addition to plate.....	108
Figure A. 7. Cellular internalization of DcMNPs by light microscopy (A) MCF-7 (6×10^3 cells/well) cells. (B) Bare DcMNPs treated MCF-7 cells. (C) lowest drug dose (2.5 μM) treated MCF-7 cells. (D). Highest drug dose (90 μM) treated MCF-7 cells.....	109

LIST OF TABLES

TABLES

Table 1.1 Classification of breast cancer.....	3
Table 1.2. Relationships between particle size distribution and removal from the capillaries of the human vascular system (Arruebo et al. 2007).....	20
Table 3.1. Loaded amounts of Gemcitabine to 2.5 mg/ml G5.5 DcMNPs on different drug concentration.....	52
Table 3.2. Loaded amounts of Gemcitabine to 2.5 mg/ml CSMNPs using different initial drug loading concentrations.....	65
Table 3.3. Loaded amounts of Gemcitabine to PHB-MNPs using different initial drug loading concentrations.....	78
Table A. 1. Effect of initial drug concentration and solvent on encapsulation efficiency of G4 and G7 DcMNPs at various solvents.....	103
Table A. 2 Zeta potential results for different half generations of PAMAM number.....	105
Table B. 1. Loading efficiencies of different initial Gemcitabine loading concentrations on 2.5 mg/ml Chitosan magnetic nanoparticles in various solvents.....	110

CHAPTER 1

INTRODUCTION

1.1 Biology of Cancer

Cancer is an expression used for diseases by out-of-control cell growth that could invade other tissues. It is the result of unregulated cell dividing. The cells divide when they are not assumed and do not stop dividing when they are assumed and do not die when they must. In the harmful cases, cancer cells could spread to all of the body through the lymphatic and blood systems and arose metastases. There are over than 100 different types of cancer. Each cancer type is classified by the organ or the cell in which they start and initially affected (Cancer.gov 2014a).

The body can be harmed by cancer when cells divide uncontrollably and form tumors. The grown tumor can intervene with the circulatory, digestive and nervous. Also all body function can be modified by release of hormones from tumors (Crosta 2014). The out of control development of cancer cell take place in a multi-step procedure. The more abnormal cells obtain new capabilities, such as release of digestive enzymes and growth factors. The cells keep on dividing and so reduce the function of the damaged organ. It takes many years for a tumor to reach the size that can be diagnosed. Cancer cells do not exactly share the similar steps for development. Development of blood vessels (angiogenesis) is the critical step for growing a tumor which provides nutrients and transports away waste (Cancerquest 2014).

Cancer tumors can invade surrounding areas or metastasize to areas beyond the nearby tissue. Metastatic tumors would be the most hazardous and also explain to a lot of large proportion of cancer deaths.

1.1.1 Breast Cancer

Breast cancer is a heterogeneous disease which is seen among women and men in the world. Two common types of breast cancer are ductal carcinoma and lobular carcinoma. Ductal carcinoma in situ (DCIS) develops in the milk ducts, which carry milk from the lobules to the nipple, hence, lobular carcinoma develops in the milk glands. Ductal carcinoma was the majority of in situ breast cancers between 2004-2008 years, which caused about 83% of breast cancer instances (DeSantis, Siegel, and Jemal 2012).

In recent years, the occurrence and mortality of breast cancer could be seen in the USA (Figure 1.1).

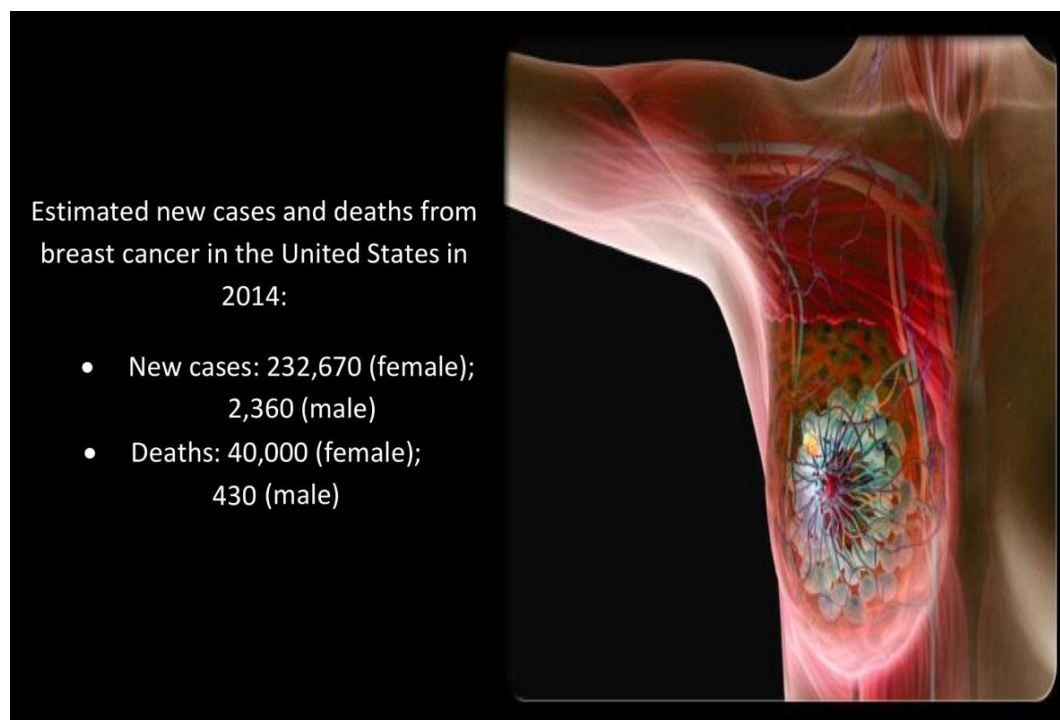


Figure 1.1. New cases of breast cancer in the USA (Cancer.gov 2014b).

Breast cancer classified as, HER2, luminal A and B, normal and basal subtypes due to progesterone receptor (PR), estrogen receptor (ER) and human epidermal growth factor receptor 2 (HER2) (Holliday et al. 2011). Each subtype has various prognosis and treatment response. The luminal A and luminal B subtypes are ER⁺, are responsive to hormone therapy. Also, luminal B and HER2 groups are HER2⁺ and they are potential candidates for trastuzumab, labatinip and pertuzumab therapy (Table 1.1) (Mohamed *et al.* 2013).

Table 1.1. Classification of breast cancer (Holliday et al. 2011).

Classification	Immunoprofile	Other characteristics	Example cell lines (adapted from [13,22])
Luminal A	ER ⁺ , PR ⁺ , HER2 ⁻	Ki67 low, endocrine responsive, often chemotherapy responsive	MCF-7, T47D, SUM185
Luminal B	ER ⁺ , PR ⁺ , HER2 ⁺	Ki67 high, usually endocrine responsive, variable to chemotherapy. HER2 ⁺ are trastuzumab responsive	BT474, ZR-75
Basal	ER ⁻ , PR ⁻ , HER2 ⁻	EGFR ⁺ and/or cytokeratin 5/6 ⁺ , Ki67 high, endocrine nonresponsive, often chemotherapy responsive	MDA-MB-468, SUM190
Claudin-low	ER ⁻ , PR ⁻ , HER2 ⁻	Ki67, E-cadherin, claudin-3, claudinin-4 and claudinin-7 low. Intermediate response to chemotherapy	BT549, MDA-MB-231, Hs578T, SUM1315
HER2	ER ⁻ , PR ⁻ , HER2 ⁺	Ki67 high, trastuzumab responsive, chemotherapy responsive	SKBR3, MDA-MB-453

EGFR, epidermal growth factor receptor; ER, oestrogen receptor; HER2, human epidermal growth factor receptor 2; PR, progesterone receptor.

Alternative treatments for breast cancer are surgery, systemic therapy and radiation therapy. Systemic therapies cover hormonal therapies, chemotherapy and also targeted therapies (DeSantis et al. 2012).

1.1.2 Physiopathological Characteristics of Tumor Tissues

1.1.2.1 Leaky Vasculature

In 1–2 mm³ sized solid tumors; diffusion is the simple way to transport nutrients and oxygen to the center of the tumor. Cellular hypoxia begins, when tumors reach to 2 mm³ and induces angiogenesis. Angiogenesis is essential step for survival and cell function, which involves the formation of new bloodstream from existing ones, delivery of vital nutrients and oxygen to newly forming cells. In this manner, tumors become capable to attain their own blood vessels (Danhier *et al.* 2010). The rapid and uncontrollable dividing is the characteristic of tumor cells, which leads to hypoxic conditions, as a result of restrictions of nutrients and oxygen within the tumor environment. For that reason, a series of steps to the development of the capillary tubing occurs, to be able to make new vessels. The proangiogenic growth factors, including; basic fibroblast growth factor, vascular endothelial growth factor, nitric oxide, prostaglandins, bradykinins, and so on, mediate this process at the tumor site. In contrast to the normal cells, the new tumor blood supplies in this abnormal growth condition present a tortuous structure and are disorganized, with holes between endothelial cells, making a porous and leaky vasculature, leading to a heightened vascular permeability to macromolecules (Egusquiaguirre *et al.* 2012).

1.1.2.2 Enhanced Permeability and Retention Effect

Reducing the lymphatic canalization and chaotic leakiness of the newly formed tumor bloodstreams, is named enhanced permeability and retention effect (EPR). Abnormal characteristics of the tumor blood vessels, such as; higher ratio of proliferating endothelial cells, abnormal bottom membrane formation and pericyte deficiency, lead the tissues to an enhanced vascular permeability (Figure 1.2) (Danhier et al. 2010).

The EPR effect is probably the most significant mechanism whereby the macromolecules and nanoparticles can be accumulated in the tumor interstitium (Egusquiaguirre et al. 2012).

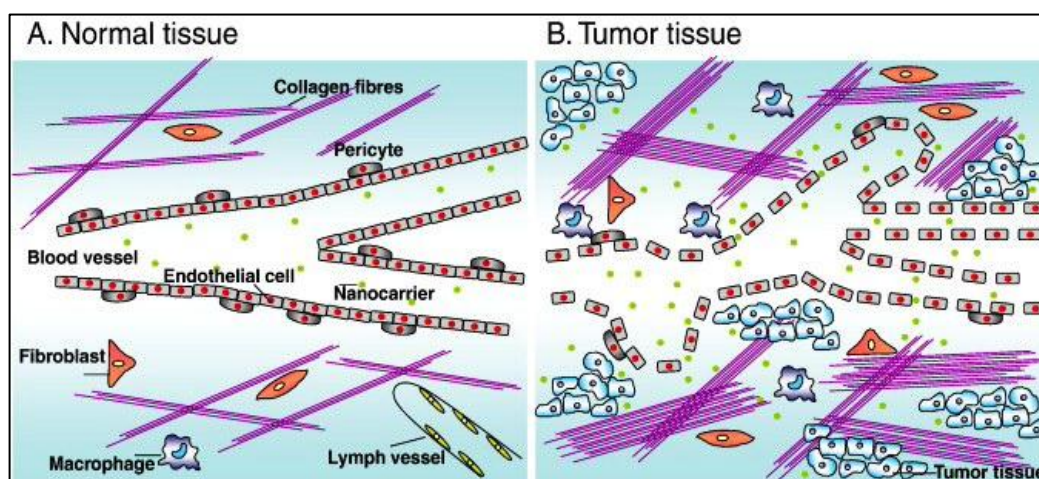


Figure 1.2. Differences between normal (A) and tumor tissues (B) (Danhier et al. 2010).

Normal tissues comprise linear blood vessels kept up by fibroblasts and pericytes. Macrophages, lymph vessels and collagen fibers are present in the extracellular matrix (Figure 1.2 A). Many abnormal blood vessels with cavities and fenestrations could be seen in tumor tissues. Also more macrophages and collagen fibers, fibroblasts could be seen in the extracellular matrix of the tumor tissue than that of normal tissue. Lymph vessels are missing (Figure 1.2 B).

1.1.2.3 Acidic Tumor Microenvironment

In addition to the EPR effect, remarkably proliferative cancer cells show a greater metabolic ratio. To complement their needs tumor cells should receive additional energy by glycolysis. These cells could not properly drain the waste products because of not organized lymphatic network. Therefore, the amount of wastes and protons concentration increases in these tissues. As a result, these generate a minor extracellular pH than normal tissues (Figure 1.3) (Gu et al. 2007).

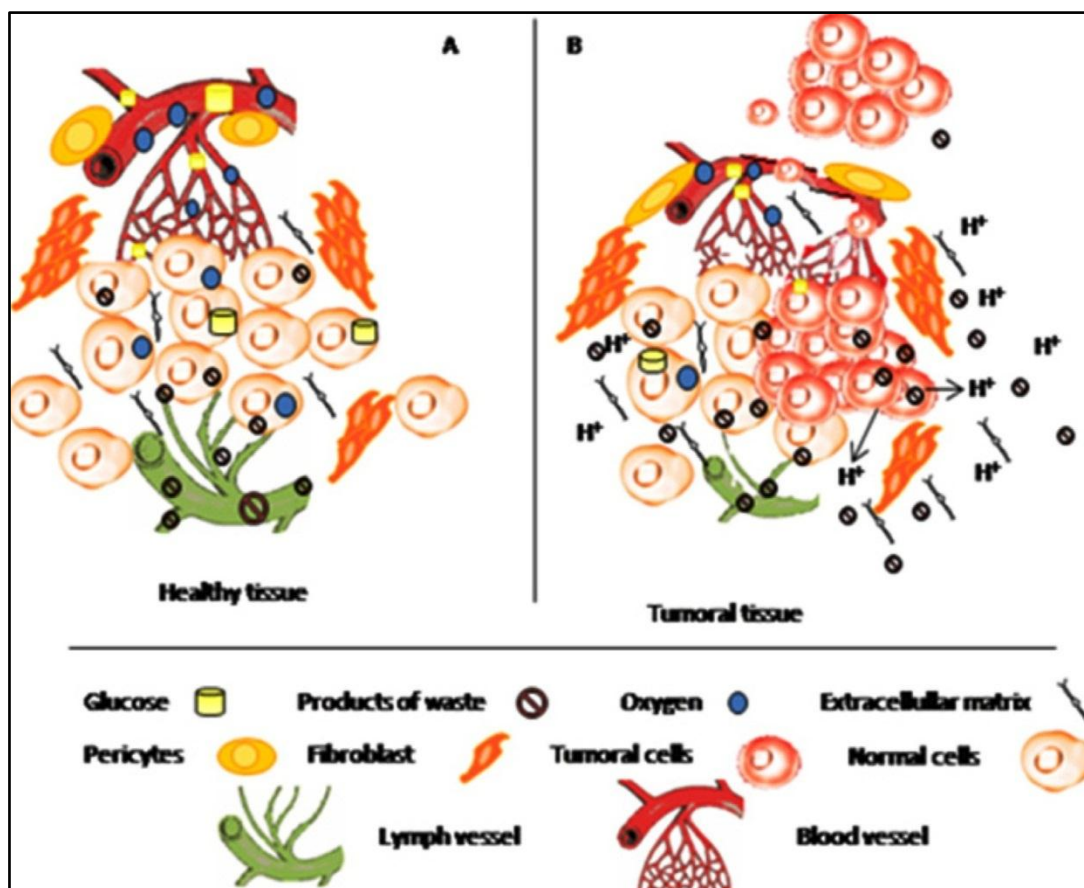


Figure 1.3. Differences between healthy (A) and tumor tissues (B) (Gu et al. 2007).

1.2 Treatment of Breast Cancer

Systemic and local therapies are the two common methods for the treatment of breast cancer. Targeted therapy, hormone therapy, and chemotherapy are the types of systemic therapy, which make it possible for traveling the drugs all over the body in bloodstream to destroy cancer cells. Surgery and also radiation therapies are local therapies hoping to treat simply at tumor site and they do not affect the whole body (Figure 1.4) (National Cancer 2014).



Figure 1.4. Treatment modalities of early stage and metastatic breast cancer (National Cancer 2014).

1.2.1 Surgery

The principle of breast cancer surgery is to eliminate the cancer through the breast and also to assess the actual stage of disease. A simple mastectomy includes removal of the whole breast. In a modified radical mastectomy involves removal of the whole breasts and also lymph nodes under the arm, without removing the underlying chest wall muscle, as which has done in radical mastectomy. In a lumpectomy, just malignant tissue along with a rim of healthy tissue is taken out. Lumpectomy is actually accompanied by radiation therapy. The survival chance of radiation therapies beside lumpectomy are the same as mastectomy (National Cancer Institute 2014).

1.2.2 Hormone Therapy

Estrogen encourages the development of numerous breast cancers. The positive estrogen test women could be handed a drug, which is known as hormone therapy to reduce estrogen levels or by blocking the consequences of estrogen on the growth of breast cancer tissues. Toremifene (Fareston) and Tamoxifen are drugs which prevent the binding of estrogen to breast cancer cells. They have effective range in premenopausal and postmenopausal patients.

The mechanism of Fulvestrant is reducing the number of estrogen receptors on breast tumors. It is usually efficacious in postmenopausal women still when the breast cancer is not answering to tamoxifen (National Cancer 2014).

1.2.3 Radiation Therapy

Watching over the operation, radiation therapy is commonly given to patients to eliminate the any leftover cancer cells. It damages cancer cells by higher energy beams or particles leading to harm at DNA level. X-ray, Gamma ray and charged particles are used in radiation therapy.

The external beam radiation therapy is applied to body from outside. In brachytherapy the radioactive material is put near by the tumor site in breast tissue (National Cancer 2014) (DeSantis et al. 2012).

1.2.4 Chemotherapy

The main benefit of chemotherapy depends on various factors, such as the size of tumors, the actual presence of progesterone or estrogen receptors, the amount of lymph nodes involved and the amount of HER2 protein. In most cases, it was shown that the combinations of drugs will more effective than a single drug for cancer treatments. Based on the combination of drugs which are used, adjuvant chemotherapy is normally offered for 3 to 6 months.

Chemotherapy is actually effective when the cycle and full dose of drugs are completed regularly (DeSantis et al. 2012).

1.2.4.1 Gemcitabine (Gemzar)

Gemcitabine (2', 2'-difluorodeoxycytidine) is an analogue of deoxycytidine which is structurally different, by its fluorine exchange on position 2' of furanose ring (Figure 1.5) (Alexander et al. 2005)(Mini et al. 2006). It is potent nucleoside analogue inducing S-phase detention and inhibiting DNA synthesis.

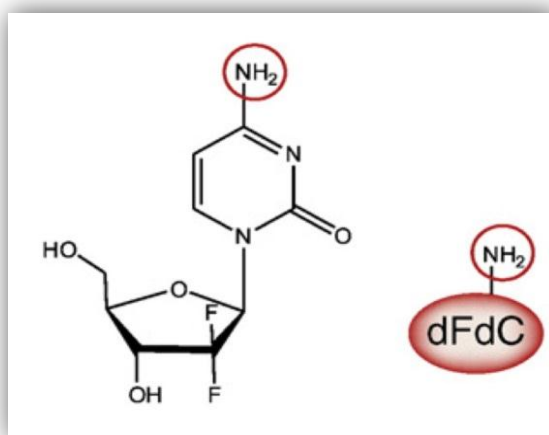


Figure 1.5. Chemical structure of Gemcitabine (Bildstein et al. 2011).

Gemcitabine is used as anticancer drug against several solid tumors, including pancreatic, lung, ovarian, colon, bladder and breast cancers (Chitkara et al. 2013)(Martín-Banderas et al. 2013).

It had been initially investigated as an antiviral agent then produced as an anticancer drug based on its impressive *in vivo* and *in vitro* anti-tumoral activity. Evidence of the effectiveness of gemcitabine to prevent the growth of human neoplasms had been obtained in a broad range of hematological and solid cancer cell lines, in addition to *in vivo* murine solid tumors and also human tumor xenografts in nude mice (Mini et al. 2006).

Due to Gemcitabine hydrophilicity it could not cross the plasma membrane passively; therefore the therapeutic effectiveness is reduced. This inhibits a higher payload and also prolonged drug release. Therefore, it must be transported into the cells by nucleoside transporters (NTs), such as the human Equilibrative Nucleoside Transporters (hENT) or human sodium gradient coupled nucleoside transporters (Mini et al. 2006)(Bildstein et al. 2010)(Chitkara et al. 2013).

Gemcitabine is a prodrug; its mechanism of action is based on cellular uptake and also intracellular phosphorylation. In the cytoplasm of the cell, it is converted into biologically active form by phosphorylation. Deoxycytidine kinase (dCK) phosphorylated gemcitabine to monophosphate (dFdCMP), and then it is changed to gemcitabine di-(dFdCDP) and triphosphate (dFdCTP), respectively. (Figure 1.6) Gemcitabine has several intracellular locations. Its antiproliferative action is considered to be dependent mostly on several inhibitory steps of DNA synthesis (Bildstein et al. 2010)(Mini et al. 2006). Gemcitabine triphosphate (dFdCTP) can inhibit DNA polymerase and become incorporated into DNA. After its incorporation, DNA polymerase could add only one nucleotide by into the DNA chain, which leads to termination of chain elongation (Alexander et al. 2005)(Mini et al. 2006).

Also non-terminal position of dFdCTP in the DNA chain inhibits recognition and restoration by DNA repair enzymes (masked chain termination). Masked termination obviously locks the drug into DNA and the proofreading enzymes are unable to eliminate gemcitabine from this position, which cause inhibition of DNA synthesis and induce apoptotic cell death (Mini et al. 2006).

Inhibition of ribonucleotide reductase (RR) is the other mechanism of action of gemcitabine, which causes a loss of competing deoxyribonucleotide pools required for DNA synthesis (Alexander et al. 2005).

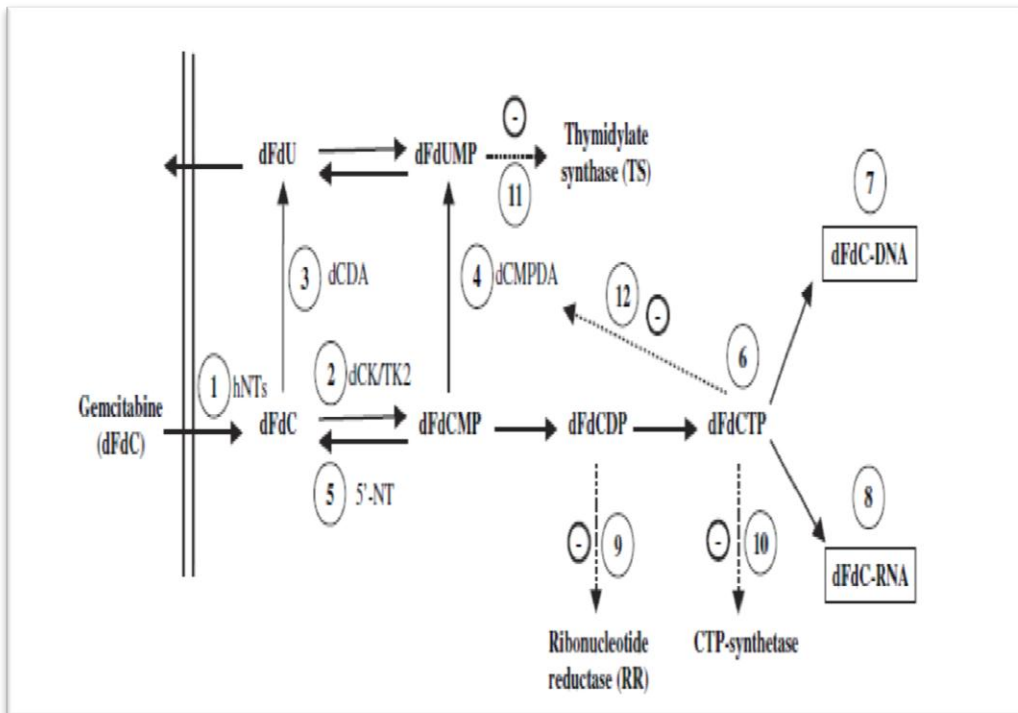


Figure 1.6. Gemcitabine metabolism, self-potential and mechanisms of actions (Mini et al. 2006).

Inhibition of deoxycytidylate deaminase (dCMP deaminase) and cytidine triphosphate syntheses (CTP syntheses) by dFdCTP are the other reported activities of gemcitabine metabolites (Mini et al. 2006)(Robinson et al. 2001).

Clinical data demonstrated that patients with tumors along with a lowered expression of hENT1 have a considerably lower survival rate following gemcitabine therapy compared to patients with tumors that convey a higher level of hENT1. In excess of 90% Gemcitabine which have been internalized in to cells are phosphorylated to Gemcitabine triphosphate (dFdCTP) and they generally deaminated by deoxycytidine deaminase (dCDA) to make inactive metabolite 2'-deoxy-2', 2'-difluorouridine (dFdU). As a result, deamination influences the actual efficiency of gemcitabine adversely (Lansakara-P et al. 2012)(Chitkara et al. 2013)(Sloata et al. 2011).

1.2.4.2 Side Effects of Chemotherapy and Gemcitabine

Chemotherapeutic drugs target the dividing cells, so they cannot identify between healthy and cancerous cells. In many healthy cells, such as, bone marrow, hair follicle, gastrointestinal track and reproductive track, dividing occurs as a normal function. Toxicity and numerous side effects are noticed in these tissues and organs by this method of treatment. In addition, at molecular level, it could also cause to the drug resistance (Liu et al. 2014).

Genetic background of a person, period and type of treatment and also type and dosage of drugs could cause a long term and short term effects in patients.

Many solid tumors are treated by Gemcitabine, but due to some aspects, its clinical benefits have been limited. The short plasma half-life of Gemcitabine (less than 20 min in human plasma) after intravenous administration and rapid metabolism into inactive form 2,2–difluorodeoxyuridine (dFdU) by cytidine deaminase, display the main restrictions of this drug (Martín-Banderas et al. 2013). Moreover, a poor diffusion directly into cells leads to the use of its higher doses, so it cause to major systemic toxicity and drug resistance, which usually restricts its therapeutic efficiency (Maksimenko et al. 2013).

Acute adverse effects of gemcitabine are (American Cancer Society 2013):

- The increasing risk of infection because of reducing the number of white blood cells in the blood.
- The increasing risk of bleeding because of reducing the number of platelets in the blood.
- Anemia; decreasing number of red blood cell in the blood.
- Feeling sick ; symptoms like tiredness, weakness, or shortness of breath
- Nausea
- Hair loss
- Vomiting and loss of appetite
- Fever
- Swelling of the arms and legs or other parts of the body

1.2.5 Targeted Therapy

Targeted treatment is one of the significant concepts that has been rising for the fight against cancer and also for avoiding the side effects of chemotherapeutic drugs through the last few years (Sawyers 2004).

1.2.5.1 Tumor Specific Targeting

Various cell specific targeted treatments with an essential role in growth and tumor progression, are designed to particular molecular target. In the breast cancer treatment estrogen receptor (ER) and human epidermal growth factor receptor 2 (HER2) are actually the main targets for therapy and also drug development (Figure 1.7).

For ER⁺ patients, Tamoxifen, Aromatase inhibitors (AIS) and Fulvestrant are among the hormonal targeting agents that are used. For HER2⁺ patients usually Lapatinib Trastuzumab, and Pertuzuman have been used (Mohamed et al. 2013).

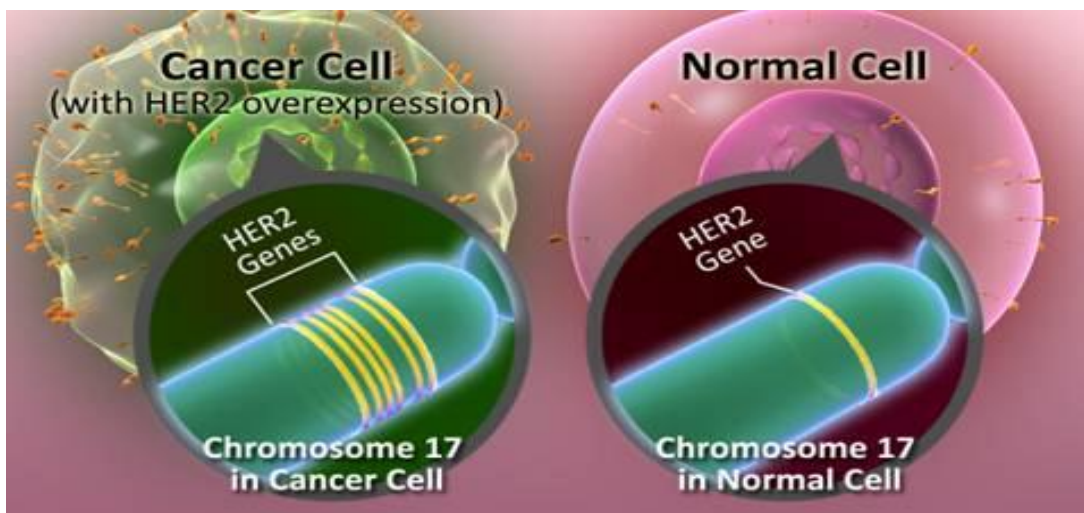


Figure 1.7. HER2 Targeted Therapy (cancer.gov n.d.).

1.2.5.2 Targeting by Drug Delivery Systems

One of the distinguished methods that have been used for targeted drug delivery is controlled drug delivery systems (DDS), which usually combined of polymers and/or lipids. Magnetic nanoparticles, dendrimers, polymers, carbon materials and liposomes, are the different nanostructures, which are used as carriers in drug delivery systems.

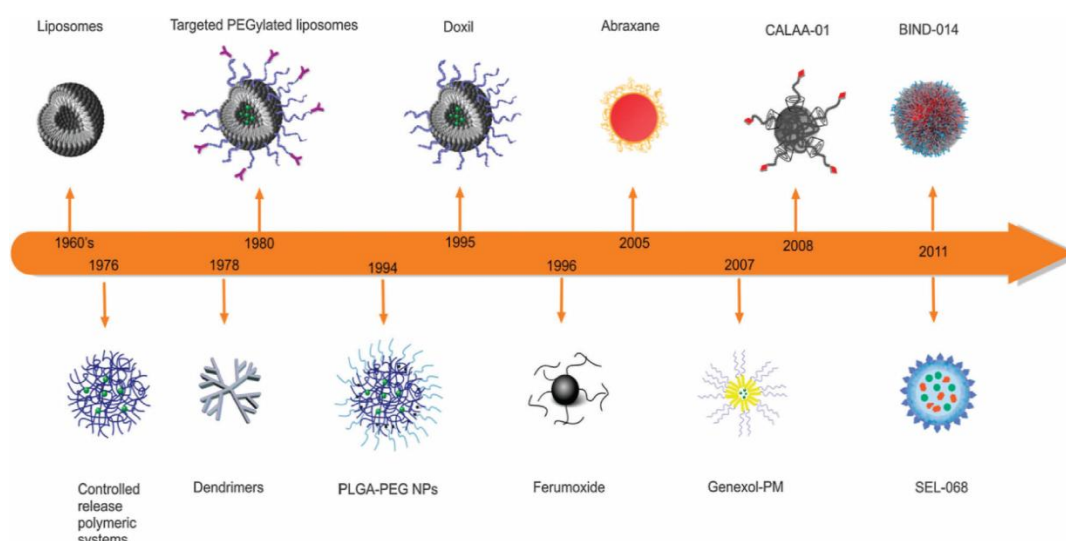


Figure 1.8. Time line of clinical stage for nanomedicine (Kamaly et al. 2012).

They have several positive aspects when compared with classic drug applying methods; especially it seems the severe difference between the dose of a drug and toxic effects. Also drug can be delivered to the cancer tissue and it cause minimizing the side effect of the drug on undesirable tissues. It has efficient, increase on drug accumulation in the tumor tissue; therefore, the specified doses of drugs are decreased significantly (Wilczewska et al. 2012).

1.3 Nanoparticles in Drug Delivery Systems

In the last two decades, the design of nanoparticles (NPs) with specific functional properties in therapeutics and diagnostics has gained attention for a drug delivery system. Nanoparticles have enabled more efficient and safer drug delivery for many drugs and help for improving the treatment of different pathologies. Their nanoscale size, high surface area and their ability to reach the different areas of the body make nanoparticles a promising tool for drug delivery system. Reducing the side effects of drugs and prolonging circulation half-times are another advantages for delivery of drugs by this system (Viota et al. 2013) (Hu et al. 2010).

1–100 nm size range of nanoparticles makes it different from bulk materials, and therefore, have great potential for using in the chemical, biological, mechanical and electronic industries (Inkyo et al. 2006) (Figure 1.9). Metal, metal oxide and semiconductor nanoparticles coupled to biomolecules have recently attracted a great interest because the resulting hybrid materials call for new applications in biological systems (Egusquiaguirre et al. 2012).

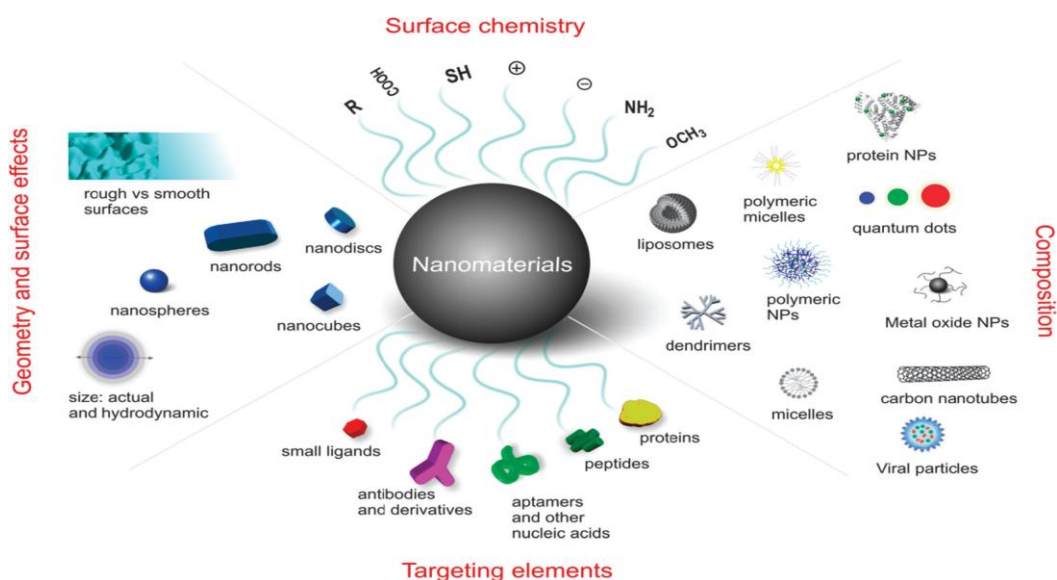


Figure 1.9. NPs and their physicochemical characteristics which affect their performance both *in vitro* and *in vivo* (Kamaly et al. 2012).

In cancer treatments, the leaky tumor vasculatures cause the better accumulation of nanoparticles in tumor site. These benefits make therapeutic nanoparticles a promising candidate to replace traditional chemotherapy (Viota et al. 2013).

1.3.1 Principal Mechanisms of Drug Targeting to Tumors

In the last few years, targeted NP therapeutics have shown great attention for cancer therapy, as they lead to increased internalization of drugs and supply enhanced efficacy and more importantly, reduced side effects and systemic toxicities. NP drug delivery to tumor tissues consists passive, active or triggered targeting.

Passive delivery refers to nanoparticles extravasations by enhanced permeability and retention effect through leaky tumor vascularization. The 'leaky' vascularization refers to the EPR effect which causes to accumulation of nanoparticles and drug within the tumor microenvironment followed by the release and diffusion of drug through the tumor tissue. Nanocarriers show more accumulation in tumor tissues than normal tissues because they have longer circulation times in the blood vessels and it drives more chances for reaching the tumor area and releasing a greater amount of drug in this area. The result is efficient anti-cancer therapy with less toxic effect. Some nanoparticles are designed to acquire “pH-controlled response and drug release” characteristic, due to acidic environment of the tumor (Egusquiaguirre et al. 2012; Kamaly et al. 2012). Although passive targeting has several limitations due to less diffusion efficiency of some drugs, also sometimes it is difficult to control the process of delivery due to many nature approaches, beside all of these limitations some tumors do not exhibit an EPR effect. Active and passive targeting are deeply dependent to each other because the active targeting occurs only after accumulation of drug in tumors after passive targeting.

Active targeting requires the use of affinity ligands to direct binding of NPs to peptides, antigens, monoclonal antibodies which are differentially overexpressed on

the membrane of diseased cells or to the extracellular matrix proteins that are differentially overexpressed in the disease tissue (Kamaly et al. 2012).

Triggered targeting is another type of drug targeting mechanism. In this method by the help of some external stimulus such as magnetic field, hyperthermia, ultrasound, electrical irradiation, and light nanocarriers could release their payloads (Egusquiaguirre et al. 2012).

1.3.2 Magnetic Nanoparticles

Magnetic micro/nanoparticles ranging from micrometer to nanometer scale are being used in an increasing number of medical and biological applications such as magnetic resonance imaging (MRI), magnetic cell separation, enzyme and protein immobilization, hyperthermia, RNA and DNA purification, and targeted drug delivery systems (Douziech-Eyrolles et al. 2007). The important properties of magnetic particles for medical applications are their nontoxicity, biocompatibility, and high-level accumulation in the target tissue or organ (Ito et al. 2005).

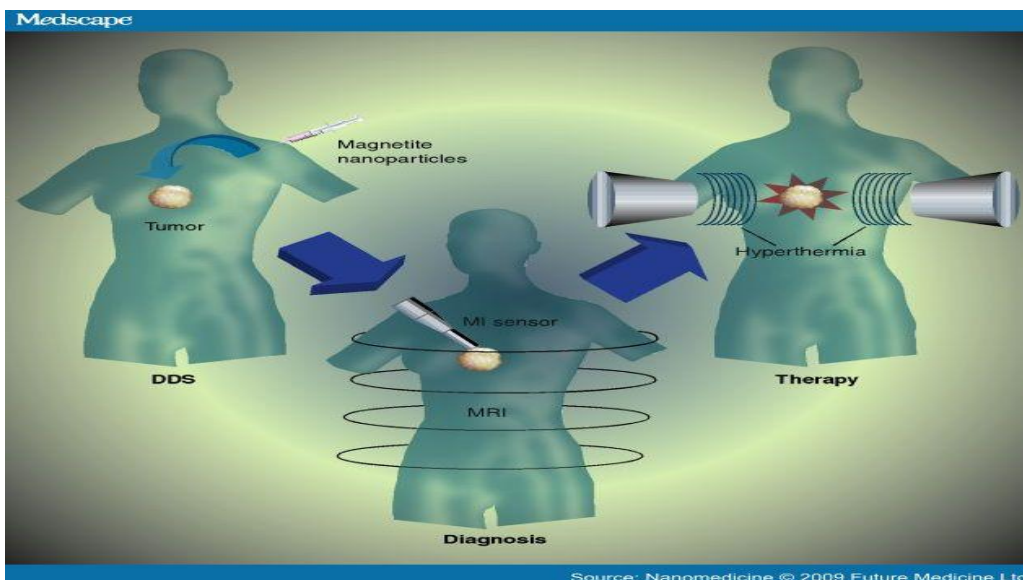


Figure 1.10. Therapeutic strategy using magnetic particles (medscape.com 2014).

Efforts in implementing magnetic particles for medical applications are based on their lack of toxicity, biodegradability, good biocompatibility, and absorption. In addition, controllable sizes and targeting ability to the desired site by an external magnetic field are the advantages of magnetic nanoparticles. Magnetic nanoparticles provide an opportunity for the development of the next generation of focused diagnostic and therapeutic oncological applications. MNPs deliver in manageable sizes, which range from a few up to tens of nanometers; therefore, their particular optimization easily matches with the interest of study. Magnetic nanoparticles could be manipulated by an external magnetic field. This is the main advantage of MNPs. Another tremendous advantage of MNPs is the role them in visualization, which is used as MRI agents (Gao et al. 2009).

Different physicochemical factors control the biodistribution of drug-loaded nanoparticles in the body, such as surface charge, the size of nanoparticles, drug loading and release, stability, toxicity, surface hydrophobicity, hydration behavior, molecular weight and crystallinity. Nevertheless, the destiny of magnetic nanoparticles also depends upon the dosage and the administration route (intravenous, pulmonary, oral, transdermal, and ocular) (Arruebo et al. 2007).

Ferrous or ferric oxide and metals such as nickel and cobalt are the main fields of magnetic particles (Ito et al. 2005). Food and Drug Administration approved iron oxide nanoparticles for clinical use (Wilczewska et al. 2012). Iron oxide magnetite and maghemite occur naturally in human heart, spleen and liver, which mark their biocompatibility and non-toxicity at a physiological concentration. In addition, easy synthesis by alkaline co-precipitation of Fe^{2+} and Fe^{3+} , chemical stability in physiological conditions and possibility of coating iron oxide cores with various shells make iron oxide nanoparticles favorable for biomedical use (Ahmed et al. 2013).

Smaller MNPs could escape from opsonisation by the reticuloendothelial system and be retained within the systemic circulation. This leads to longer circulation times of

these nanoparticles in the body (Table 1.2). Magnetic nanoparticles with less than 5 nm hydrodynamic diameter have short blood circulation times and rapidly extravasate across the endothelium. MNPs around 6 nm in size go through renal clearance and glomerular filtration. MNPs more than 8 nm in size, and with specific surface properties such as charge and hydrophobicity, are phagocytosed by Kupffer cells and they also undergo clearance via the biliary system (Ahmed et al. 2013).

Table 1.2. Relationships between particle size distribution and removal from the capillaries of the human vascular system (Arruebo et al. 2007).

		Size	System/Organ
Particle removal*	Tight-junction capillaries	< 1 nm	Central nervous system, blood-brain barrier
	Continuous capillaries	~ 6 nm	Tissues such as muscle, skin, and lung
	Fenestrated capillaries	~ 50-60 nm	Kidney, intestine, and some endocrine and exocrine glands
	Sinusoidal capillaries	~ 100-1000 nm	Liver, spleen, and bone marrow
Particle delivery	Arteriole radius	0.005-0.07 mm	Circulatory system. Particles supplied by intravenous administration. Elimination involves opsonization and removal by monocytes in blood
	Artery radius	0.08-7.5 mm	
	Venule radius	8-100 μ m	
*It is noted that this table expresses only the morphological pores contributing to diffusive permeability. Actual transcapillary exchanges are modified by vesicular transports, which are able to internalize particles with sizes up to 20-30 nm.			

Magnetic nanoparticles have responsive surface that can be readily modified with biocompatible coatings and loaded with drugs (Sun et al. 2008)(Nune et al. 2009).

These magnetic nanoparticles are generally composed of magnetite (Fe_3O_4) core and a polymeric shell where the drugs, nucleic acids, and proteins are bound. The polymeric shells such as dendrimers, dextran, PEG, PLGA, PHB and chitosan must have active groups for conjugation to biomolecules.

1.4 Coating of Magnetic Nanoparticles for Drug Delivery

Surface coatings on magnetic nanoparticles often serve several purposes. The coating of MNPs have essential role for protecting against agglomeration and also provide a chemical handles for the conjugation of drug to MNPs. It is retards clearance by reticuloendothelial system (RES) and limits non-specific cell interactions. Low toxicity is another important thing that causes the surface coating for magnetic nanoparticles. Also the coating often facilitates the stabilization of MNPs in a partly alkaline pH environment or a high salt concentration. Uncoated magnetic nanoparticles were shown to be cleared immediately after injection to the body by phagocyte system, Kupffer cells in the liver, spleen and bone marrow (Arruebo et al. 2007).

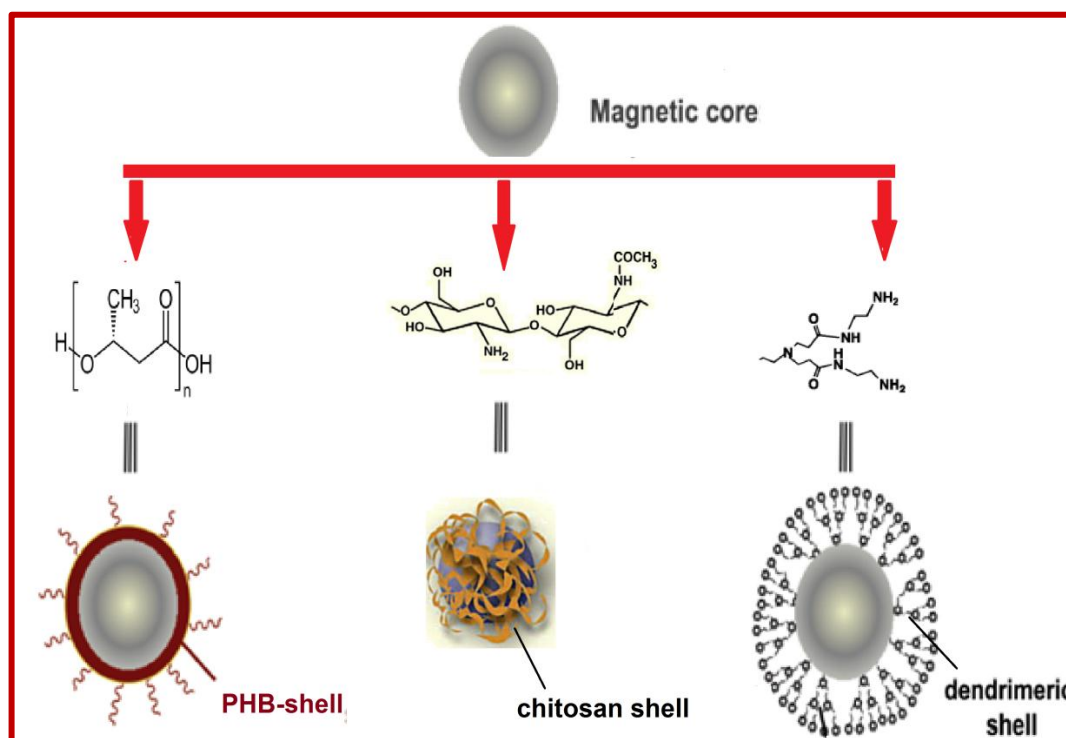


Figure 1.11. Surface coating of magnetic nanoparticles.

Many different coating materials can be used for preventing of nanoparticles opsonization and permitting a longer circulation time. Various kinds of polymers, dendrimers and chitosan have been used for coating of magnetic iron oxide nanoparticles (Figure 1.11).

Loading of a drug with MNPs may be achieved by electrostatic interactions, covalent binding, adsorption, or encapsulation process. Targeting of drug-MNP conjugates to diseased tissues can be carried out by passive or active mechanism depending on their size and surface chemistry (Wilczewska et al. 2012).

1.4.1 Dendrimers for Surface Coating of Magnetic Nanoparticles

In the 1830's, synthetic polymers were introduced as macromolecules that had been typically synthesized with a cascade of chemical reactions of monomers. Those linear polymers had been focused by traditional chemistry and technology. Starting point for the synthesis of dendritic polymers was the synthesized a branched polypropylene-amine "cascade molecules" that were generated through repetitive monomers by Vogtle *et al.* in 1978 (Walter et al. 2012).

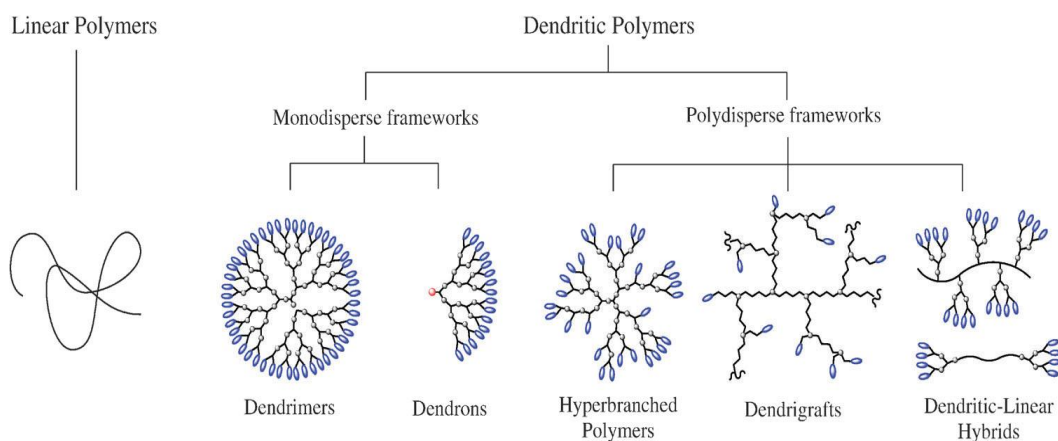


Figure 1.12. Schematic overview of the sub-classes of dendritic polymers family. (Walter et al. 2012).

Dendrimers are new classes of spherical and highly branched polymeric macromolecules introduced by Tomalia et al. as a monodisperse poly(amidoamine), (PAMAM), and by Newkome et al. as a poly(etheramide) arborols at the end of 1980's (Walter et al.2012).

The dendrimers demonstrate an exponential increase of surface groups as a purpose of generation. The molecular weight of the dendrimer nearly doubles with each additional generation, though the volume of the sphere improves with the cube of the generation. Numerous functional groups, dendrons, from center to arms give nearly-perfect 3D geometric structure in nanometer size range. These characteristics supply a high degree of functionality and wide variety of skills to dendrimers (Shcharbin et al. 2009).

Dendrimers possess three components: an initiator core (G0), interior layers (branches), and exterior (terminal functional groups). The polyfunctional initiator core is in the heart of the molecule, and interior layers composed of repeating units which extend outward from it. The monomers attached to the G0, are called first generation monomers (G1) and repeating generation monomers are attached to the previous generation monomers (Bharali et al. 2009). The chemistry of the terminal functional groups provides many of the special properties of dendrimers such as solubility and reactivity. In addition, terminal groups can be modified to get both a charged (cationic or anionic), and hydrophilic or lipophilic properties for the ideal biological and drug delivery applications (Majoros et al. 2003).

The structure of dendrimers offers various advantages over other architectural forms of polymers which used in drug delivery systems. They can be synthesized and designed for specific applications. They have narrow polydispersity; they are in the nanometer size range from 1 to 100 nm, which allows less susceptible for RES uptake; host–guest chemistry can take place either in the interior for drug entrapment or on the terminal groups of the dendrimer for drug adsorption (Pan et al. 2005; Jain et al. 2010).

Polyamidoamine (PAMAM), polyethyleneimine, polyarylether and polypropyleneimine are samples of dendrimers that have been investigated for biopharmaceutical applications.

1.4.1.1 PAMAM Dendrimer

Poly-amidoamine (PAMAM) dendrimer is a well-defined, special three-dimensional structure and has a multivalent surface and internal cavities that can play an important role in drug delivery systems suitable. Several experiments indicated that higher transfection efficiency and lower toxicity can be obtained by using completion of DNA with PAMAM, as well as for the completion between siRNA and PAMAM dendrimers (Jain et al. 2010)(Vasumathi et al. 2010).

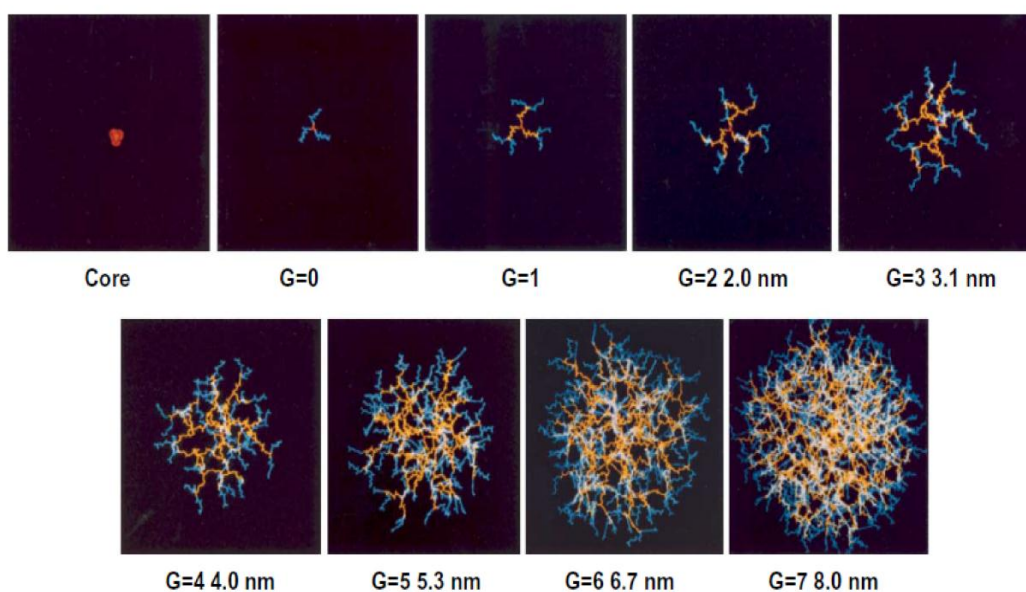


Figure 1.13. Graphical presentation of PAMAM dendrimers from core to G7 (Svenson et al. 2005).

PAMAM synthesized by the divergent method starting from an ethylenediamine interior core and an amidoamine repeat branches. They can be synthesized in a diversity of molecular weights. Their surface functionality and size are explained by

the number of monomeric units added dendrimers at different generations are obtained (up to generation 10^9) (Boas et al. 2006) (Figure 1.13).

Their great monodispersity, bioavailability and biocompatibility make PAMAM dendrimers excellent candidates for drug delivery (Taghavi Pourianazar et al. 2014). Despite these advantages, it is usually necessary to change the surface cationic amine groups of dendrimers to avoid the toxicity and liver (Gillies et al. 2005).

1.4.1.2 Dendrimers in Biomedical Applications

PAMAM dendrimers are water-soluble and they are the only type of dendrimer that are mono-dispersed. In these dendrimers charge denseness is high and the surface of molecules limits this charge. The synthesis of PAMAM can be carried out due to the need for a cationic or anionic surface charge. Full generations such as 1, 2, have cationic amine surface charge; while half generations such as 1.5, 2.5. etc., have anionic carboxylic acid groups at the surface (Figure 1.14) (Pan et al. 2005).

Masking the cationic charge of dendrimers and converting them into biocompatible and less toxic dendrimers surface engineering is a rewarding strategy (Yang et al. 2012). PEGylation, folate, acetylation, peptide, and carbohydrate conjugation or by introducing anionic charge such as half-generation dendrimers are the engineering methods to neutralize the charge of PAMAM dendrimers (Taghavi Pourianazar et al. 2014). Previously Jin et al performed a surface modification with diethylenetriamine by a amidation reaction of PAMAM (G3.5) dendrimer resulting in a 1,2-diaminoethane surface. They depicted that DNA delivery could be increased by appropriate modification and amine surface structure changing of PAMAM dendrimers (Jin et al. 2011).

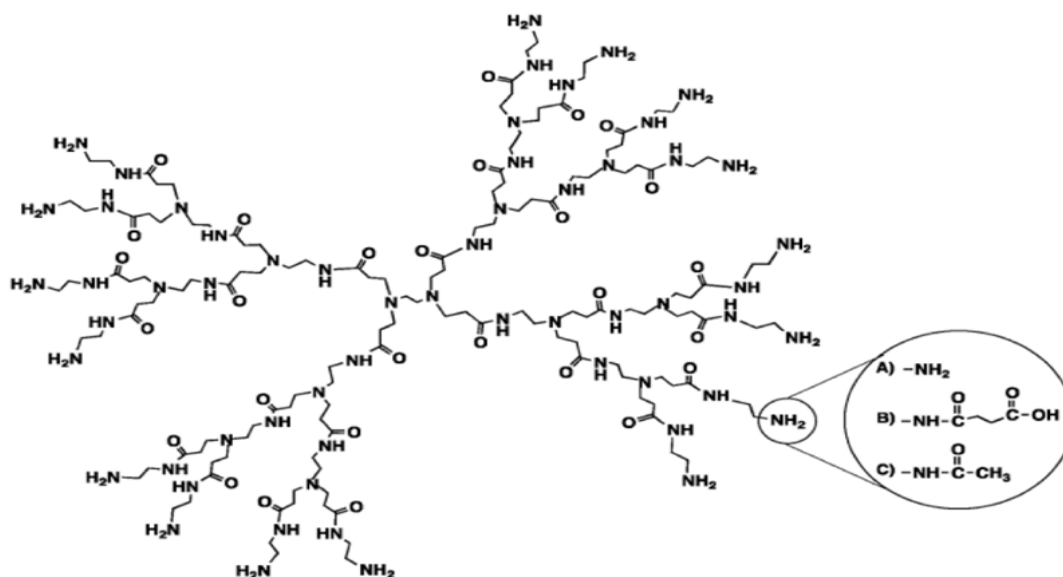


Figure 1.14. chemical structure of G2 PAMAM dendrimer. The representative structure of the surface modified dendrimers: (A) amine-, (B) carboxyl-, and (C) acetyl-terminated dendrimers (Yang et al. 2012).

1.4.1.3 Interaction Between Dendrimer and Drugs

The perfectly branched structures and external surfaces of dendrimers have been assembled a potential sites for encapsulation and interaction with drugs. The loading capacity of the drug extremely depends on the surface group of dendrimers. Large numbers of ionisable groups, which increases two fold with each generation, on the surface of dendrimer provides an opportunity for electrostatic interaction with drugs. Electrostatic interaction can occur between the anionic carboxyl end groups of the dendrimers and the cationic amine groups of the drugs, or vice versa between the cationic amine group of dendrimers and carboxyl or hydroxyl groups of drugs (Figure 2.2 C) (Garg et al. 2011). Hydrolyzable and biodegradable linkage in covalent attachment of drug and surface groups of the dendrimers provide the opportunity for drug release control. Host and guest interaction causes to dramatically an increase in the encapsulation of drug between branches (Garg et al. 2011)(Jain et al. 2010)(Pan et al. 2005).

1.4.2 Chitosan for Surface Coating of Magnetic Nanoparticles

Recently, there has been an increasing attention to use nanoparticles for drug deliveries particularly in cancer treatment. Tumor-specific targeted delivery of anticancer drugs will reduce systemic toxicity and, hence, increase the efficacy of the drug and decrease side effects. Among the various drug delivery systems, chitosan has gained considerable attention due to its biocompatibility, biodegradability, and non-toxicity.

Chitosan is a polycationic natural linear polysaccharide which is achieved by partial N-deacetylation of chitin and it plays an important role in controlling the proteins, peptides and release of drugs. The solubility and cationic character on one side, and biodegradability and mucoadhesivity on the other side make chitosan very attractive for biological applications. It has been examined greatly in the pharmaceutical industries for its outstanding potential in the evolution of drug delivery systems. Chitosan has been extensively investigated for biological and medical applications such as drug delivery systems, tissue engineering, wound healing, agricultural industries and magnetic nanoparticles coatings. The degradation products of chitosan are nontoxic, nonimmunogenic, and noncarcinogenic (Ibezim et al. 2011).

The solubility of chitosan salts in water depends on the degree of deacetylation and the pH of the solution. In this regard, highly deacetylated chitosan (85%) is readily soluble in solutions of pH up to 6.5, but as the deacetylation degree decreases, the solubilization becomes more difficult (Cho et al. 2000).

Chitosan promotes cross linkage with sodium tripolyphosphate (TPP) anions to provide an effective mesh work for entrapment of the drugs. To increase the magnetic nanoparticles conjugation efficiency and for targeting the drug or antibodies to the specific tissues, chitosan coated MNPs had been synthesized (Arya et al. 2011).

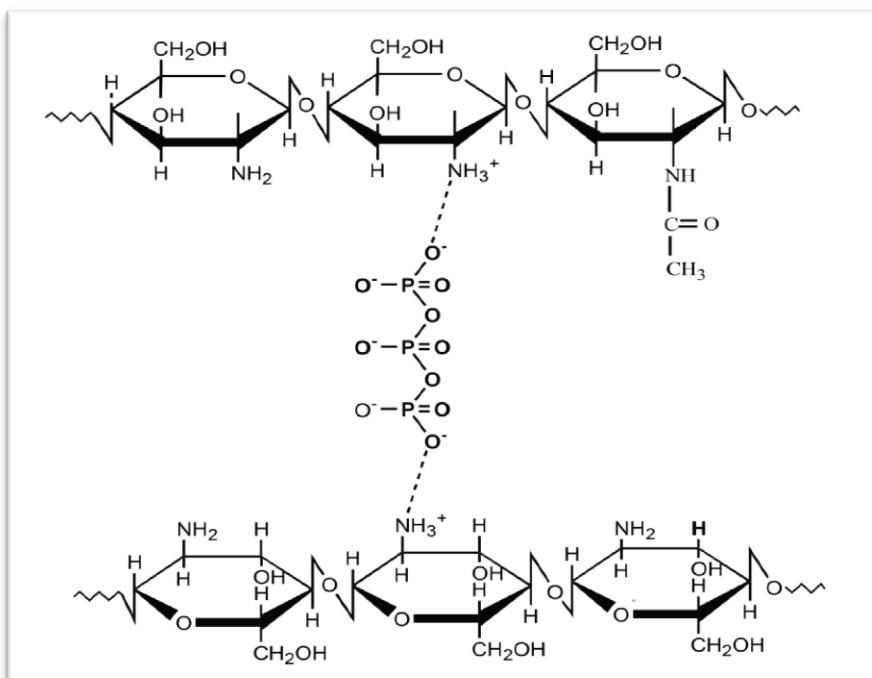


Figure 1.15. The interaction between Chitosan and TPP (Unsoy et al. 2012).

Likeness other polymers, the chitosan molecules contain a number of free amine groups, which allow binding of many agents such as; drugs, antibodies, DNA. Chitosan has been used in binding and delivering DNA to cells for transfection, while chitosan magnetic nanoparticles are unable to bind and deliver DNA (Kievit et al. 2009)(Arya et al. 2011).

Recently synthesized nanocarriers, composed of a magnetite core and chitosan coating was synthesized in this study. The aim of using the magnetic core is to actively target the drug loaded nanoparticles to the tumor site by an externally applied magnetic field.

1.4.3 Polyhydroxybutyrate (PHB) for Surface Coating of Magnetic Nanoparticles

There are many different biodegradable synthetic and natural polymers used for coating of nanoparticle such as dendrimers, chitosan, polyesters such as polylacticacid and polyhydroxybutyrate. In this study polyhydroxybutyrate (PHB) which belongs to Polyhydroxyalkanoates (PHAs) family is used as a coating polymer (Yalcin et al. 2014).

Polyhydroxybutyrate (PHB) is a linear biodegradable biopolymer that has been widely used in biomedical applications. PHB is naturally produced by a variety of microorganisms. In PHB commercially production many cheap substrates such as cane and beet molasses, ethanol, methanol and starch have been used. Nonetheless, it is commonly nontoxic, because it is degraded to end products (CO₂ and H₂O) which are naturally occurring in human body (Chaijamrus et al. 2008)(Larsson et al. 2014).

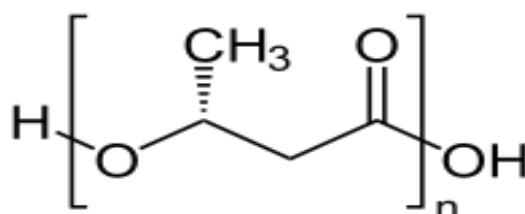


Figure 1.16. Polyhydroxybutyrate (PHB) structure.

PHB is used as a storage polymer in microorganisms due to excess carbon and energy sources and also under the environmental stress conditions such as nutrient, phosphorus, nitrogen and oxygen limitations (Althuri et al. 2013). PHB can be degraded to carbon and energy sources when the sources of limiting nutrient is restored (Choi et al. 1999). PHAs and PHB are beneficial candidates for use in nerve scaffolding and bone tissue engineering and drug delivery systems. They possess all the properties required for these systems (Pidubnyak et al. 2004).

1.5 Aim of the Study

The aim of this study was to obtain an effective targeted delivery system for Gemcitabine by using PAMAM dendrimer, Chitosan and Polyhydroxybutyrate (PHB) coated magnetic nanoparticles (MNPs).

Gemcitabine were conjugated onto different half-generations of synthesized PAMAM dendrimer, chitosan and PHB coated magnetic nanoparticles. The loading efficiency, surface and conjugation characters, release and stability profiles of Gemcitabine loaded magnetic nanoparticles as well as their antiproliferative effect on SKBR-3 and MCF-7 cells were investigated.

CHAPTER 2

MATERIALS AND METHODS

2.1 Materials

Iron (II) chloride tetrahydrate ($\text{FeCl}_2 \cdot 4\text{H}_2\text{O}$), iron (III) chloride hexahydrate ($\text{FeCl}_3 \cdot 6\text{H}_2\text{O}$), 3-aminopropyl trimethoxysilane (APTS) [$\text{NH}_2(\text{CH}_2)_3\text{-Si-(OCH}_3)_3$], ethanol, methanol, methyl acrylate, ethylene di amine, phosphate buffer saline (PBS), dimethylsulfoxide (DMSO), Chitosan (LMW, 85% deacetylated), polyhydroxybutyrate (PHB), and Gemcitabine hydrochloride, were purchased from Sigma-Aldrich (U.S.A).

Sodium tripolyphosphate (TPP, Sigma-Aldrich Chemie GmbH, Germany) was provided by Assoc. Prof. Dr. Ayşen TEZCANER's Lab.

Acetic acid (CH_3COOH), ammonium hydroxide solution (32%, NH_4OH) was obtained from Merck (Germany). Nitrogen gas was provided from Asya Gaz (Turkey).

Trypsin-EDTA, gentamycin sulphate, trypan blue and XTT cell proliferation kit were purchased from Biological Industries, Israel.

MCF-7 cells were provided by SAP Institute (Ankara, Turkey) and SKBR-3 was donated by Assoc. Prof. Dr. Rengul Atalay, Bilkent University. The cells were grown in RPMI 1640 medium supplemented with 10% heat-inactivated fetal bovine serum, 1% L-glutamine, 1% gentamicin (Biological Industries, Israel) and maintained at 37°C in a humidified air atmosphere with 5% CO_2 .

2.2 Methods

2.2.1 Synthesis of PAMAM Coated Magnetic Nano Particles (DcMNPs)

2.2.1.1 Preparation of Bare Magnetic Nano Particles (MNP)

In recent years, many different methods were used to synthesize magnetic nanoparticles (Gupta et al. 2005). Co-precipitation is one of them that was used in this study. Because of spherical shape and small size (10-15 nm) MNPs are mostly used in biomedical applications (Gao et al. 2009)(Khodadust et al. 2013)

Under nitrogen environment and mixing with a mechanical stirrer (Heildolf RZR 2021, Germany), Fe (II) and Fe (III) salts (by 1:2 ratios) were dissolved in 150 ml distilled water and heated until 90°C (Figure 2.1). After 1 hour, ammonia hydroxide solution was added to the system dropwise for the next 2 hours. Obtained black precipitate was washed by distilled water and then by ethanol (Khodadust et al. 2013).

The chemical reaction for MNPs is given below:



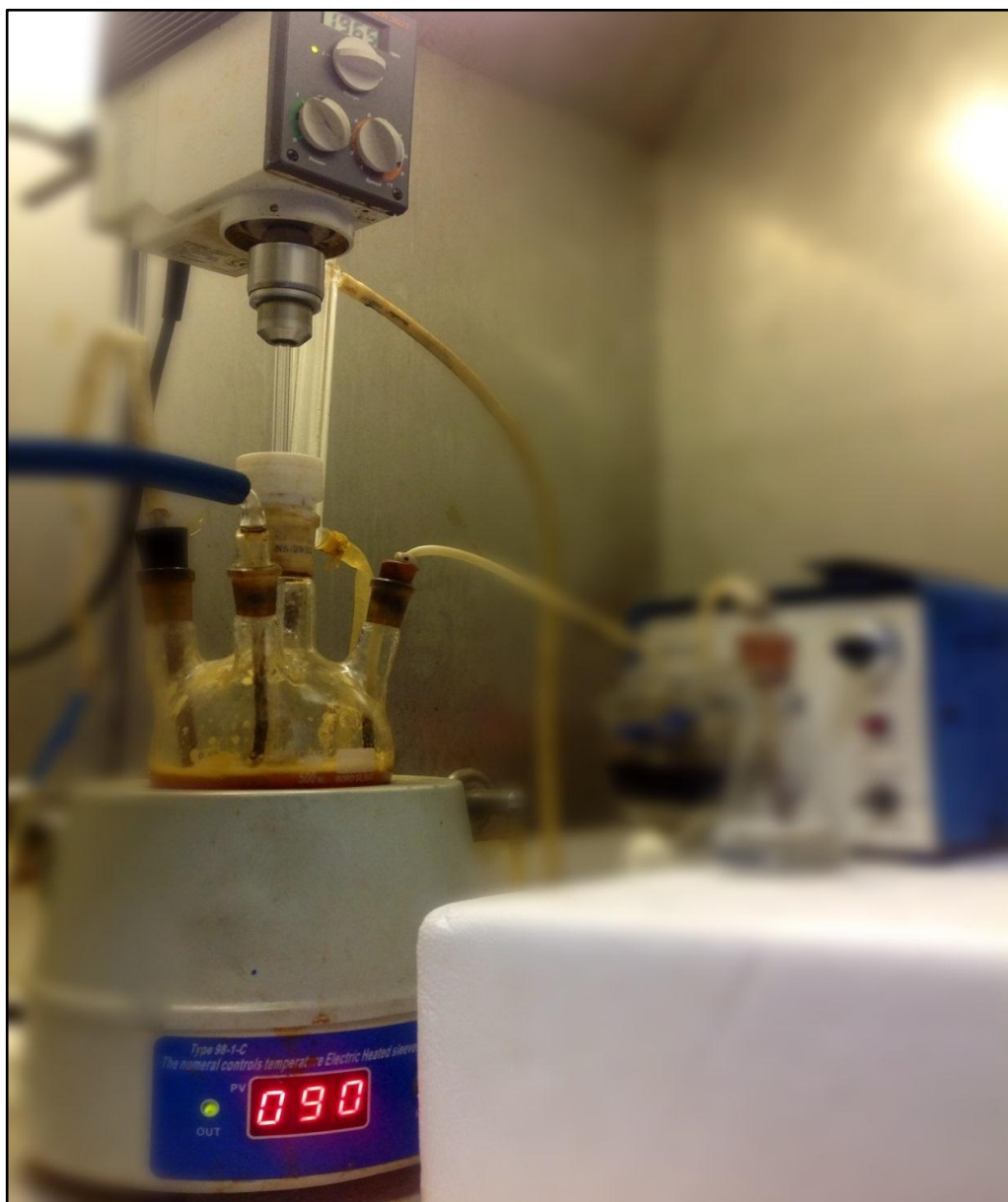


Figure 2.1. The bare MNP experimental synthesis setup. Magnetic iron oxide synthesis in balloon which placed in mantle (90 °C) and stirred by mechanical stirrer (2000 rpm). Cooling, temperature and nitrogen gas probes were attached to fine necked balloon. Ammonia solution pumped by a peristaltic pump within the balloon.

2.2.1.2 Coating of Bare Magnetic Nanoparticles by APTS

The agglomeration was the main problem of bare nanoparticles due to Van der Waals forces between the nanoparticles. For preventing this problem, bare MNPs were coated with 3-aminopropyl trimethoxysilane (APTS). For obtaining APTS coated G0 MNPs, 10 ml 3-aminopropyl trimethoxysilane was added to MNPs with sonication (Bandelin Sonopuls Ultrasonic Homogenizer HD 2200, Berlin, Germany). The process was continued by stirring the solution at 2000 rpm for 15 hours at room temperature. The black precipitate was washed by ethanol several times by the help of magnetic field (Gao et al. 2009)(Khodadust et al. 2013).

Previously characterization of the bare and APTS-modified MNPs were performed in our lab by transmission electron microscopy (TEM), X-ray diffraction (XRD), Fourier transform infrared spectroscopy (FT-IR), dynamic light scattering (DLS), thermal gravimetric analysis (TGA), X-ray photoelectron spectroscopy (XPS), and vibrating sample magnetometer (VSM) analyses (Khodadust et al. 2013).

2.2.1.3 Surface Coating of MNPs with PAMAM Dendrimer

Divergent synthesis was initially applied in the synthesis of PAMAM dendrimers. To be able to synthesize a PAMAM dendrimer, a two-step series should be repeated. The first step produces a half generation, starting with a Michael addition of methyl acrylate which followed by amidation with ethylenediamine to complete the full generation (Taghavi Pourianazar et al. 2014). The first step started by adding methylacrylate methanol solution (20%, v/v) to the G0 DCMNPs, and mixed at room temperature for 7 h by ultrasonic water bath or mechanical stirrer. The obtained G0.5 DcMNPs were separated by the help of magnetic decantation and washed with methanol. The second step for completing the full generation started by adding the ethylenediamine-methanol solution (50%, v/v) and suspension was mixed for additional 3 hours. The obtained G1 DcMNPs were separated by magnetic decantation and washed several times with methanol. The stepwise growth of dendrimers was repeated until the desired numbers of generations were achieved (Gomez et al. 2009)(Yang et al. 2012)(Khodadust et al. 2013). For achieving the half-generation of PAMAM (DcMNPs), after synthesis the desired generation of PAMAM dendrimer, methylacrylate solution was added to particles for additional 7 hours. By this method the end group of PAMAM becomes anionic carboxyl group (Figure 2.2a).

2.2.2 Synthesis of Chitosan Coated Magnetic Nano Particles

Precipitation of Fe(II) and Fe(III) salts in the presence of chitosan and TPP molecules was used to in situ synthesize of Chitosan coated magnetic iron oxide nano particles. Under nitrogen condition with mixing by a mechanical stirrer (Heildolf RZR 2021, Germany), iron salts (1:2 ratios) dissolved in 30 ml of 0.5% chitosan solution, in which 0.15 g chitosan was dissolved in 30 ml of 1% acetic acid and pH was adjusted to 4.8 by NaOH (10 M). 10 ml of 7.5% TPP, used for cross-linking of low molecular weight chitosan and 25 ml NH₄OH (32%), were added slowly to the solution to produce smaller sized chitosan coated magnetic nanoparticles (CSMNPs). The solution was stirred for an additional 1 hour at room temperature. The synthesized CSMNPs were extensively washed with deionized water and methanol for several times and separated by the help of magnetic field (Unsoy et al. 2012).

2.2.3 Synthesis of PHB Coated Magnetic Nano Particles

Previously Xiong et al. synthesized PHB coated MNPs by the co-precipitation method (Xiong et al. 2010). Under nitrogen (N₂) gas flow and stirring at 2500 rpm, iron oxide II (1.34 g) and iron (III) (3.40 g) salts were dissolved in 30 ml of 1 % PHB solution. Then ammonium hydroxide was added slowly by the help of the peristaltic pump. The solution was stirred for more 2h at room temperature. The colloidal PHB-MNPs were washed with ethanol and then with methanol for several times (Yalçın et al., 2014).

2.2.4 Gemcitabine Loading, Release and Stability on DcMNPs

2.2.4.1 Loading of Gemcitabine on Different Half-Generation of DcMNPs

In this study, G4.5, G5.5, G6.5, G7.5 DcMNPs (2.5 mg/ml) and various amount of Gemcitabine in methanol solution were incubated on rotator (10 rpm with five-second vibration intervals) for 24h at room temperature while being protected from light (Figure. 2.2 c). After the incubation period, Gemcitabine-conjugated DcMNPs were separated by magnetic field and conjugation efficiency was quantified by measuring the absorbance of the supernatant at 269 nm by a UV spectrophotometer (Multiskan GO, Thermo Scientific). The amount of Gemcitabine was calculated with the help of standard solution. (Equation 2.2) The conjugation of maximum Gemcitabine to G5.5 DcMNPs was confirmed by FT-IR, XPS and Z-potential analysis.

$$\text{Loading efficiency (\%)} = \frac{\text{Calculated drug concentration}}{\text{Theoretical drug concentration}} \times 100 \quad \text{Equation 2.2}$$

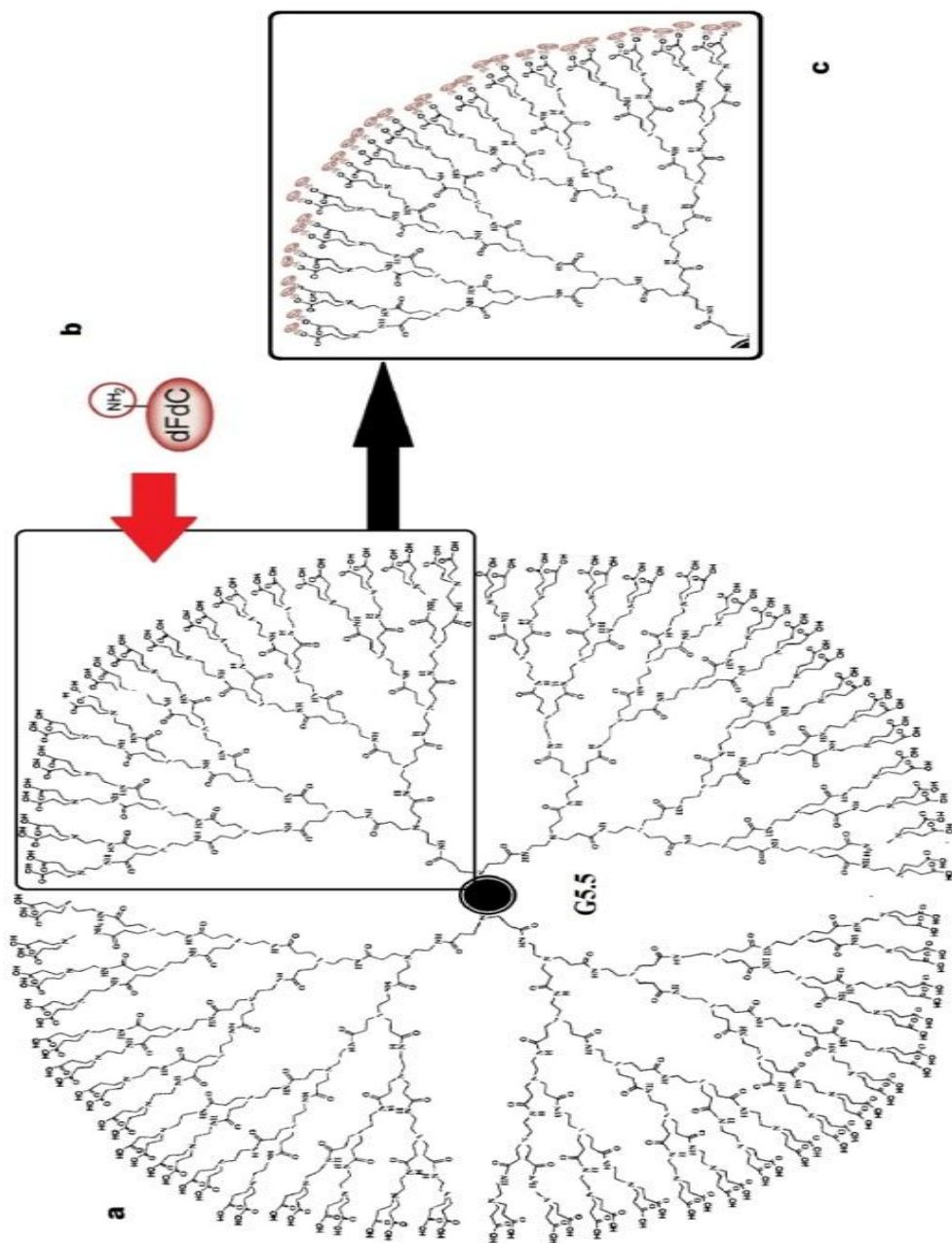


Figure 2.2. (a) G5.5 PAMAM dendrimer magnetic nanoparticle (G5.5 DcMNPs), (b) Gemcitabine (dfdc), (c) G5.5 DcMNPs conjugated by dfdc.

2.2.4.2 Release of Gemcitabine from DcMNPs

The release of Gemcitabine (6.47 - 6.62 $\mu\text{g/ml}$) from G5.5 DcMNPs (2.5 mg/ml) was analyzed in acetate buffer at 4.2 and 5.2 pH value for 24 h. The amount of released Gemcitabine was determined by measuring the absorbance of the supernatant at 269 nm using acetate buffer standard curve (Appendix A. Figure A.4B,C).

2.2.4.3 Stability of Gemcitabine on DcMNPs

The stability of G5.5 DcMNPs loaded with the highest amounts of Gemcitabine (6.57 $\mu\text{g/ml}$) was perused in PBS buffer (pH 7.2) up to 6 weeks at 37°C. The release of Gemcitabine from magnetic nanoparticles in PBS buffer was determined by spectrophotometric measurements at 269 nm by using standard curve constructed with different concentrations of Gemcitabine in PBS buffer (Appendix A. Figure A.4, A).

2.2.5 Gemcitabine Loading, Release property and Stability of CSMNPs

2.2.5.1 Loading of Gemcitabine on CSMNPs

Gemcitabine loading on CSMNPs (2.5 mg/ml) was performed in methanol with different drug concentrations in order to obtain the highest drug loading efficiency. The mixture of CSMNPs and Gemcitabine in methanol was rotated (Biosan Multi RS-60 Rotator) at 90 rpm with 5 seconds vibration intervals for 24 hours in the light protected tubes at room temperature. After 24h, Gemcitabine conjugated CSMNPs was quantified by determining drug concentration in the supernatant. The amount of Gemcitabine was found by measuring absorbance at 269 nm and determining the concentration with the help standard solution (Equation 2.2). The loading of Gemcitabine to CSMNPs was confirmed by FT-IR, XPS and Z-potential analyses.

2.2.5.2 Release of Gemcitabine from CSMNPs

The release of Gemcitabine (8.65 $\mu\text{g/ml}$) from CSMNPs (2.5 mg/ml) was studied in acetate buffers at pH 4.2 and 5.2 for 24 h. The amount of released Gemcitabine was determined by measuring the absorbance of the supernatant at 269 nm by using the calibration curve constricted (Appendix A. Figure A.4.B,C).

2.2.5.3 Stability of Gemcitabine on CSMNPs

The stability of CSMNPs loaded with the highest amounts of Gemcitabine (9.1 $\mu\text{g/ml}$) was determined in PBS buffer (pH 7.2) up to 72h at 37°C. The release of Gemcitabine from nanoparticles in PBS buffer was measured by a UV spectrophotometer at 269 nm.

2.2.6 Gemcitabine Loading, Release and Stability on PHB-MNPs

2.2.6.1 Loading of Gemcitabine on PHB

The different drug concentrations of Gemcitabine were conjugated on PHB-MNPs (2.5 mg/ml) in methanol for 24h to obtain the highest drug loading efficiency. The solution was rotated (Biosan Multi RS-60 Rotator) at 90 rpm with 5 seconds vibration intervals in the light protected tubes at room temperature. Gemcitabine conjugated PHB-MNPs was quantified by measuring the absorbance of supernatant at 269 nm. The amount of Gemcitabine was calculated with the help of standard solution (Equation 2.2). The loading of maximum Gemcitabine to PHB-MNPs was confirmed by FT-IR, XPS and Z-potential analyses.

2.2.6.2 Release of Gemcitabine from PHB-MNPs

The release of Gemcitabine (6.5 $\mu\text{g/ml}$) from PHB-MNPs (2.5 mg/ml) was studied in acetate buffer at 4.2 pH value for 24 h. The amount of released Gemcitabine was determined by measuring the absorbance of the supernatant at 269 nm.

2.2.6.3 Stability of Gemcitabine on PHB-MNPs

The stability of PHB-MNPs loaded with the highest amounts of Gemcitabine (6.4 $\mu\text{g/ml}$) was determined in PBS buffer (pH 7.2) up to 36h at 37°C. The release of Gemcitabine from nanoparticles in PBS buffer was determined by measuring absorbance at 269 nm.

2.2.7 Chemical Characterizations

Previously, Khodadust et al. performed the characterizations of full generation dendrimer coated MNPs (Khodadust et al. 2013). Characterization and comparison of half-generation PAMAM dendrimers with full generation and Gemcitabine conjugated half-generation DcMNPs were done by Fourier Transform Infrared (FT-IR) Spectroscopy, Transmission Electron Microscopy (TEM), X-Ray Diffraction spectroscopy (XPS) and Zeta-Potential analyses.

The same analyses were also performed for chitosan coated magnetic nanoparticles (DCMNPs) and PHB coated magnetic nanoparticles before and after loadings by Gemcitabine, too. The Fourier Transform Infrared Spectroscopy analyses were performed in Hacettepe University and METU Central Laboratory. The Transmission Electron Microscopy, X-Ray Diffraction spectroscopy and Zeta-Potential measurements were carried in METU Central Laboratory.

2.2.8 Cell Culture

2.2.8.1 Cell Lines and Culture Conditions

MCF-7 and SKBR-3 human breast cancer cell lines were grown in RPMI 1640 medium (Biochrom AG, Berlin), supplemented with 10% (v/v) fetal bovine serum (FBS) (Biochrom AG, Berlin) and 10% (w/v) gentamicin (Biological Industries, Israel).

Cells were cultured under sterile laminar flow (BioAir, Italy), cells were seeded in cell culture dishes and were passaged by using trypsin-EDTA (1 ml for 75cm² culture flasks) when cell growth reached 80% confluency. The cells were passaged at a 1:3 ratio and incubated at 37°C in a humidified atmosphere with 5% CO₂, in incubator (Heraeus, Germany).

2.2.8.2 Cell Proliferation Assay with XTT Reagent

Cytotoxicity of bare DcMNPs, CSMNPs, PHB-MNPs and Gemcitabine conjugated nanoparticles was determined by using XTT cell proliferation assay kit. SKBR-3 and MCF-7 (6x10³ cells/well) cells were seeded to 96 well plates at 37°C. Cells that were exposed to free MNPs, Gemcitabine and Gemcitabine conjugated nanoparticles were incubated for 72 h at 37°C. Viability of cells was determined by XTT assay and 50% viability of treated cells was calculated from the relative viability curves for which the viability of the untreated control cells was taken as 100%.

CHAPTER 3

RESULTS AND DISCUSSION

3.1 Characterization of Half Generation of PAMAM Magnetic Nano Particles (DcMNPs)

Poly(amidoamine) (PAMAM) dendrimers play an important role in drug delivery systems, because of their special three-dimensional architecture, presence of internal cavities and multifunctional surface (Jain et al. 2010). Their great monodispersity, bioavailability and biocompatibility make PAMAM dendrimers excellent candidates for drug delivery (Taghavi Pourianazar et al. 2014). Despite these advantages, it is generally necessary to modify the surface amine groups of these dendrimers to avoid the toxicity and liver accumulation associated with their polycationic surfaces (Gillies et al. 2005). For masking the cationic charge of dendrimers and convert them into biocompatible and less toxic dendrimers surface engineering is a rewarding strategy (Yang et al. 2012). Previously, Jin et al. performed a surface modification with diethylenetriamine by an amidation reaction of PAMAM (G3.5) dendrimer resulting in a 1, 2- diaminoethane surface. They depicted that DNA delivery could be increased by appropriate modification and amine surface structure changing of PAMAM dendrimers (Figure 3.1) (Jin et al. 2011).

Recently, characterizations of full generation dendrimer coated MNPs were performed (Khodadust et al. 2013). Amine end group of full generation PAMAM prevented the conjugation of our drug, therefore half generation of PAMAM dendrimers having free carboxyl group were used in this study. Loading studies demonstrated that generation 5.5 had the best conjugation efficiency. Therefore generation 5.5 DcMNPs were used for further analysis in this study.

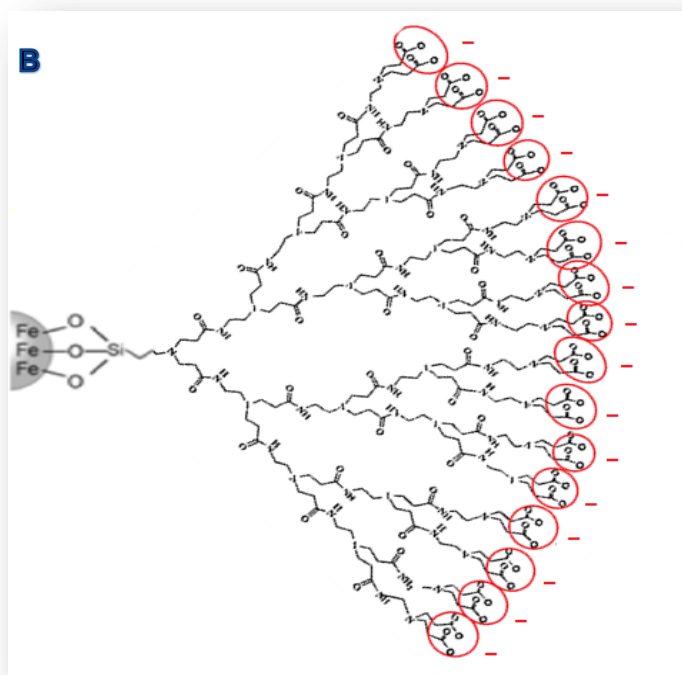
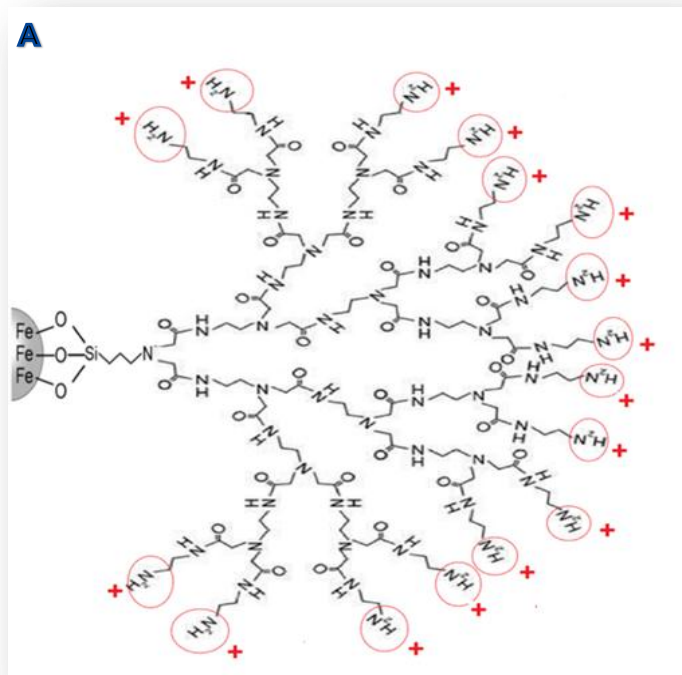


Figure 3.1. (A) Full generation PAMAM dendrimer, (B) Half generation PAMAM dendrimer.

3.1.1 Analysis of PAMAM DcMNPs

3.1.1.1 TEM Analyses

The morphology and size of synthesized full and half generations of PAMAM magnetic nanoparticles have been examined with TEM in this study. TEM images of G5DcMNPs and G5.5 DcMNPs are shown in Figure 3.2. However, there were no significant differences between the sizes and shapes of full and half generations of dendrimeric nanoparticles. The average diameters of G5DcMNPs and G5.5 DcMNPs were around 12 nm and almost 13-14 nm, respectively.

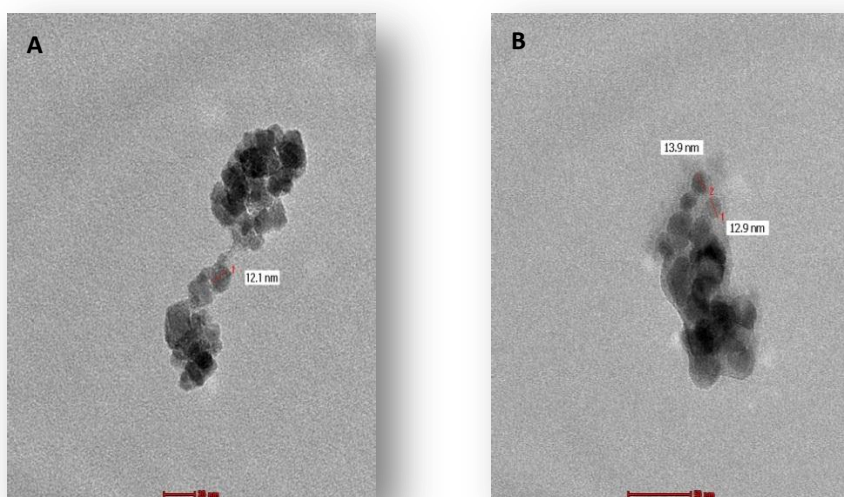


Figure 3.2. (A) TEM images of G5DcMNPs, (B) G5.5 DcMNPs.

3.1.1.2 Zeta (ζ) Potential Analyses

Zeta potential supplies a measure of the electrostatic potential at the surface of nanoparticles. Nanoparticle surface charge and size can activate platelets and induce platelet aggregation *in vitro*. Many researches indicated platelet aggregation just only done by large, cationic dendrimers (Dobrovolskaia et al. 2013).

The zeta potential values of DcMNPs were measured at pH 7.2. Full generation DcMNPs were positively charged with a surface potential greater than +19 mV due to the presence of protonated amino groups of dendrimer on particle surface. On the other hand, G5.5 DcMNPs had negative zeta potential (-10 mV) due to the presence of terminal carboxyl groups (Figure 3.3).

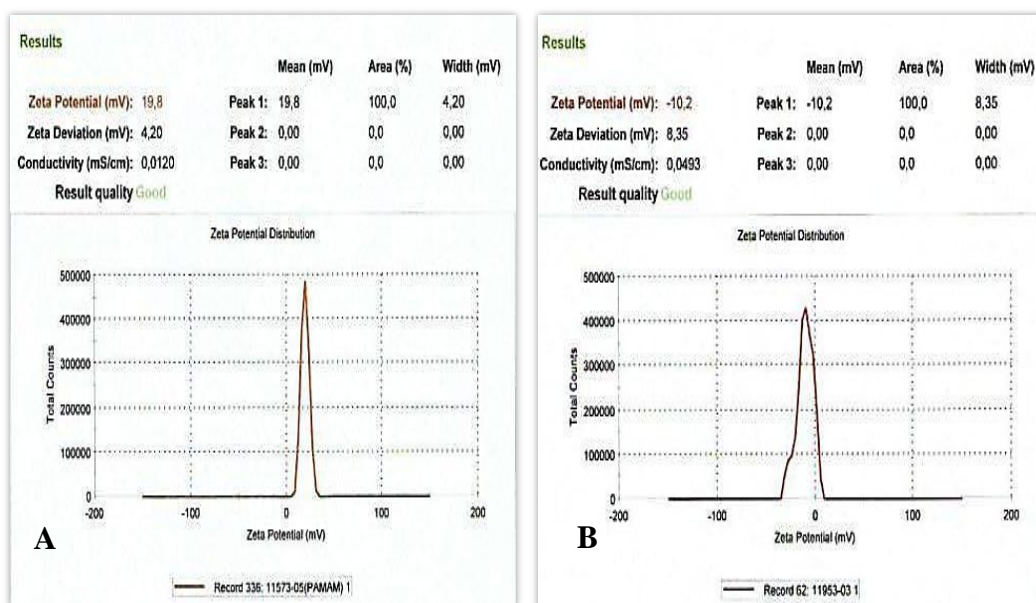


Figure 3.3. Zeta (ζ) Potential of G5 DcMNPs (A) and G5.5 DcMNPs (B).

Previously, Dobrovolskaia et al. showed that the hydroxyl and carboxyl terminated PAMAM dendrimers and also small amine terminated (cationic) dendrimers (G3) did not result in aggregation of human platelets *in vitro*. However, large cationic PAMAM dendrimers (G4, G5 and G6) resulted in platelet aggregation in human plasma and caused lysis of red blood cells. There was significant difference between 3rd generation PAMAM dendrimer and larger dendrimers. However, no clear difference was observed between G4, G5 and G6 dendrimers for platelet aggregation. These results demonstrated that both surface charge and particle size are important physicochemical properties which determine dendrimer interaction with human platelets (Dobrovolskaia et al. 2013).

3.1.1.3 Fourier Transform-Infrared Spectroscopy (FT-IR)

The coatings of DcMNPs with a PAMAM dendrimer layer of G5.5 and G5 were validated by FT-IR. Significant difference was seen at 1650-1750 cm^{-1} and 2800-3000 cm^{-1} between G5 DcMNPs and G5.5 DcMNPs (Figure 3.4). The COOH bonds related to G5.5 DcMNPs can be seen at 1730 cm^{-1} . Vibrations of $-\text{CO}-\text{NH}-$ bonds for G5 DcMNPs were observed at 1450, 1490, 1530, and 1620 cm^{-1} , which were not seen in G5.5 DcMNPs. Also the vibration after 3000 cm^{-1} that mostly belongs to N-H bonds were not observed for G5.5 DcMNPs.

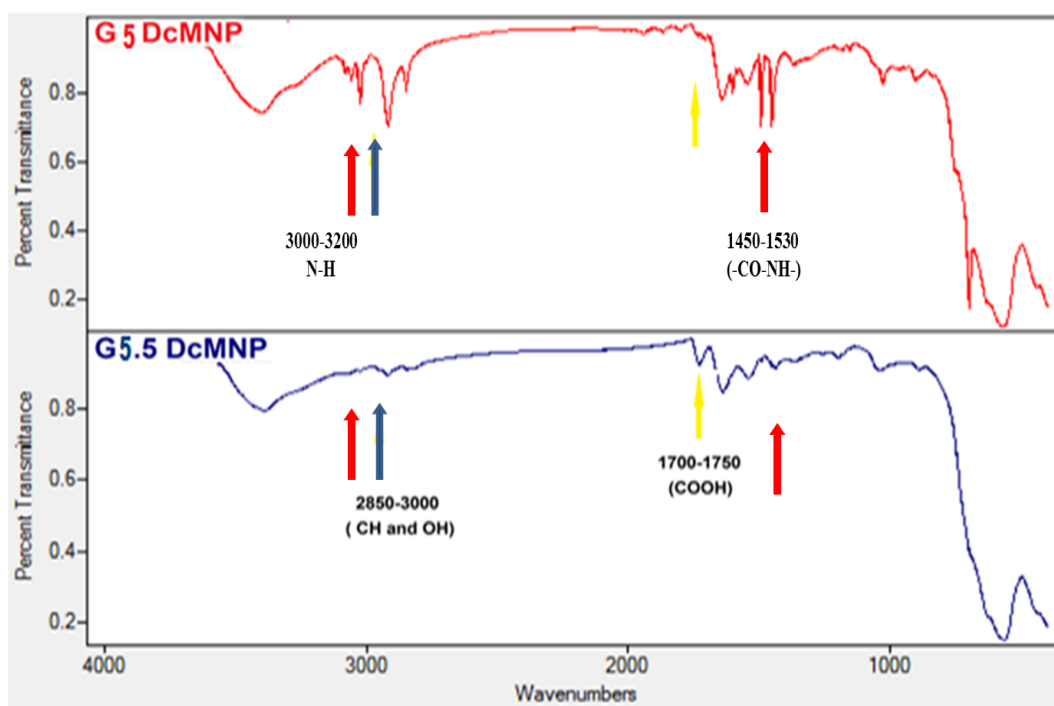


Figure 3.4. FT-IR spectra of the G5 DcMNPs and G5.5 DcMNPs.

3.2 Gemcitabine Loading Efficiencies on various half generation of DcMNPs

Covalent conjugation of drug molecules to PAMAM dendrimer surface due to multivalency of PAMAM is an alternative access to the development of PAMAM dendrimer as anticancer drug carriers (Garg et al. 2011). The direct coupling of the drugs with terminal functional groups of PAMAM dendrimer which occurs via electrostatic or covalent bonds is useful for controlling spatial and temporal release of the attached drugs.

The interaction of hydrophobic drug and the non-polar PAMAM via hydrophobic bonds and release control of these encapsulated molecules in an aqueous environment is passively done by non-covalent interactions including hydrophobic forces, hydrogen bonding, steric hindrance, and electrostatic interactions. It seems possible by using different generations of dendrimers or by changing the coupling conditions (Taghavi Pourianazar et al. 2014).

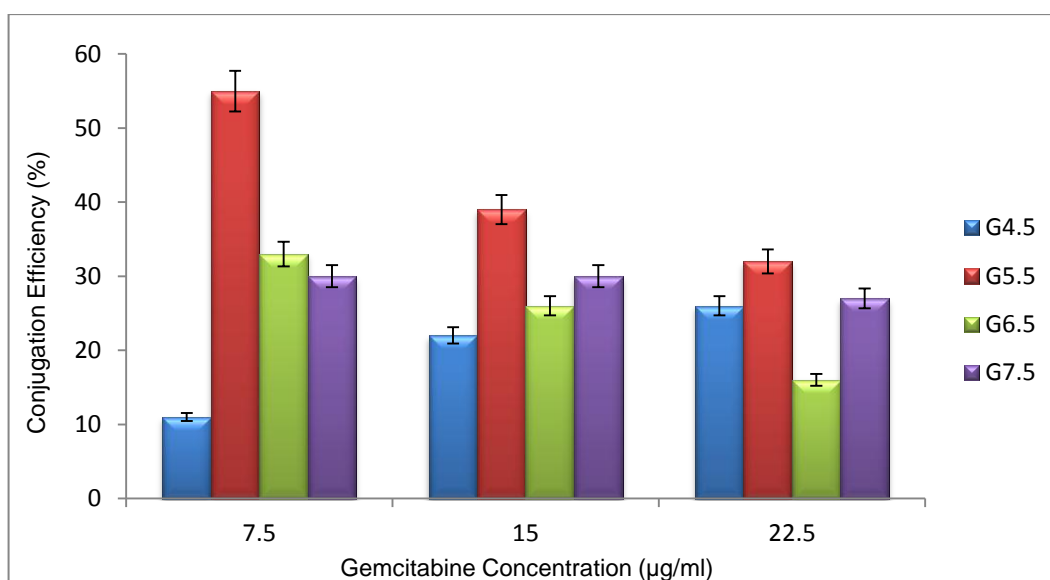


Figure 3.5. Loading efficiencies of Gemcitabine conjugated to different half-generations for DcMNPs. The data are represented as the mean \pm SEM (n = 3).

Loading efficiencies were tested in methanol with different drug concentrations and different half generations (4.5, 5.5, 6.5, and 7.5) of DcMNPs (2.5 mg/ml). The loading efficiencies of 7.5, 15 and 22.5 $\mu\text{g/ml}$ Gemcitabine were conjugated 55%, 39% and 32% in methanol to G5.5 DcMNPs, respectively (Figure 3.5). The highest and most efficient drug conjugation concentration was obtained for 22.5 $\mu\text{g/ml}$ with generation 5.5 which is around 24 μM (Table 3.1).

Conformation of the conjugation of Gemcitabine to G5.5 PAMAM DcMNPs was done by TEM, Zeta (ζ) potential, FT-IR and XPS analyses.

Table 3.1. Loaded amounts of Gemcitabine to 2.5 mg/ml G5.5 DcMNPs using different initial drug loading concentrations.

Gemcitabine concentration ($\mu\text{g/ml}$)	7.5 $\mu\text{g/ml}$	15 $\mu\text{g/ml}$	22.5 $\mu\text{g/ml}$
Loaded amount of Gemcitabine (μg)	4.1 μg	5.9 μg	7.2 μg
Loaded amount of Gemcitabine (μM)	14 μM	19.5 μM	24 μM

In our initial attempts, we tried to load Gemcitabine (7.5, 15 and 22.5 $\mu\text{g/ml}$) on 2.5 mg/ml of PAMAM dendrimers (G4-DcMNP and G7-DcMNP) in methanol, PBS, water and TPP. However, Gemcitabine binding was not observed on full generations of (G4 and G7) PAMAM dendrimers. Then, we synthesized and characterized the half-generations of PAMAM DcMNPs (G4.5 up to G7.5) (Appendix A. Table A1).

3.2.1 Characterization of Gemcitabine Loaded G5.5 PAMAM DcMNPs

3.2.1.1 TEM Analyses

TEM images of G5.5 DcMNPs and Gemcitabine conjugated G5.5 DcMNPs (Figure 3.6) show the particle sizes around 12 nm and ~12-14 nm, respectively. There were no remarkable differences between the sizes DcMNPs after conjugation with Gemcitabine.

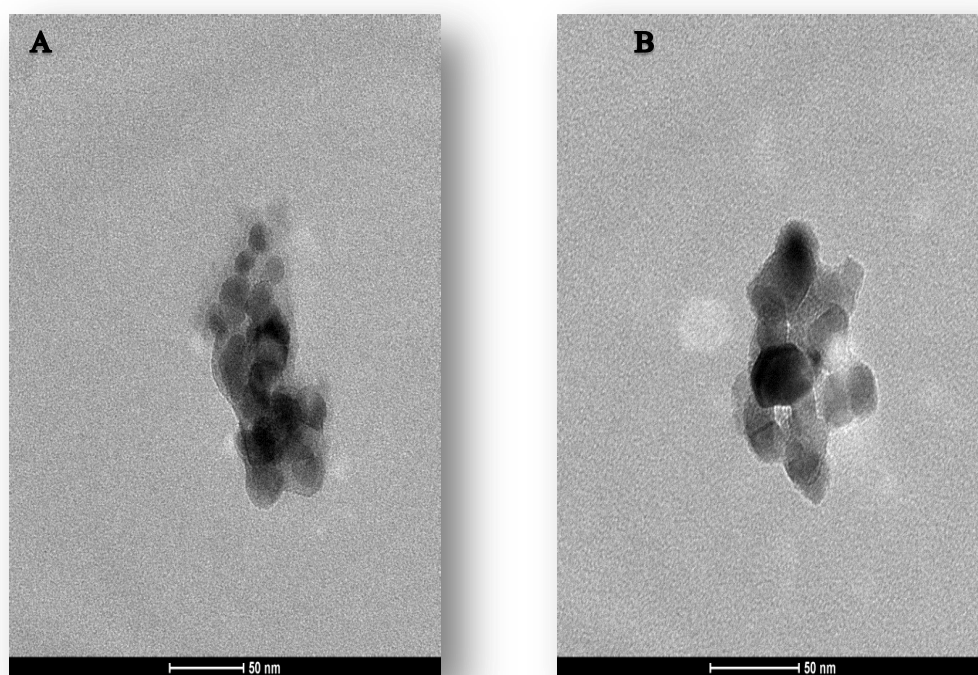


Figure 3.6. TEM images of G5.5 DcMNPs (A) and Gemcitabine conjugated G5.5 DcMNPs (B).

3.2.1.2 X-Ray Photoelectron (XPS) Analyses

XPS was used to examine shell structure of the synthesized product because core electron lines of ferrous and ferric ions can both be detectable and distinguishable in XPS.

Figure 3.7 shows representative XPS spectrum of the DcMNPs and Gemcitabine conjugated DcMNPs. The peaks obtained upon XPS analysis belong to C 1s (286 eV), N 1s (400 eV), O 1s (531 eV), and Fe 2p (721 eV). The N1s band of DcMNPs at 400 eV is assigned to amino groups ($-\text{NH}_2$). There was an increase in the oxygen (O1s) and nitrogen (N1s) contents in Gemcitabine conjugated DcMNPs.

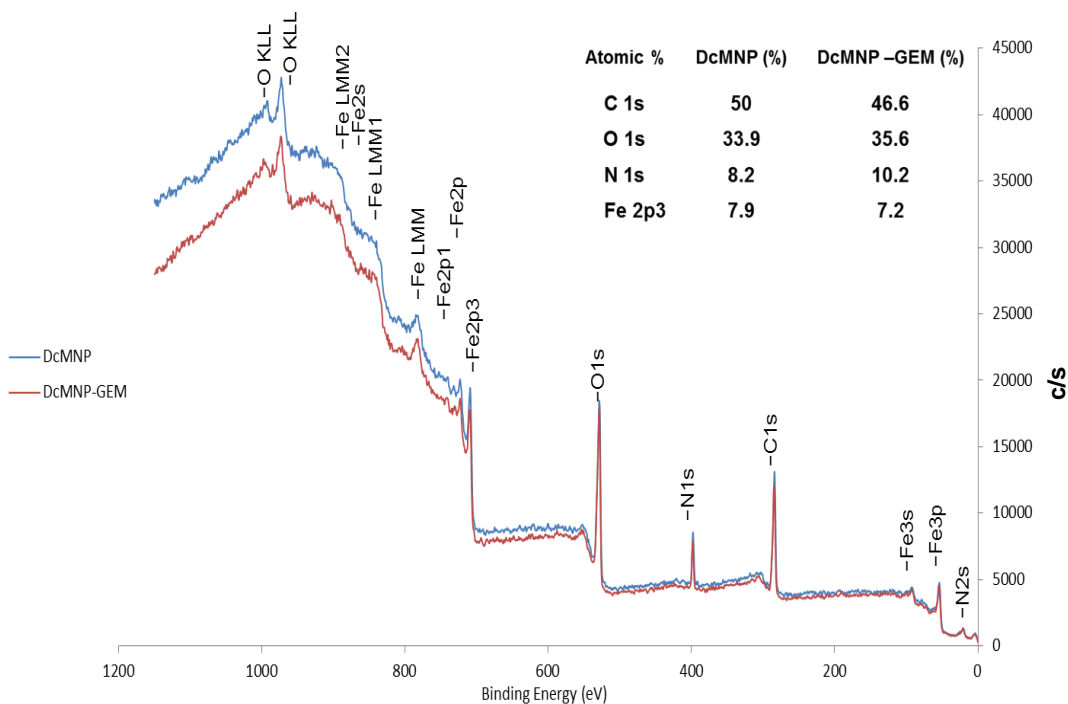


Figure 3.7. XPS spectra of G5.5 DcMNPs, and Gemcitabine conjugated G5.5 DcMNPs.

The fluorine atom was observed in XPS specific spectra analysis between 650-700 eV binding energy and under 4000 c/s of Gemcitabine conjugated DcMNPs (Figure 3.8). These results demonstrated that the Gemcitabine was conjugated successfully to G5.5 PAMAM dendrimer coating magnetic nanoparticles.

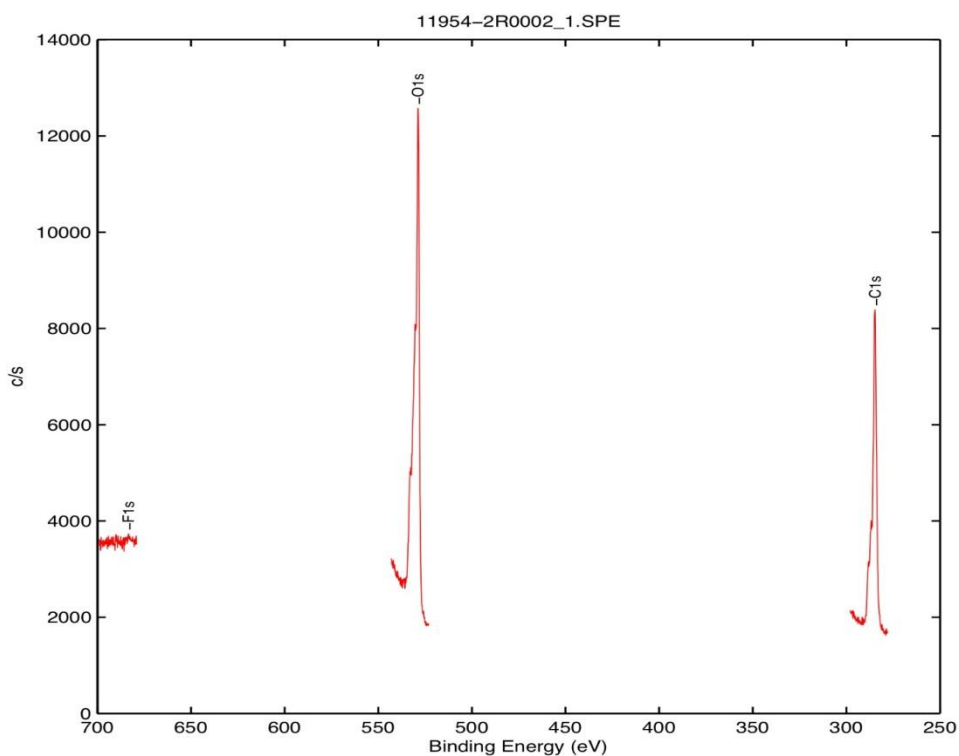


Figure 3.8. XPS particular Fluorine analyses of Gemcitabine conjugated DcMNPs.

3.2.1.3 Fourier Transform-Infrared spectroscopy (FT-IR)

In FT-IR, Gemcitabine absorption bands at 1280 cm^{-1} and 1220 cm^{-1} belong to C-N stretching and vibration 1450 cm^{-1} and 1540 cm^{-1} is due to NH bonds. Furthermore, peaks at 1660 cm^{-1} and 1710 cm^{-1} show the presence of C-C and C-O groups, respectively. The peak at $3200\text{--}3400\text{ cm}^{-1}$ shows stretching vibration of OH and band at 3320 cm^{-1} which is due to stretching vibration of NH group (Figure 3.9).

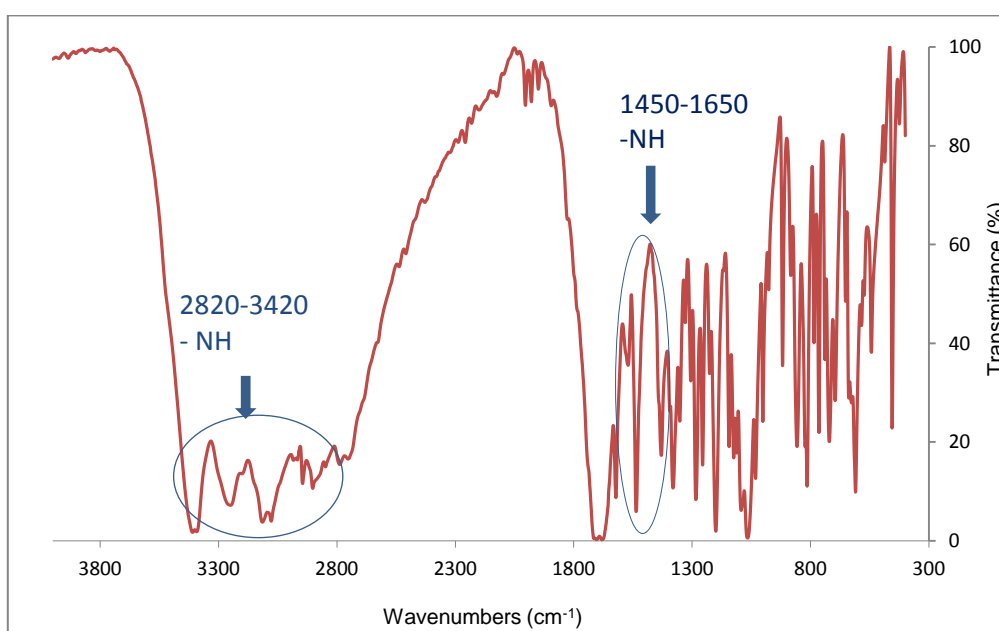


Figure 3.9. Gemcitabine FT-IR spectra.

In the case of the absorption values of G5.5-Gemcitabine solution there was a shift in the absorption of NH group. Band at 3320 cm^{-1} broadened and shifted to higher wavelength at 3510 cm^{-1} which caused by the interaction of DcMNPs and NH group of drug molecule (Figure 3.10). These peaks have also been observed in the spectrum of Gemcitabine loaded DcMNPs as shifted to $1697\text{--}1835\text{ cm}^{-1}$ (C=O) and 1616 cm^{-1} (NH_2).

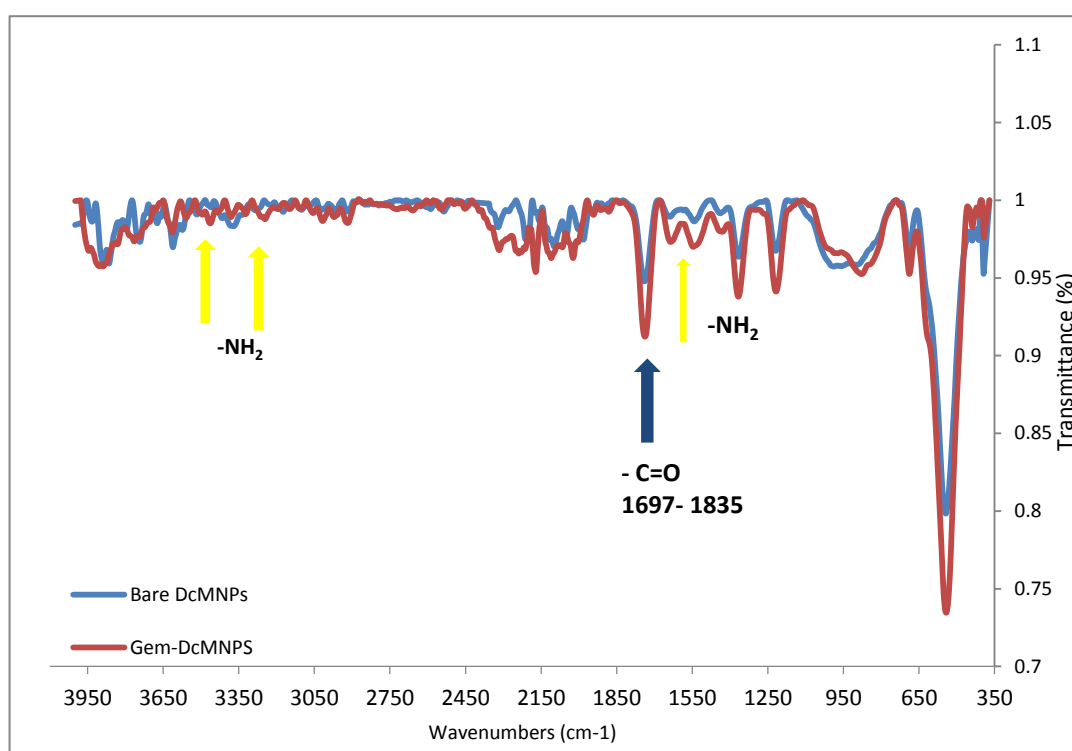


Figure 3.10. FT-IR spectra of (A) Gemcitabine conjugated G5.5 dendrimer coated magnetic nanoparticles, (B) G5.5 dendrimer-modified magnetic nanoparticles.

3.2.1.4 Zeta (ζ) Potential Analyses

The zeta potential of G5.5 DcMNPs in aqueous dispersion was determined to be about -10.2 mV. On the other hand, the zeta potential of Gemcitabine conjugated G5.5 DcMNPs was slightly negative (-4.85 mV) (Figure 3.11).

This results support our hypothesis that Gemcitabine conjugation was achieved at the negative carboxylic groups of the nanoparticles.

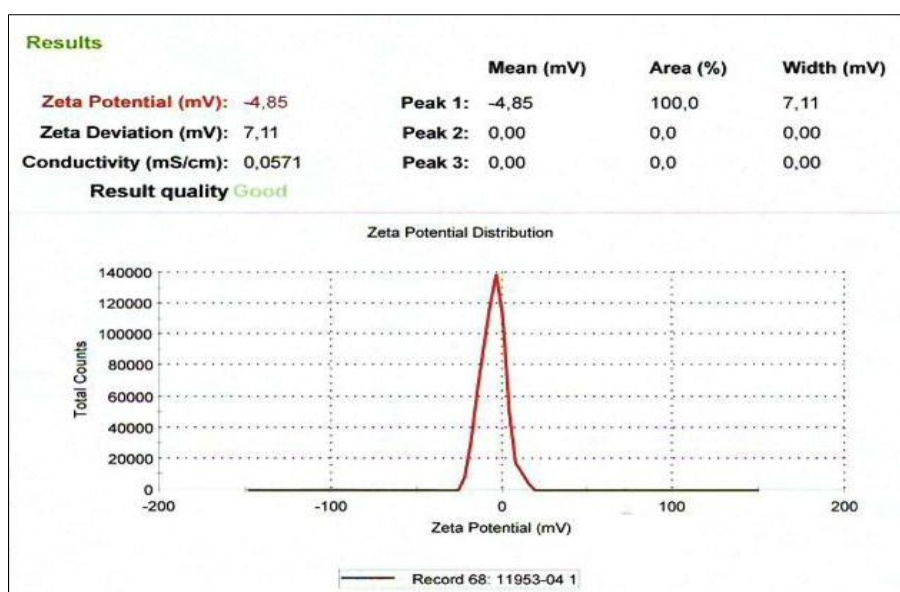


Figure 3.11. Zeta (ζ) potential graphs of Gemcitabine conjugated to G5.5 DcMNPs.

3.2.2 Release and Stability Efficiencies of Gemcitabine from G5.5 PAMAM DcMNPs

3.2.2.1 Release Profiles

Gemcitabine release studies were performed in acetate buffer at pH 4.2 and 5.2 and the amount of drug release was determined using calibration curves constructed with known concentrations of Gemcitabine in acetate buffer at relevant pH (Appendix A. Figure A.4 (B),(C)).

The release profiles of the drug from DcMNPs at pH 4.2 and pH 5.2 are given in Figure 3.12. The release studies were continued up to 24 h. The entire drug (100%) was released within first 15 h at pH 4.2, and nearly 75% of the drug was released at pH 5.2. Gemcitabine release was higher at pH 4.2 compared to pH 5.2. Electrostatic interactions between protonated amino residues on Gemcitabine and anionic groups on nanoparticles are responsible for the surface interactions involved in the burst release (Khaira et al., 2014).

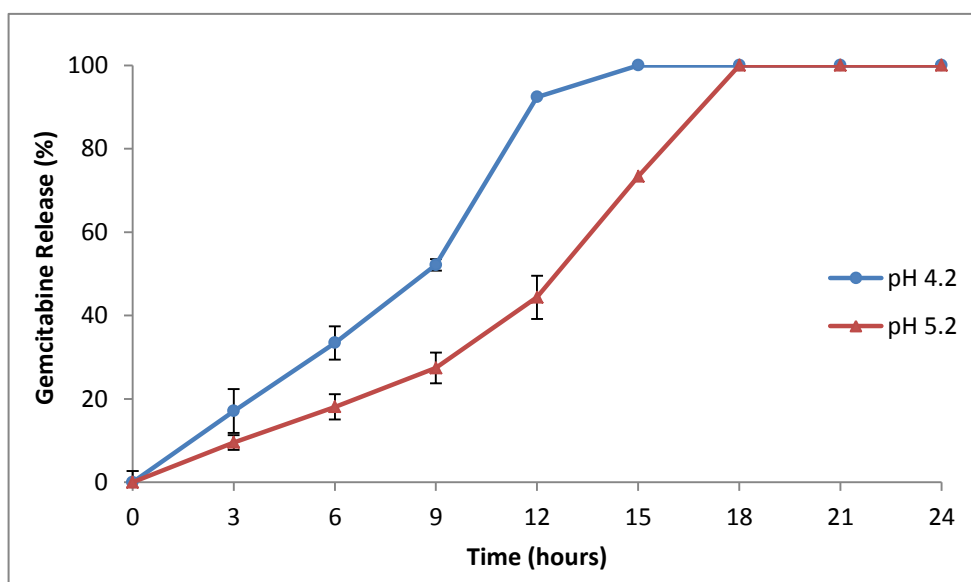


Figure 3.12. Gemcitabine release profile of DcMNPs at pH 4.2 and pH 5.2. The data are represented as the mean \pm SEM (n = 3).

It was shown Gemcitabine release was higher at pH 4.2 compared to pH 5.2. As the pH decreased, the drug release increased. Then, the drug is expected to be released at the targeted cancer cells, because the pH of tumor tissue and endosomes are acidic. Burst release of Gemcitabine from nanoparticles at initial stage will occur. Nearly the whole drug was released within first 15 h from all nanoparticles in pH 4.2.

3.2.2.2 Stability Efficiencies

The stability of Gemcitabine loaded nanoparticles was evaluated up to 6 weeks in PBS (pH 7.2) at 37°C by the help of standard curve (Appendix A. Figure A.4,A), which mimics the physiological conditions (Figure 3.13). Results showed that the stability of Gemcitabine loaded G5.5 DcMNPs were around 94 % at 37°C.

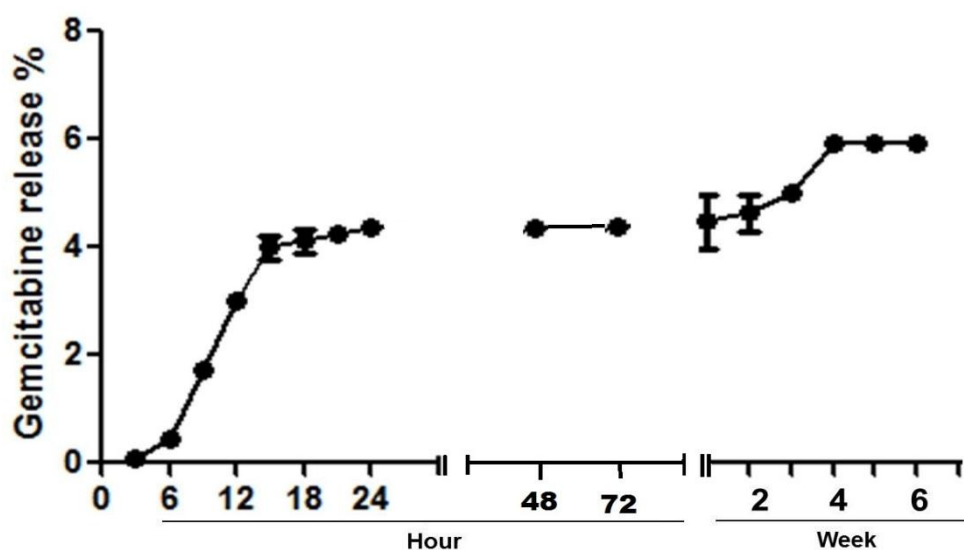


Figure 3.13. Gemcitabine release of G5.5 DcMNPs in PBS (pH 7.2) results for stability test. The data are represented as the mean \pm SEM (n = 3).

The results indicated that only 6% of Gemcitabine drug content was released after 6 weeks showing that DcMNPs were stable at 37°C in PBS buffer. This is a desirable property, which provides an advantage in the storage of Gemcitabine conjugated DcMNPs.

3.2.3 *In vitro* Cytotoxicity Studies of Bare and Gemcitabine Conjugated G5.5 PAMAM DcMNPs on SKBR-3 and MCF-7 Cell Lines

Cytotoxicities of G5.5 DcMNPs, free Gemcitabine and Gemcitabine conjugated G5.5 DcMNPs were investigated by XTT cell proliferation assay using SKBR-3 and MCF-7 breast cancer cell lines. MCF-7 and SKBR-7 cells were treated with bare G5.5 PAMAM dendrimers for 72 hours in 96- well plates. After incubation period, cell viability was determined for each cell type.

Previously, Khodadust et al. (2013) reported empty G4DcMNPs as significantly cytotoxic at concentrations of more than 250 $\mu\text{g/ml}$ (Khodadust et al. 2013). Our results demonstrated that the bare half generation PAMAM dendrimers have no cytotoxicity on SKBR-3 and MCF-7 cell lines over 250 $\mu\text{g/ml}$ concentration.

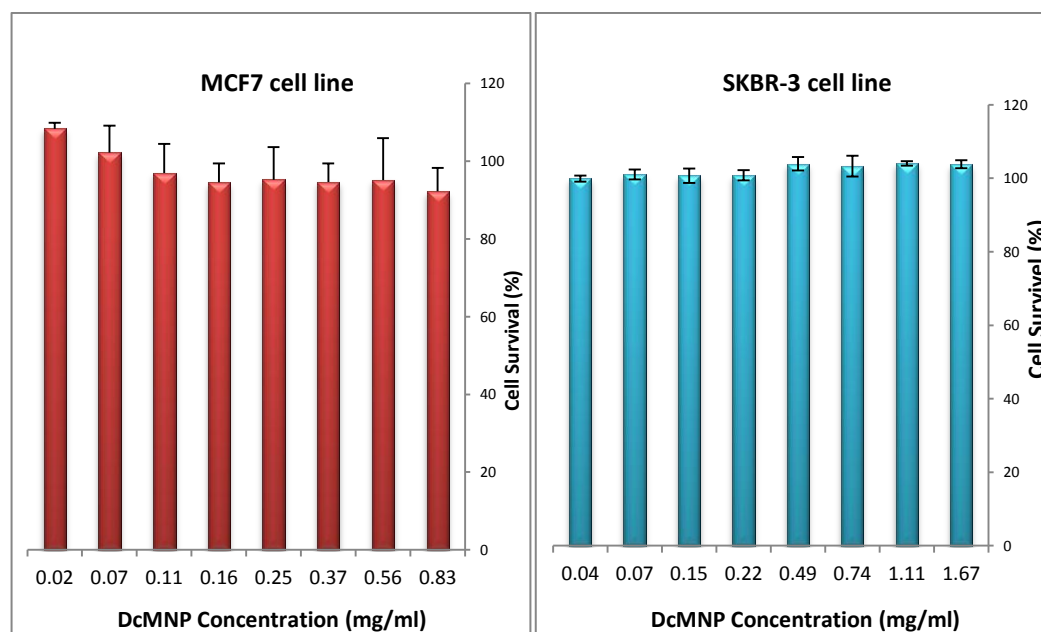


Figure 3.14. Cytotoxicity of G5.5 DcMNPs on MCF-7 and SKBR-3 cell lines. The data are represented the mean \pm SEM (n = 2)

Survival rates of G5.5 DcMNPs indicated that there was no significant cytotoxic effect of the nanoparticles on SKBR-3 and MCF-7 cells up to 1.67 mg/ml and 0.83 mg/ml concentrations, respectively (Figure 3.14).

IC₅₀ (half maximal inhibitory concentration) values for Gemcitabine and Gemcitabine conjugated G5.5 DcMNPs were determined at the 72 h treatments. IC₅₀ values were calculated from the logarithmic trend line of the cell proliferation percentage versus concentration plots.

Figures 3.15 and 3.16 demonstrated the antiproliferative effects of Gemcitabine loaded G5.5 DcMNPs with increasing concentrations on SKBR-3 and MCF-7 cell lines. As demonstrated in Figure 3.15, IC₅₀ values of Gemcitabine and Gemcitabine conjugated nanoparticles was about 6.5 μ M and 1.2 μ M on SKBR-3 cells, respectively. In Figure 3.16, IC₅₀ values of Gemcitabine and Gemcitabine conjugated nanoparticles was found as 3.9 μ M and 1.1 μ M on MCF-7 cells, respectively.

Gemcitabine conjugated DcMNPs were found as nearly 6 and 3 fold more toxic on SKBR-3 and MCF-7 cells respectively compared to free Gemcitabine. These results showed that Gemcitabine conjugated DcMNPs are more effective over breast cancer cell lines. It is suggested that these nanoparticles could overcome the drug resistance.

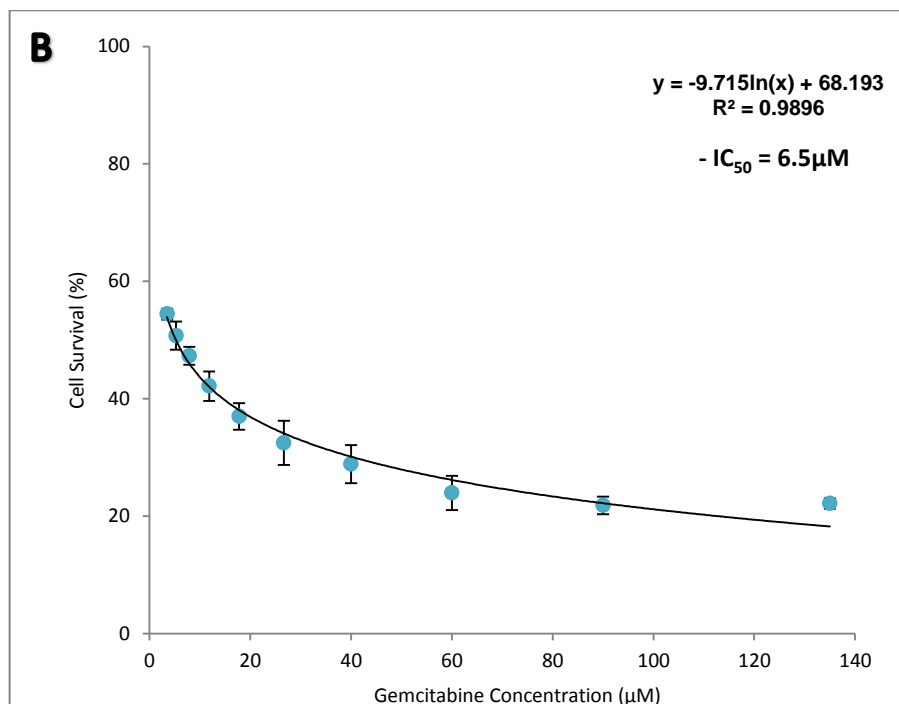
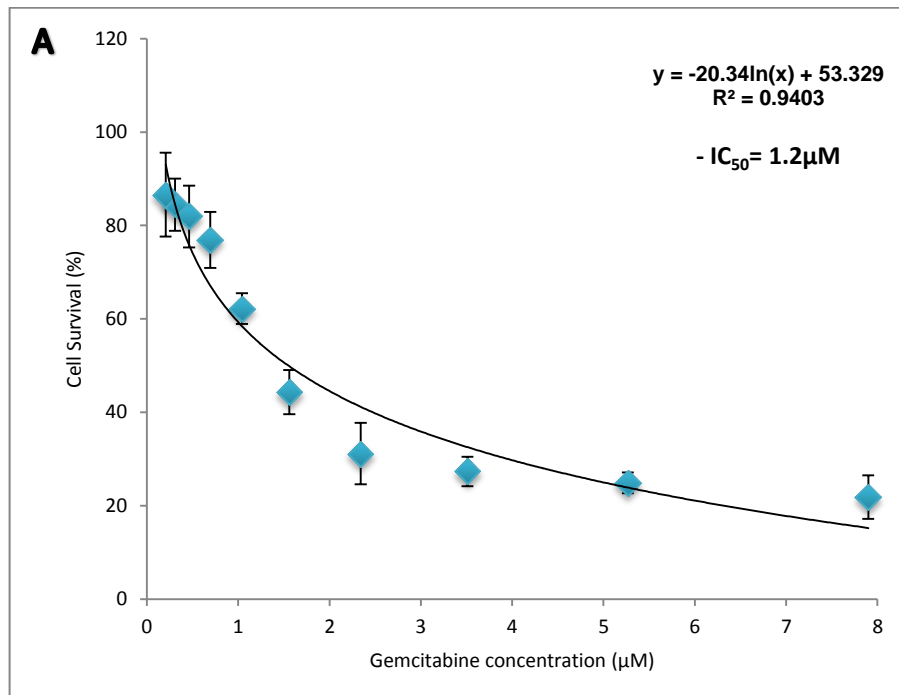


Figure 3.15. XTT cell proliferation assay of (A) Gemcitabine, (B) Gemcitabine conjugated DcMNPs on SKBR-3 cells. The data are represented the mean \pm SEM (n = 3).

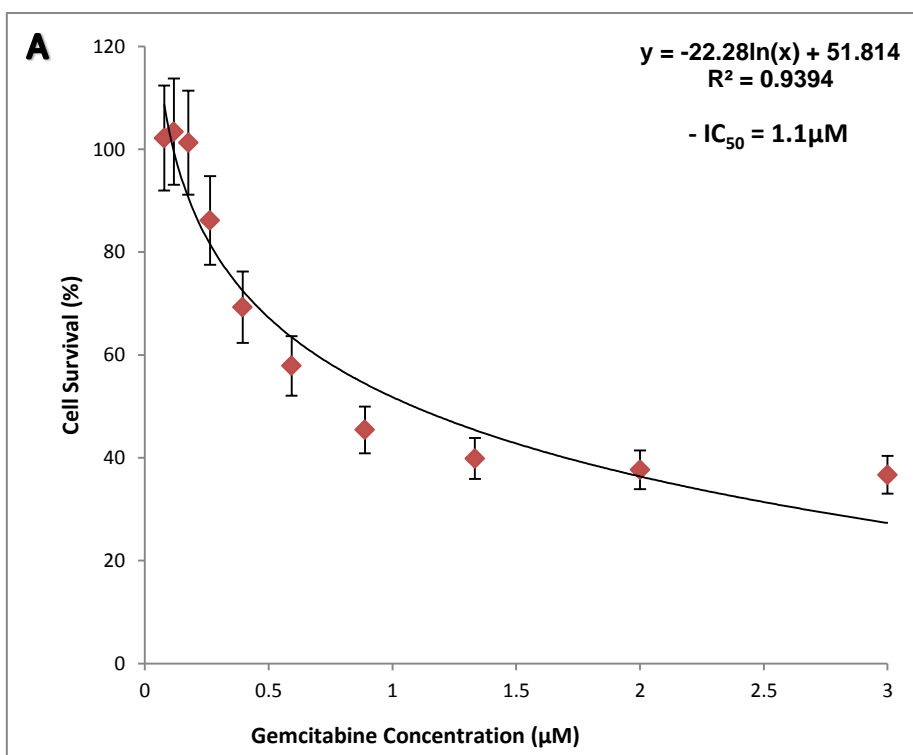
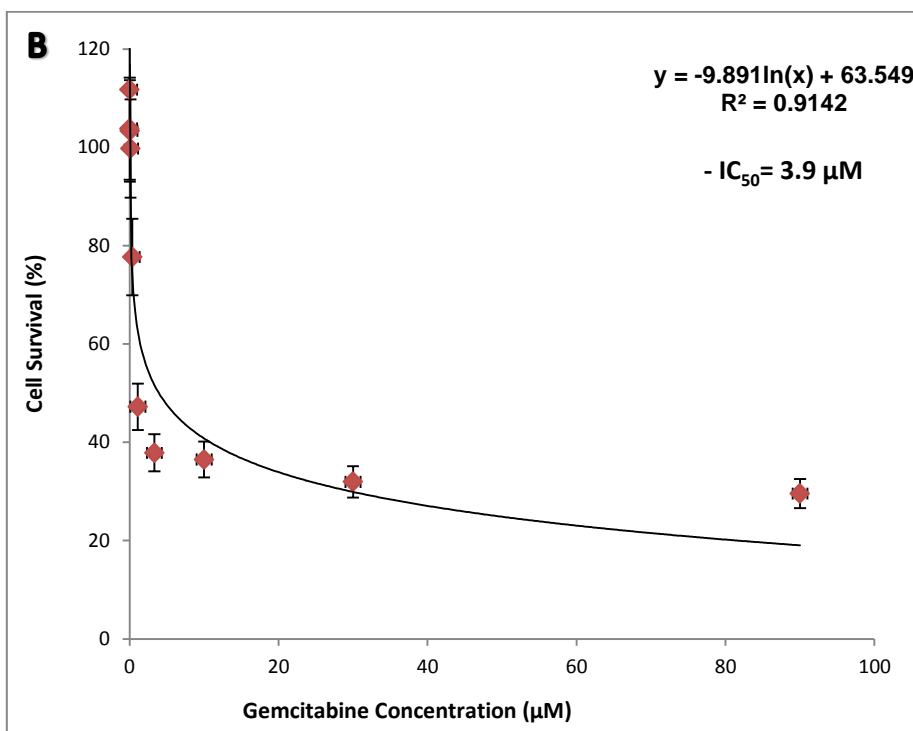


Figure 3.16. XTT cell proliferation assay of (A) Gemcitabine, (B) Gemcitabine conjugated DcMNPs on MCF-7 cells. The data are represented the mean \pm SEM (n = 3).

3.3 Gemcitabine Loading Efficiencies on Chitosan Coated Magnetic Nanoparticles (CSMNPs)

Gemcitabine loading was investigated at different drug dilutions (7.5, 15 and 22.5 $\mu\text{g/ml}$) using 2.5 mg/ml of CSMNPs (Figure 3.17). The loading efficiencies of 7.5, 15 and 22.5 $\mu\text{g/ml}$ Gemcitabine were 63%, 44% and 39% in methanol to CSMNPs, respectively.

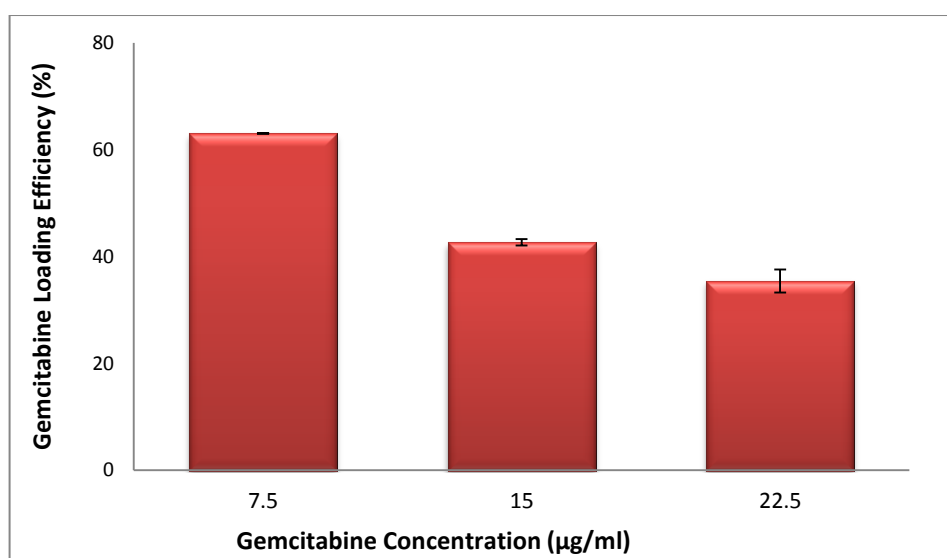


Figure 3.17. Loading efficiencies of Gemcitabine conjugated to CSMNPs. The data are represented the mean \pm SEM (n = 3)

Loading efficiency (39%) was increased up to 9 $\mu\text{g/ml}$ with the highest amount of Gemcitabine (22.5 $\mu\text{g/ml}$) in methanol solution. The highest drug loading was 30 μM (Table 3.2).

Table 3.2. Loaded amounts of Gemcitabine to 2.5 mg/ml CSMNPs using different initial drug loading concentrations.

Gemcitabine concentration ($\mu\text{g/ml}$)	7.5 $\mu\text{g/ml}$	15 $\mu\text{g/ml}$	22.5 $\mu\text{g/ml}$
Loaded amount of Gemcitabine (μg)	4.8 μg	6.6 μg	8.8 μg
Loaded amount of Gemcitabine (μM)	16 μM	22 μM	30 μM

3.3.1 Characterization of Gemcitabine Loaded CSMNPs

3.3.1.1 TEM Analyses

TEM images of CsMNPs and Gemcitabine loaded CsMNPs displayed almost spherical morphology and uniform size distribution (Figure 3.18). The average diameters of CsMNPs were 4 nm and Gemcitabine loading (9 $\mu\text{g/ml}$) did not significantly affect the diameters of nanoparticles.

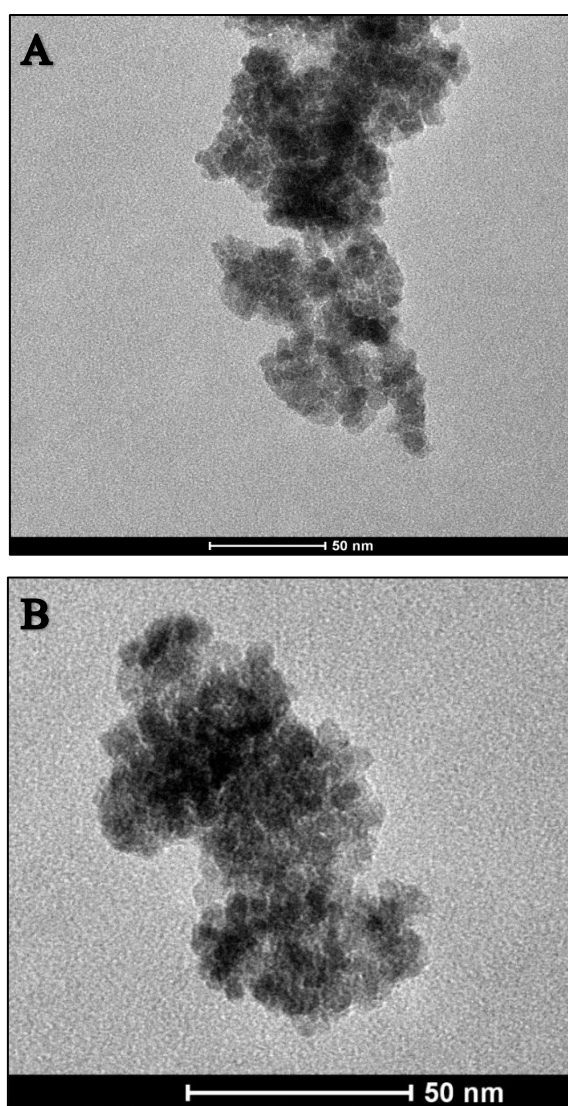


Figure 3.18. TEM images of CSMNPs (A) and Gem-CSMNPs (B).

3.3.1.2 X-ray Photoelectron (XPS) Analyses

X-ray photoelectron spectrophotometry give insight to the interactions between the surface of chitosan coated iron oxide nanoparticles and Gemcitabine. Figure 3.19 shows representative XPS spectra of the CSMNPs and Gemcitabine loaded CSMNPs. The N1s band of CSMNPs at 400 eV is assigned to amino groups ($-\text{NH}_2$). The peaks obtained upon XPS analysis belonged to C 1s (286 eV), N 1s (400 eV), O 1s (531 eV), and Fe 2p (721 eV).

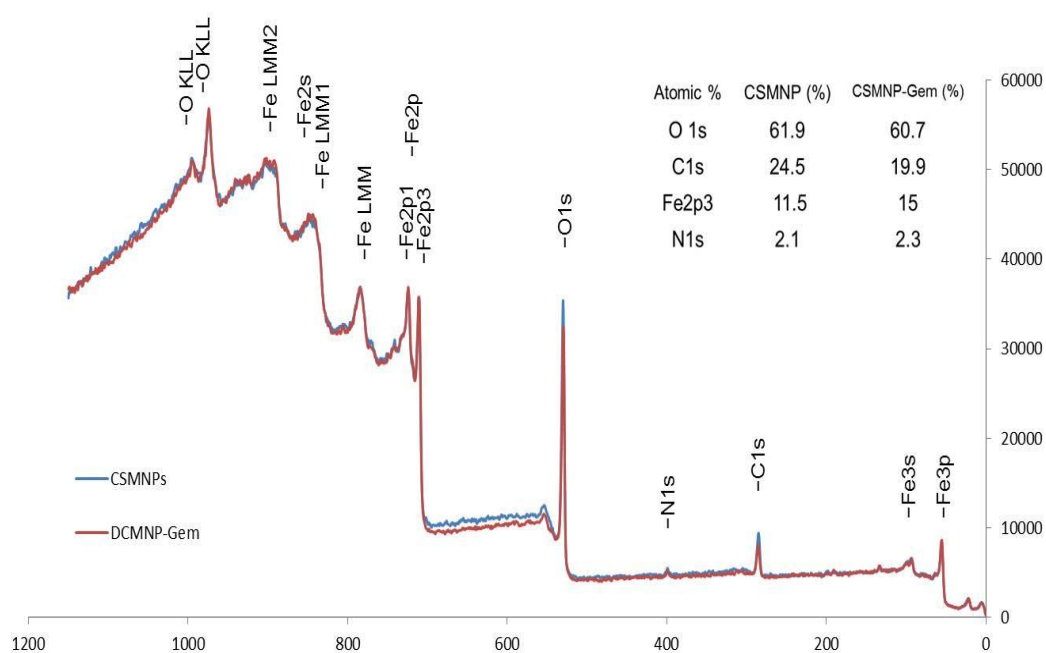


Figure 3.19. XPS scanning spectra of CSMNPs, and Gemcitabine loaded CSMNPs.

Nitrogen and oxygen amounts did not change significantly because of that XPS specifically reveals atomic composition of the surface of nanoparticles (Figure 3.19). Most of loaded Gemcitabine enters into the cavities of chitosan network rather than the surface of CsMNPs. However, the peak belonging to Fluorine atom of Gemcitabine appeared in the spectrum of Gemcitabine loaded CsMNPs, demonstrating the presence of drug on the surface of CsMNPs. Fluorine peak was between 670-700 eV binding energy and under 1200 c/s (Figure 3.20). Results demonstrated that Gemcitabine was loaded both onto the surface and into the cavities of chitosan coated magnetic nanoparticles.

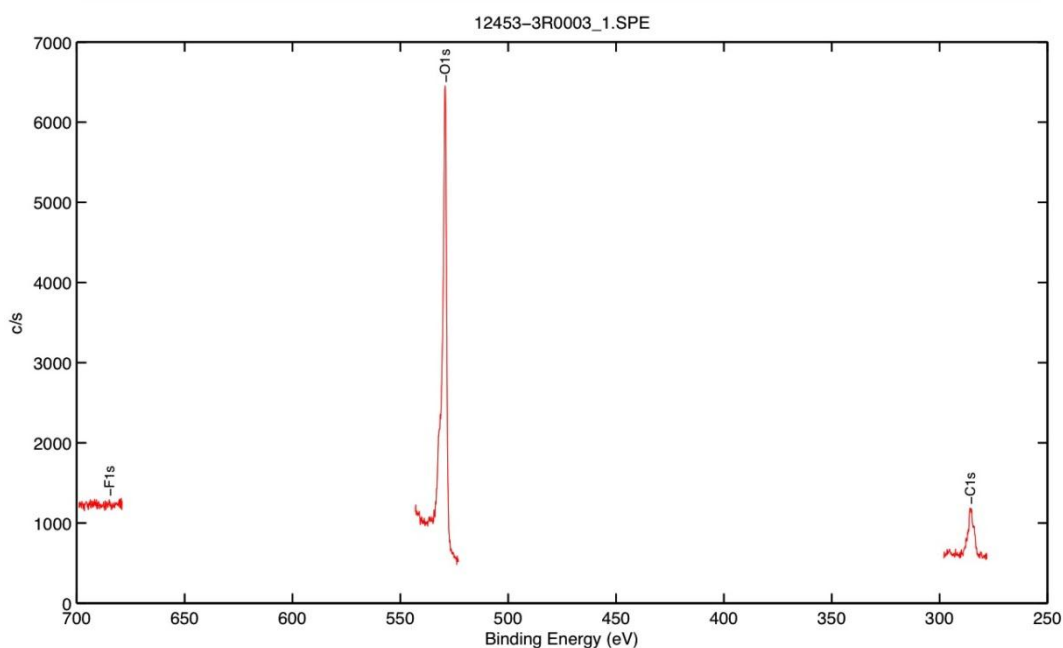


Figure 3.20. XPS particular fluorine analyses of Gemcitabine conjugated CSMNPs.

3.3.1.3 Fourier transform-infrared spectroscopy (FT-IR)

The CsMNPs and Gemcitabine loaded CsMNPs were characterized by the FT-IR. In FT-IR spectra of drug loaded nanoparticles the bands coming from both the CsMNPs and from free Gemcitabine were observed (Figure 3.9).

FTIR spectra of Gemcitabine revealed high intensity broad bands at approximately 2932, 1689, and 1055 cm^{-1} . These peaks were also observed in the spectrum of Gemcitabine (9 $\mu\text{g/ml}$) loaded CsMNPs as shifted to 2920, 2850 cm^{-1} (CH_2), 1689 cm^{-1} ($\text{C}=\text{O}$) and 1053 cm^{-1} ($\text{C}-\text{O}$). However, these peaks were not present in the spectrum of CsMNPs. The characteristic peaks in 1685 cm^{-1} and 2902 cm^{-1} due to (NH_2) band were disappeared after loading by Gemcitabine. This is a clear indication of Gemcitabine loading on chitosan coated magnetic nanoparticles.

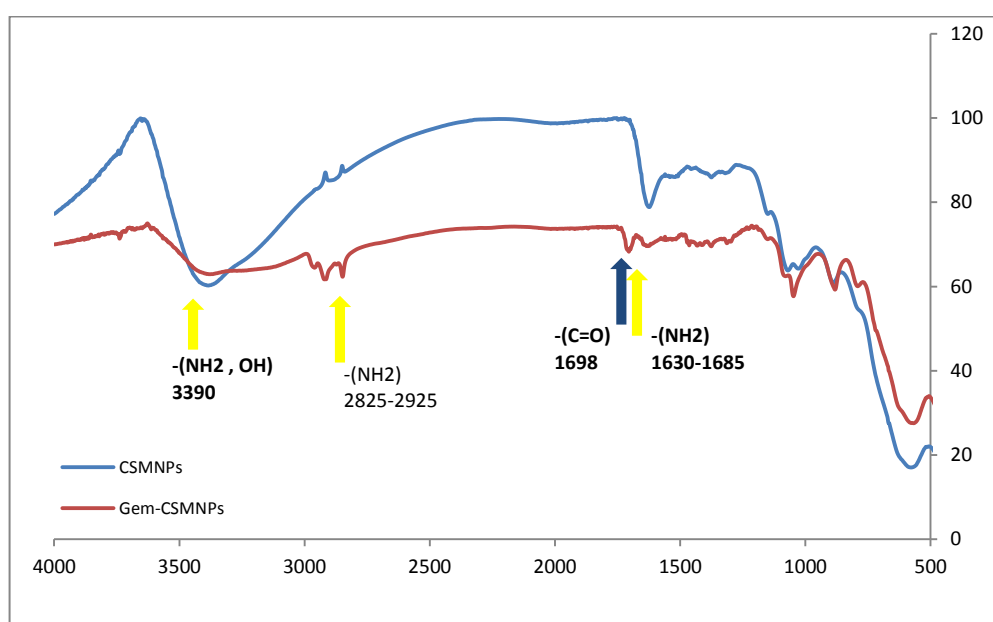


Figure 3.21. FT-IR spectra of CSMNPs and Gem-CSMNPs.

3.3.1.4 Zeta (ζ) Potential Analyses

The zeta potential of CsMNPs was determined as -19.8 mV in aqueous medium at pH 7.2. Unsoy et al. reported that CsMNPs have negative charge at pH>6.7 due to the deprotonation of amino groups on chitosan layer (Unsoy et al. 2012). An electrostatic interaction is expected between the aqueous dispersion of negatively charged CsMNPs (pH 7.2) and positively charged Gemcitabine (by the protonation of NH₂ group). Zeta potential of Gemcitabine (30 μ M) loaded CsMNPs was -8.66 mV at pH 7.2 (Figure 3.22). This significant increase in zeta potential could be explained by entrapment of Gemcitabine to the chitosan coated iron oxide nanoparticles neutralizing negative charges.

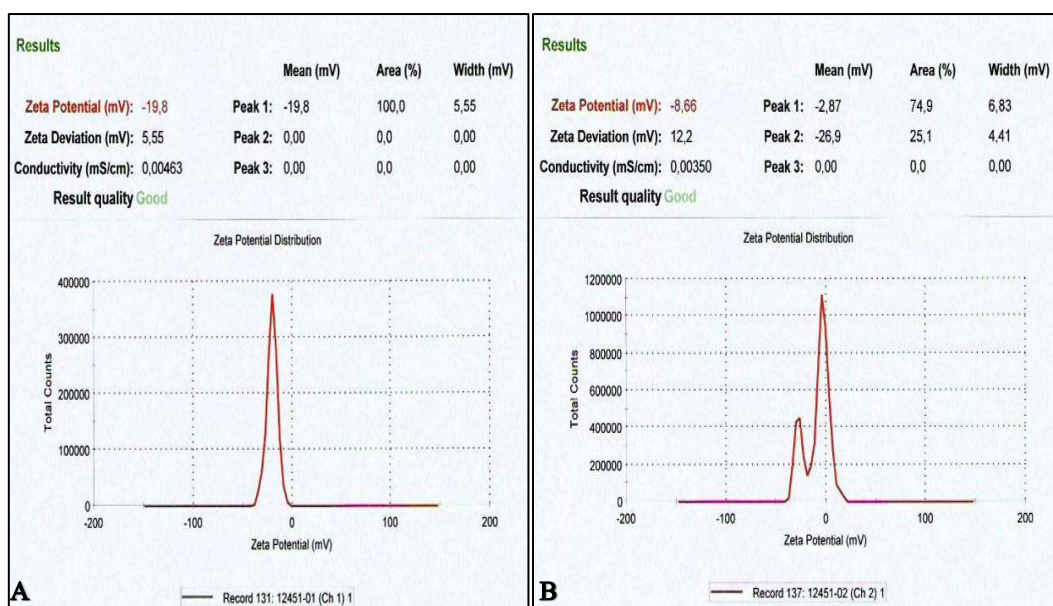


Figure 3.22. Zeta potential measurements of CSMNPs (A) and Gem-CSMNPs (B).

3.3.2 Release and Stability Efficiencies of Gemcitabine from CSMNPs

3.3.2.1 Release Profile

Gemcitabine release studies showed pH dependent release pattern. The release profiles of the drug from CSMNPs in acetate buffer at pH 4.2 and pH 5.2 are given in Figure 3.23. The release studies were continued up to 24 h. Gemcitabine release was higher at pH 4.2 (65.4%) compared to pH 5.2 (33%). This faster release at lower pH was related to the higher solubility of Chitosan at lower pH values, thus, allowing Gemcitabine to leak out at a faster rate.

CsMNPs showed 25% and 10% initial burst release of Gemcitabine at pH 4.2 and 5.2, respectively during a period of 3h. This initial rapid release, characterized as “burst effect”, occurs by desorption of Gemcitabine, localized on the surface of nanoparticles or upper layer of mesh cavities. Therefore, the entire drug entrapped in the mesh cavities shows slow release from nanoparticles.

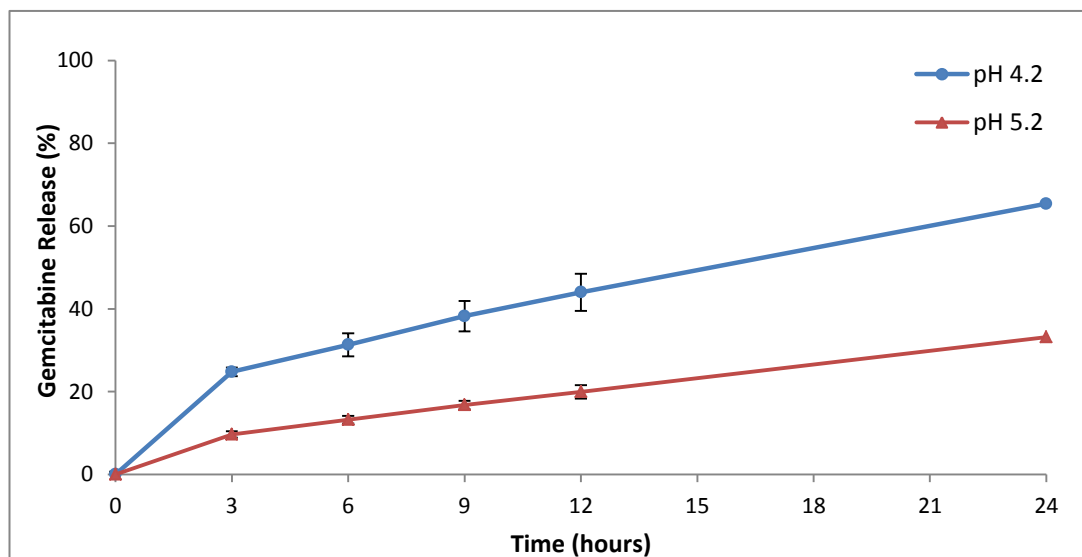


Figure 3.23. Gemcitabine release profile of CSMNPs in acetate buffer at pH4.2 and pH 5.2. The data are represented as the mean \pm SEM (n = 3).

Maximum 25% and 10% burst releases of Gemcitabine at pH 4.2 and 5.2 indicated that drug was mostly entrapped in the mesh cavities of CsMNPs more than the surface. It has been reported that chitosan starts to degrade at pH 4.2 (Rodrigues et al. 2012). So, higher release of Gemcitabine was obtained at pH 4.2 (65%). As pH of the release media was decreased, the drug release increased. Then, the drug is expected to be released at the targeted cancer cells, because the pH of tumor tissue and endosomes are acidic.

Garg et al. (2012) investigated *in vitro* release kinetics of Gemcitabine from chitosan/poly(ethylene glycol)anisamide (CTS/PEG-AA) nanoparticles by dialysis bag method using PBS (10 mM, pH 5.8) as release medium. They showed that nearly 79% of the drug was released from CsMNPs during 10 days (Garg et al. 2012). Contrarily, Arias et al. (2011) obtained much faster Gemcitabine release rate from chitosan nanoparticles at pH 5. They observed 65% release within 2 h, while the remaining drug was slowly released in the next 22 h (Arias et al. 2011). It took longer time to release whole drug load of CsMNPs compared to the study of Arias et al. because entrapped Gemcitabine amount (9 µg/ml) was higher in CsMNPs. In the study of Garg et al. they needed more time to release their drug load due to the encapsulation of drug inside the nanoparticles.

3.3.2.2 Stability Profile

The stability of Gemcitabine loaded nanoparticles was evaluated up to 72h in PBS at 37°C, which mimics the physiological conditions (Figure 3.24). Results showed 12h steady-state release (2%) continued by burst release up to 24h and again steady-state up to 72h (8%). The percentage of cumulative release was around 8% in PBS buffer (pH 7.2). Consequently, Gemcitabine conjugated CSMNPs were highly stable (92%) up to 72h.

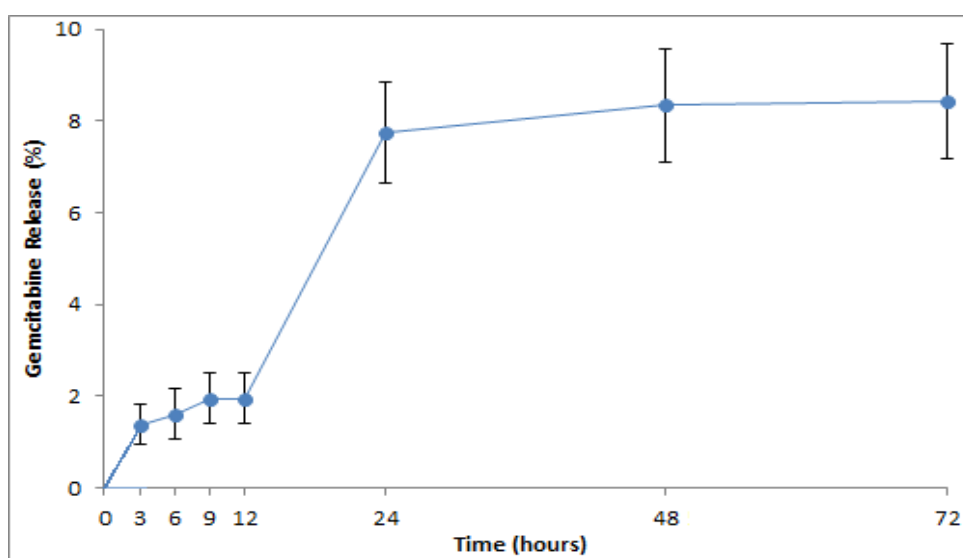


Figure 3.24. Stability of Gemcitabine conjugated CSMNPs in PBS buffer (pH 7.2). The data are represented as the mean \pm SEM (n = 3).

Arias et al. demonstrated the release of gemcitabine adsorbed onto the chitosan nanoparticles was complete within 2 h at pH 7.4. On the contrary, the entrapped gemcitabine within chitosan nanoparticles showed a burst drug release ($\approx 40\%$ in 2h), which indicates the leakage of the surface-associated and poorly entrapped drug and the remaining drug being released through next 4 days (Arias et al. 2011).

In this study, the results indicated that Gemcitabine conjugated CSMNPs were highly stable ($\approx 92\%$) up to 72h in PBS buffer. This is a desirable property, which provides an advantage in the storage of Gemcitabine conjugated CSMNPs.

3.3.3 *In Vitro* Cytotoxicity Studies of CSMNPs and Gemcitabine Loaded CSMNPs on SKBR-3 and MCF-7 Cell Lines

Cytotoxicities of CSMNPs and Gemcitabine loaded CSMNPs were investigated by XTT cell proliferation assay on SKBR-3 and MCF-7 breast cancer cell lines. MCF-7 and SKBR-7 cells were treated with CSMNPs for 72 hours in 96- well plates. After incubation period, cell viability profiles were determined for each cell type.

As previously reported by Unsoy et al., when 0.75 mg/ml CsMNPs were applied to HeLa, SiHa and MCF-7 cells, a significant toxicity was not observed on these cell lines (Unsoy et al. 2012). XTT results showed that CsMNPs were not significantly cytotoxic on SKBR-3 cells up to 1.7 mg/ml concentration. On the other hand, 0.8 mg/ml CsMNPs showed 30% cytotoxicity in MCF-7 cells (Figure 3.25). However, less CsMNP (0.5 mg/ml) is enough for Gemcitabine loading studies on MCF-7 and SKBR-3 cell lines (Figure 3.25).

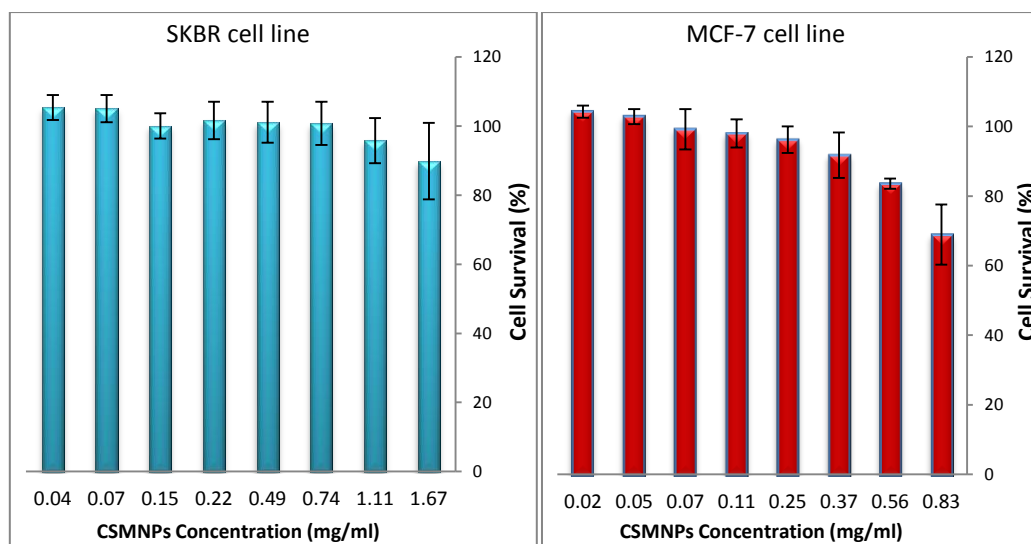


Figure 3.25. Cytotoxicity of CSMNPs on MCF-7 and SKBR-3 cell lines. The data are represented as the mean \pm SEM (n = 2).

Figures 3.26 and 3.27 demonstrate the dose dependent antiproliferative effect of Gemcitabine and Gemcitabine loaded CSMNPs on SKBR-3 and MCF-7 cell lines, respectively. IC_{50} values of Gemcitabine and Gemcitabine conjugated CsMNPs were calculated from the logarithmic trend line of cell proliferation percentage versus concentration plots. IC_{50} values of Gemcitabine and Gemcitabine conjugated CsMNPs were 6.5 μ M and 4.8 μ M on SKBR-3 cells, and 3.9 μ M and 1.5 μ M on MCF-7 cells, respectively (Figures 3.26, 3.27).

Results showed that, Gemcitabine loaded CsMNPs were found as nearly 1.4 and 2.6 fold more toxic compared to free Gemcitabine on SKBR-3 and MCF-7 cells, respectively. These results showed that loading of Gemcitabine on CsMNPs are more effective over breast cancer cell lines. Similarly, Unsoy et al (2014) reported that the efficacy of Doxorubicin loaded CsMNPs was 2 folds higher than free Doxorubicin on MCF-7 cells. In another cell proliferation assay of Bortezomib loaded CsMNPs on HeLa cells revealed that the required amount of drug decreased 2 folds compared to free Bortezomib (Unsoy et al. 2014). Consequently, the inhibition of cancer cell proliferation was achieved with less drug concentrations by CsMNPs *in vitro*.

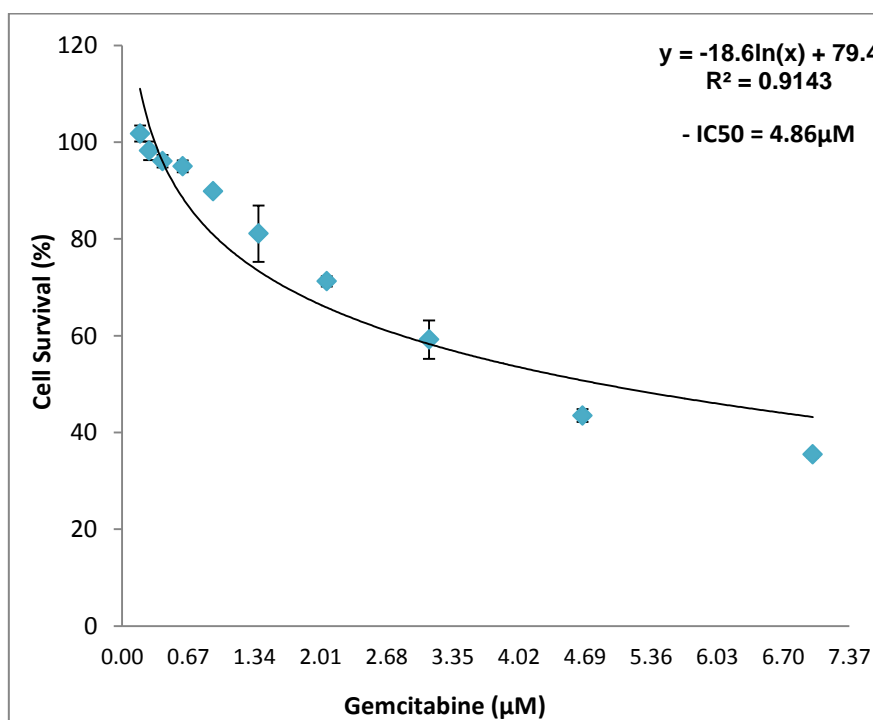
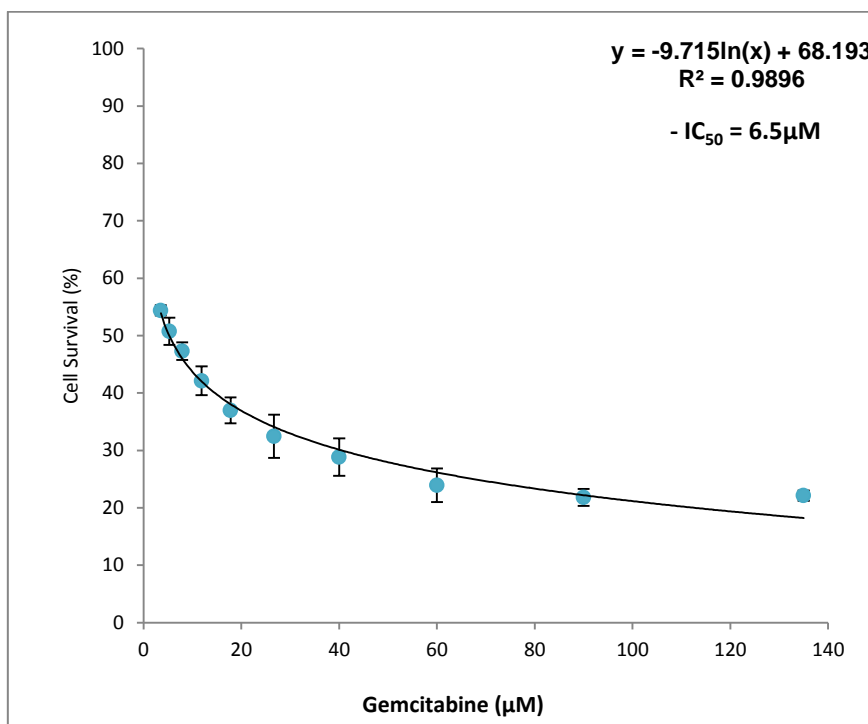


Figure 3.26. XTT cell proliferation assay of Gemcitabine and Gemcitabine conjugated CSMNPs on SKBR-3 cells. The data are represented as the mean \pm SEM (n = 3).

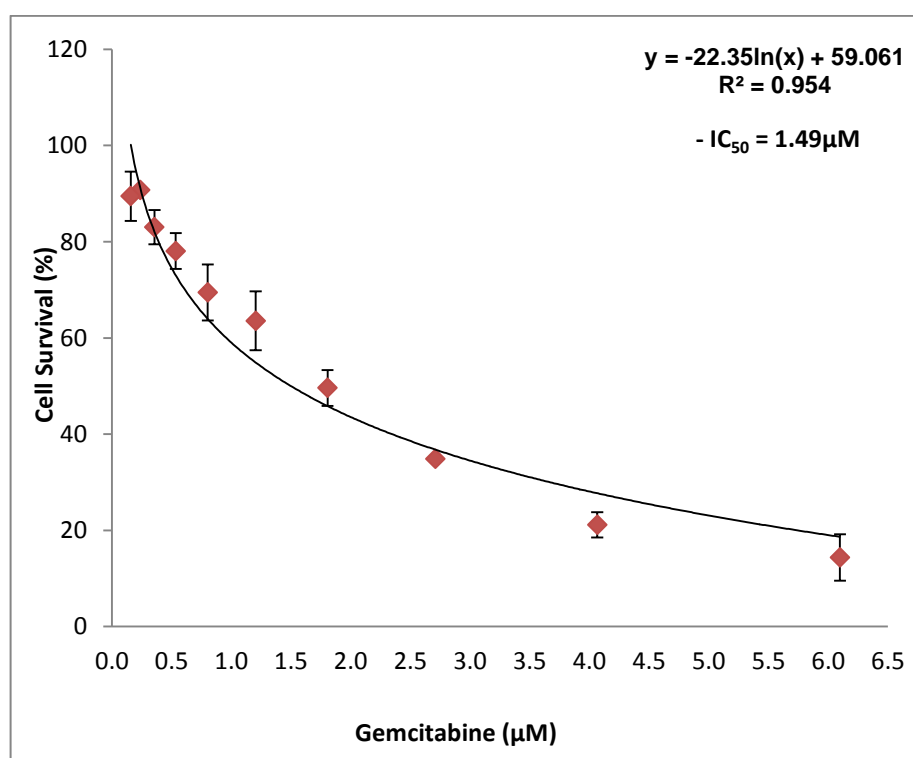
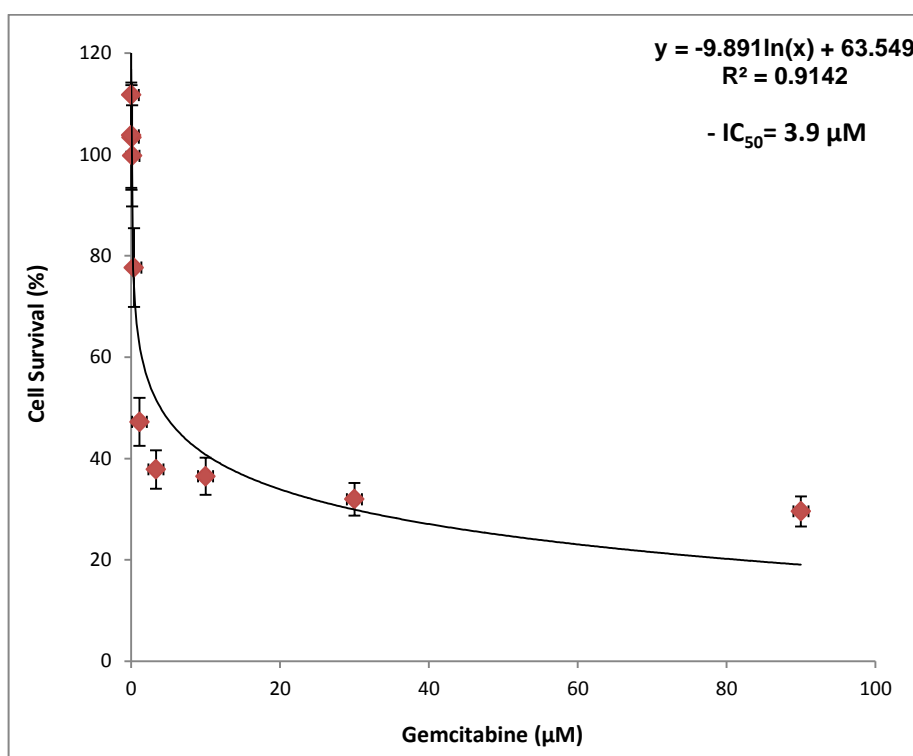


Figure 3.27. XTT cell proliferation assay of Gemcitabine and Gemcitabine conjugated CSMNPs on MCF-7 cells. The data represent the mean \pm SEM (n = 3).

3.4 Gemcitabine Loading Efficiencies on PHB Magnetic Nanoparticles (PHB_MNPs)

Loading efficiencies were investigated in methanol with different drug concentrations using (2.5 mg/ml) PHB-MNPs (Figure 3.28). The loading efficiencies of 7.5, 15 and 22.5 $\mu\text{g/ml}$ Gemcitabine were 32%, 27% and 29% in methanol to PHB-MNPs, respectively.

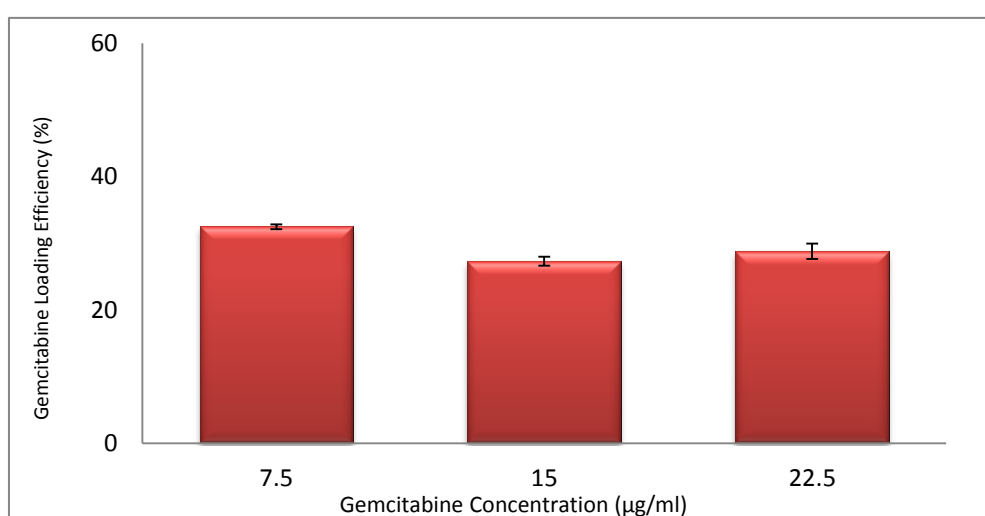


Figure 3.28. Loading efficiencies of Gemcitabine conjugated to PHB-MNPs. The data are represented as the mean \pm SEM (n = 3)

Loading efficiency (29%) was increased up to 6.5 $\mu\text{g/ml}$ with the highest amount of Gemcitabine (22.5 $\mu\text{g/ml}$) in methanol solution. The highest loaded concentration of drug was 22 μM (Table 3.3).

Table 3.3. Loaded amounts of Gemcitabine to PHB-MNPs using different initial drug loading concentrations.

Gemcitabine concentration ($\mu\text{g/ml}$)	7.5 $\mu\text{g/ml}$	15 $\mu\text{g/ml}$	22.5 $\mu\text{g/ml}$
Loaded amount of Gemcitabine (μg)	2.4 μg	4 μg	6.5 μg
Loaded amount of Gemcitabine (μM)	8 μM	13.5 μM	22 μM

3.4.1 Characterization of Gemcitabine Loaded PHB-MNPs

3.4.1.1 TEM Analyses

The sizes of magnetic polymer and morphological properties before and after conjugated by drug were observed through TEM images. TEM images of PHB-MNPs and Gemcitabine conjugated PHB-MNPs (Figure 3.29) show the particle sizes were around 13 nm and ~13-15 nm, respectively. There were no remarkable differences between the sizes of MNPs after loading with 6.5 μg Gemcitabine.

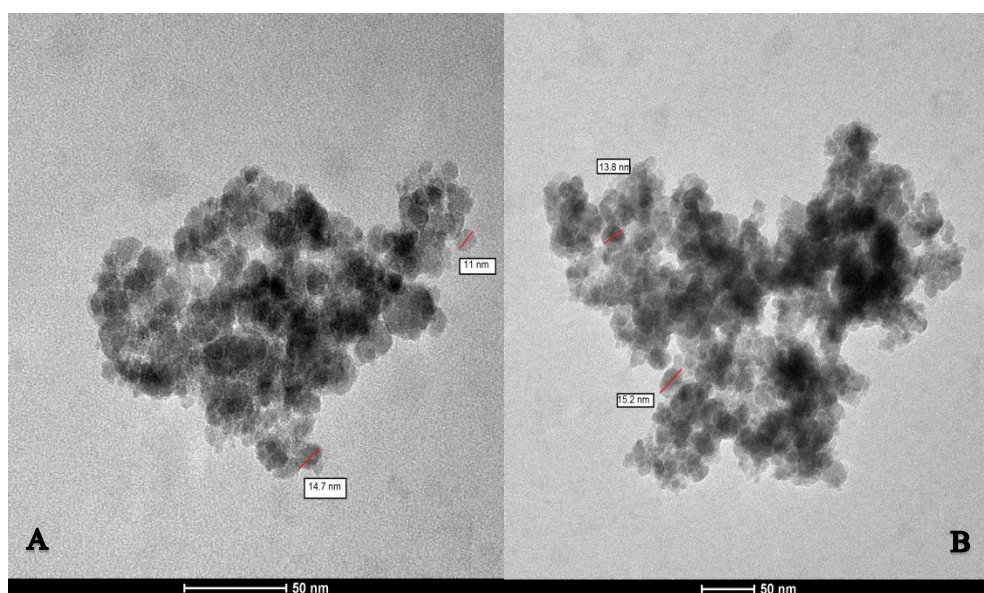


Figure 3.29. TEM images of PHB-MNPs (A) and Gemcitabine conjugated PHB-MNPs (B)

3.4.1.2 X-ray Photoelectron (XPS) Analyses

XPS was used to examine shell structure of the synthesized product. Figure 3.30 shows representative XPS spectra of the PHB-MNPs and Gemcitabine loaded PHB-MNPs. XPS specifically reveals atomic surface characteristics of nanoparticles. The peaks obtained upon XPS analysis were belonging to C 1s (286 eV), C 1s (286 eV), O 1s (531 eV), and Fe 2p (721 eV). The atomic percent of these peaks did not change significantly after Gemcitabine conjugation.

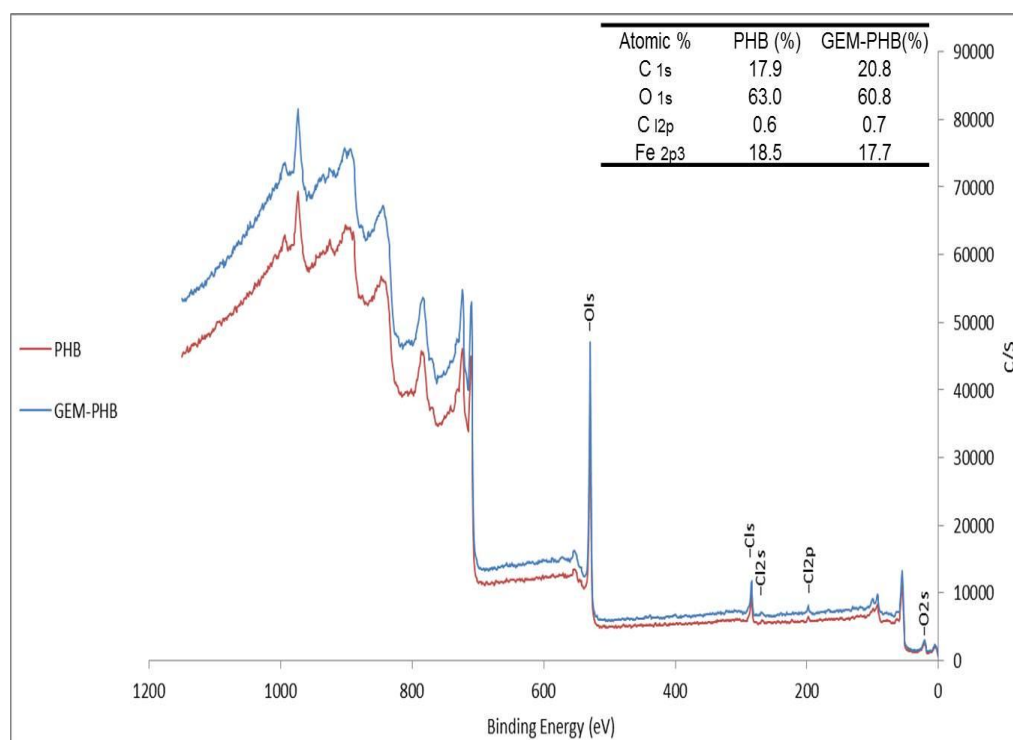


Figure 3.30. XPS scanning spectrum of PHB-MNPs, and Gemcitabine conjugated PHB-MNPs.

In figure 3.30, nitrogen peak belonging to Gemcitabine NH_2 were not seen in the Gemcitabine loaded PHB-MNPs spectra. However Fluorine atom was observed in XPS particular analysis between 670-700 eV binding energy and under 2000 C/S of Gemcitabine loaded PHB-MNPs (Figure 3.31). The absence of nitrogen atom and presence small amount of fluorine demonstrated that Gemcitabine was encapsulated within PHB-MNPs mesh-works more than surface association.

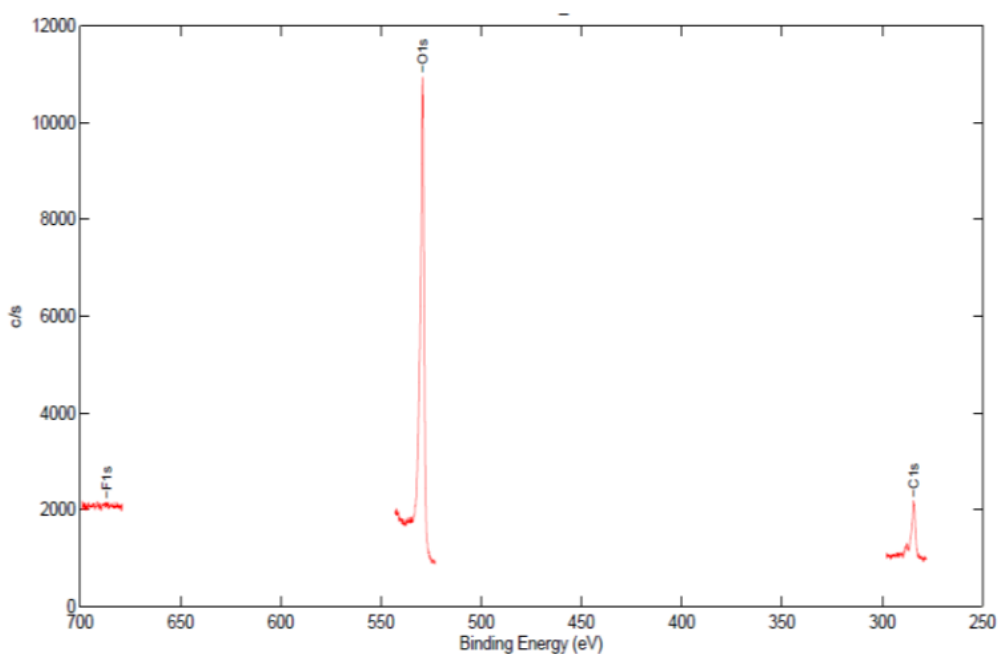


Figure 3.31. XPS results for Fluorine analysis of Gemcitabine conjugated PHB-MNPs.

3.4.1.3 Fourier Transform-Infrared Spectroscopy (FT-IR)

In order to characterize the chemical composition of synthesized PHB magnetic nanoparticles (PHB-MNPs) and to support the information of Gemcitabine loaded to PHB-MNPs, FT-IR spectra were obtained.

The peak at the 583 cm^{-1} region, characteristic for the Fe-O group, was found in PHB coated magnetic nanoparticles and Gemcitabine loaded particles spectra, confirming that the products contained magnetite. The characteristic peaks at 2750 cm^{-1} , 3050 cm^{-1} and 3390 cm^{-1} due to NH_2 band disappeared in PHB-MNPs (Figure 3.32). These peaks were seen in Gemcitabine FTIR (Figure 3.9) and also appeared in PHB-MNPs after Gemcitabine loading. This is a clear indication that Gemcitabine was efficiently entrapped into the PHB-MNPs.

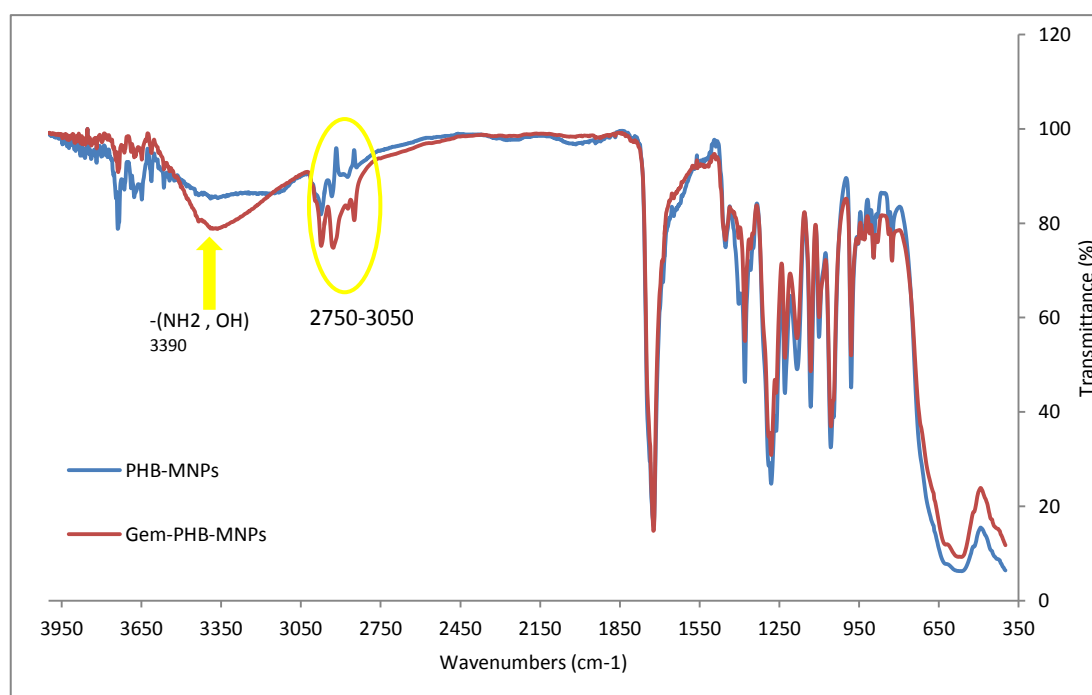


Figure 3.32. FT-IR results related to PHB-MNPs and Gemcitabine conjugated PHB-MNPs.

3.4.1.4 Zeta (ζ) Potential Analysis

The zeta potential of PHB-MNPs in aqueous dispersion was around 19.9 mV. On the other hand, the zeta potential of Gemcitabine loaded PHB-MNPs was 24.5 mV (Figure 3.33). These results demonstrated that Gemcitabine loading was achieved and the cationic charge of PHB did not so much change after drug loading.

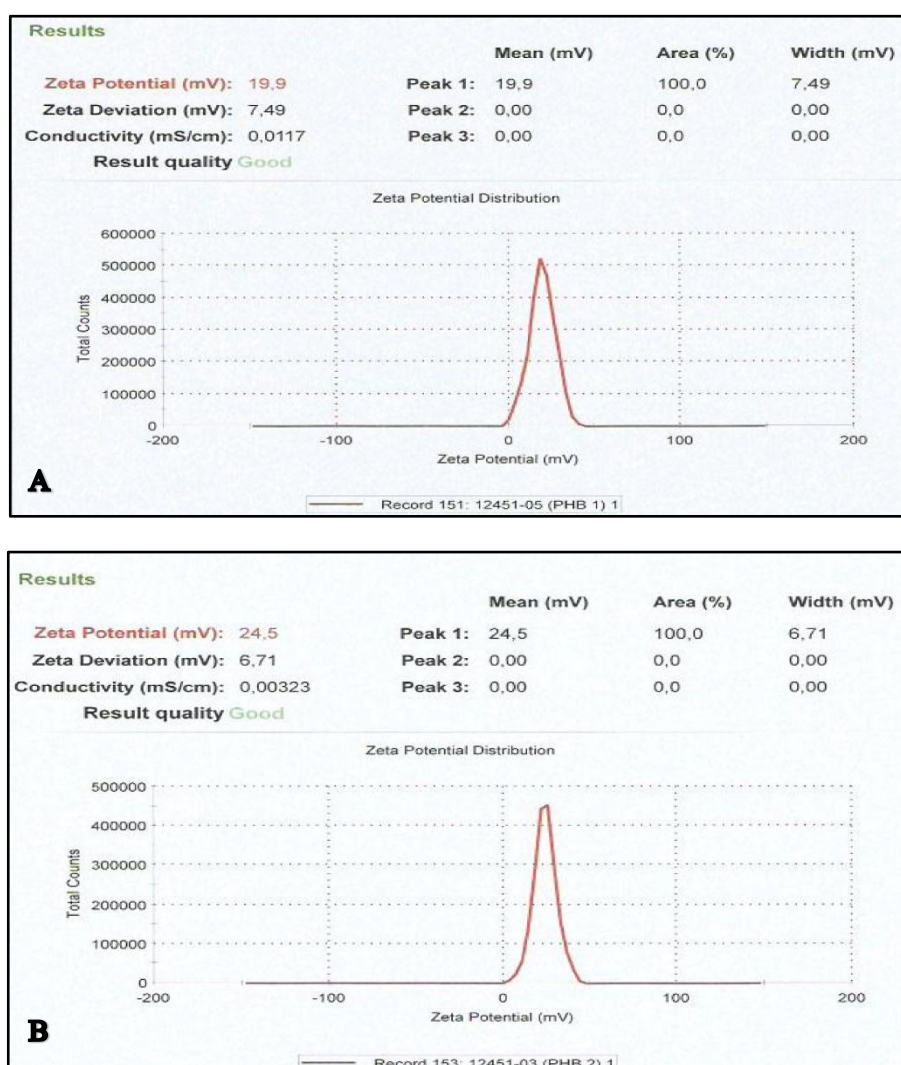


Figure 3.33. Zeta (ζ) Potential graphs of PHB-MNPs (A), and Gemcitabine conjugated PHB-MNPs (B).

3.4.2 Release and Stability Efficiencies of Gemcitabine from PHB-MNPs

3.4.2.1 Release Profile

Gemcitabine release studies were performed in acetate buffer at pH 4.2 for 24 h. The release profile of the drug from PHB-MNPs at pH 4.2 is given in Figure 3.34. The total amount of the drug released within 24h from PHB-MNPs was around 48.8 % at pH 4.2. 13% burst release was observed in first 3h which was lower than observed in DcMNPs (17%) and CSMNPs (25%). PHB-MNPs released 48.8% of drug after 24h as opposed to DcMNPs, which released whole adsorbed drug after 15h. These results indicated that firstly Gemcitabine adsorbed to the surface of PHB-MNPs or inside the upper layer of cavities were released and drug entrapped in the deeper mesh cavities needed more time for release. Yalcin et al. (2014) showed 60% of Doxorubicin loaded to PHB-MNPs needed 65h to be released at pH 4.5. It was showed nearly 50% of Doxorubicin (400 µg/ml and 500 µg/ml) were released after 24h (Yalcin et al. 2014).

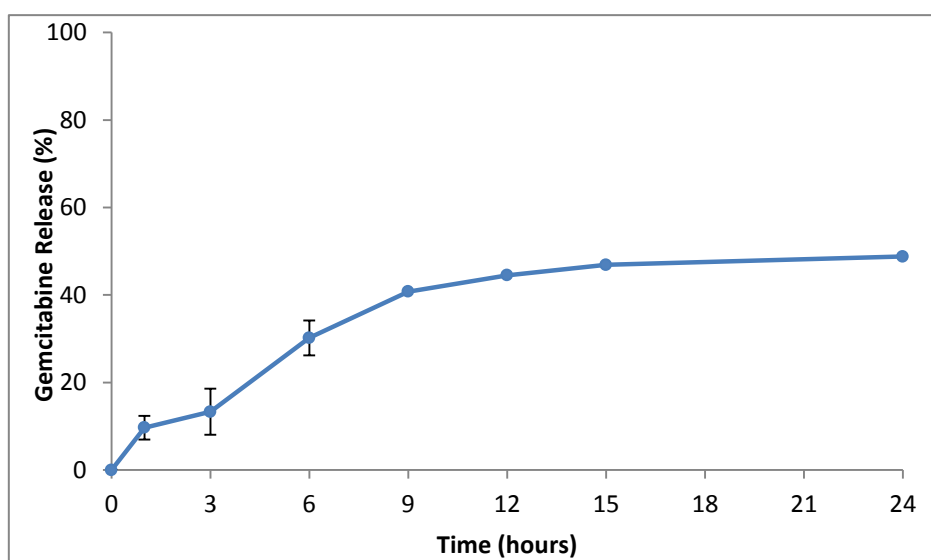


Figure 3.34. Gemcitabine release profile of PHB-MNPs at pH 4.2. The data are represented as the mean \pm SEM (n = 3).

3.4.2.2 Stability Profile

The stability of Gemcitabine loaded PHB nanoparticles was investigated up to 36 hours in PBS (pH 7.2) at 37°C, which mimics the physiological conditions (Figure 3.35). Results showed that the 15h burst release (19%) continued by steady-state release up to 36h. However only 19.4% of the drug was released after 36h of incubation.

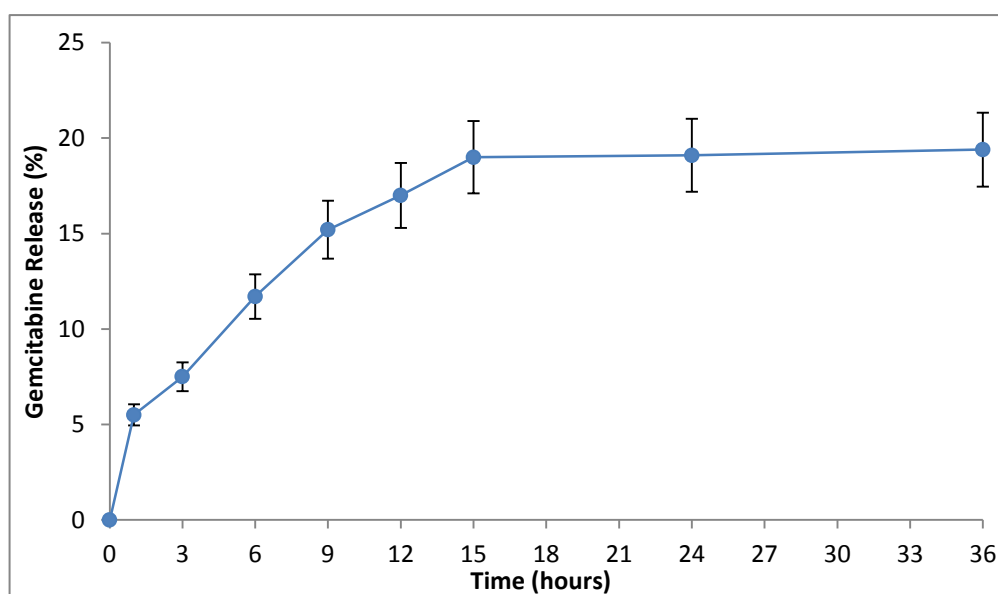


Figure 3.35. Stability of Gemcitabine loading PHB-MNPs in PBS buffer (pH 7.2). The data are represented as the mean \pm SEM (n = 3).

The results indicated that Gemcitabine loaded PHB-MNPs were stable ($\approx 80\%$) up to 36h in PBS buffer. Previously, Yalcin et al. showed that about 35% of the Doxorubicin was released from PHB-MNPs at pH 7.2 within 2 weeks, and 65% of the drug was not released up to 8 weeks (Yalcin et al. 2014). This is a desirable property, which provides an advantage in the storage of drugs conjugated PHB-MNPs.

3.4.3 *In Vitro* Cytotoxicity Studies of Bare and Gemcitabine Loaded PHB-MNPs

Cytotoxicities of PHB-MNPs, free Gemcitabine and Gemcitabine loaded PHB-MNPs on SKBR-3 and MCF-7 breast cancer cell lines were investigated by XTT cell proliferation assay. MCF-7 and SKBR-7 cells were treated with bare PHB-MNPs for 72 hours in 96-well plates. After incubation period, cell viability profiles were determined for each cell type.

Previously, Yalcin et al. (2014) reported empty PHB-MNPs were not cytotoxic in the highest dose on PHB-MNPs (500 $\mu\text{g/ml}$) at Doxorubicin sensitive and resistance MCF-7 cell lines (Yalcin et al. 2014 a) (Yalçın, S. et al. 2014 b).

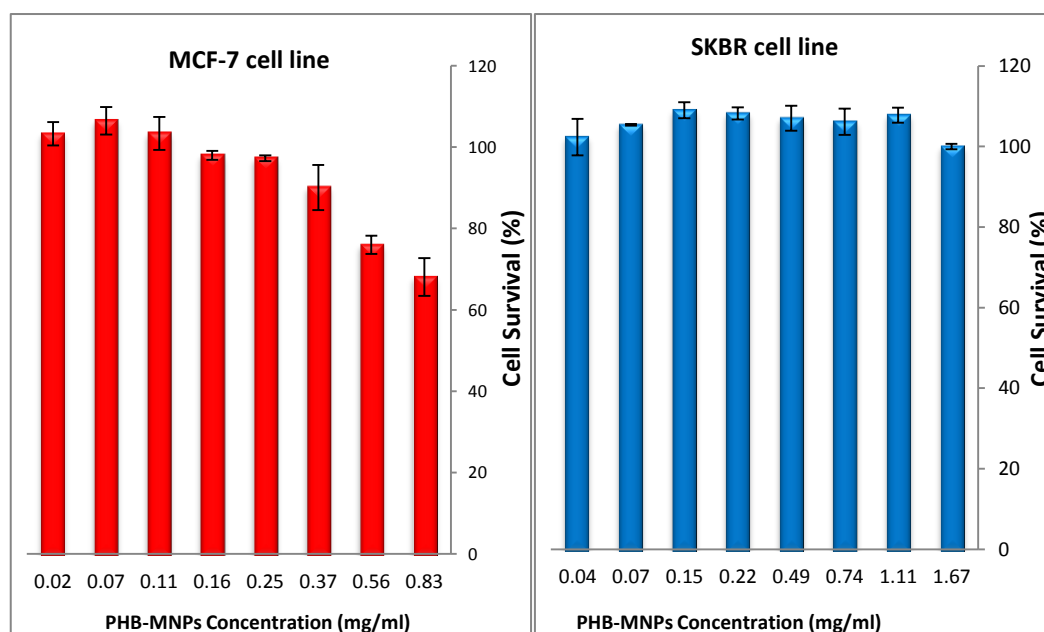


Figure 3.36. Cytotoxicity of PHB-MNPs on MCF-7 and SKBR-3 cell lines.

Cell survival rates with PHB-MNPs indicated that there was no significant cytotoxic effect of the nanoparticles on SKBR-3 cells up to 1.67 mg/ml, but has a little cytotoxic effect on MCF-7 cell lines at high MNPs concentrations (above 0.5 mg/ml) (Figure 3.36).

IC₅₀ values for Gemcitabine and Gemcitabine conjugated PHB-MNPs were determined at the 72 h treatments. IC₅₀ were calculated from the logarithmic trend line of the cell proliferation percentage versus concentration plots. Figures 3.37 and 3.38 demonstrated the antiproliferative effects of Gemcitabine loaded PHB-MNPs with increasing concentrations on SKBR-3 and MCF-7 cell lines. IC₅₀ values of Gemcitabine and Gemcitabine loaded nanoparticles was about 6.5 μM and 3.5 μM for SKBR-3 cells (Figure 3.37), and 3.9 μM and 1.98 μM for MCF-7 cell lines, respectively (Figure 3.38).

As results indicated, Gemcitabine loaded PHB-MNPs were found as nearly 2 fold more toxic on SKBR-3 and MCF-7 cells compared to free Gemcitabine. These results showed that Gemcitabine conjugated PHB-MNPs are more effective over breast cancer cell lines than free Gemcitabine and we claim that, this treatment could overcome the drug resistance.

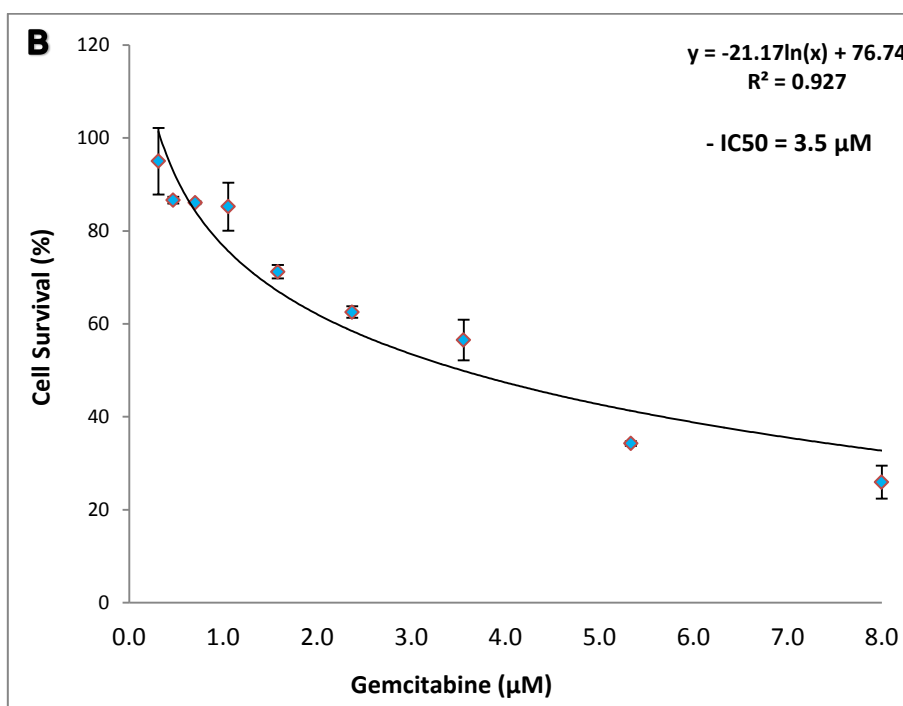
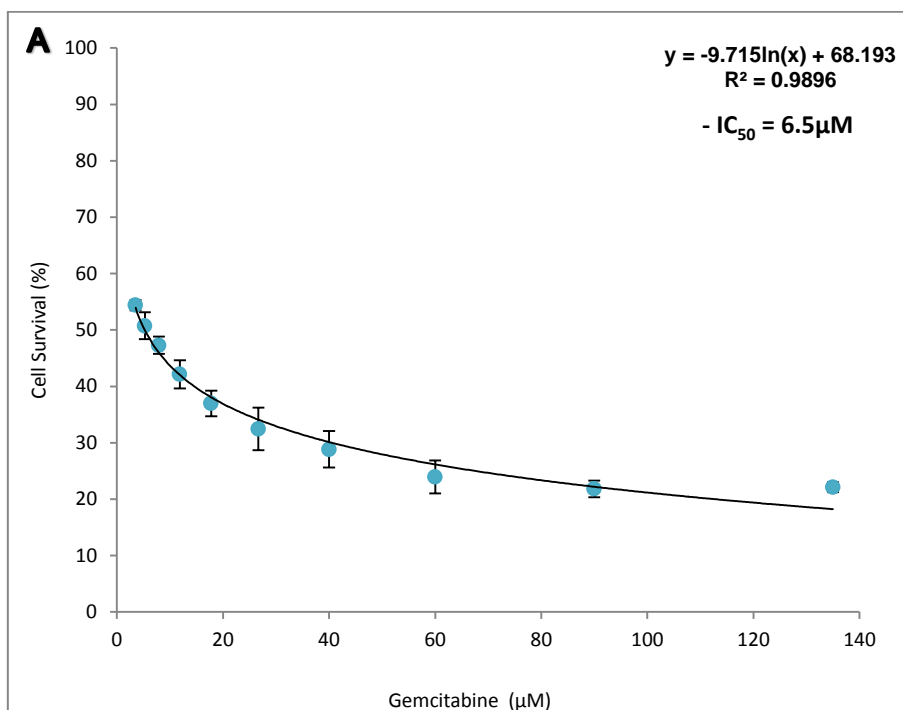


Figure 3.37. XTT cell proliferation assay results (A) Gemcitabine, (B) Gemcitabine loaded PHB-MNPs on SKBR-3 cells. The data are presented as the mean \pm SEM (n = 3)

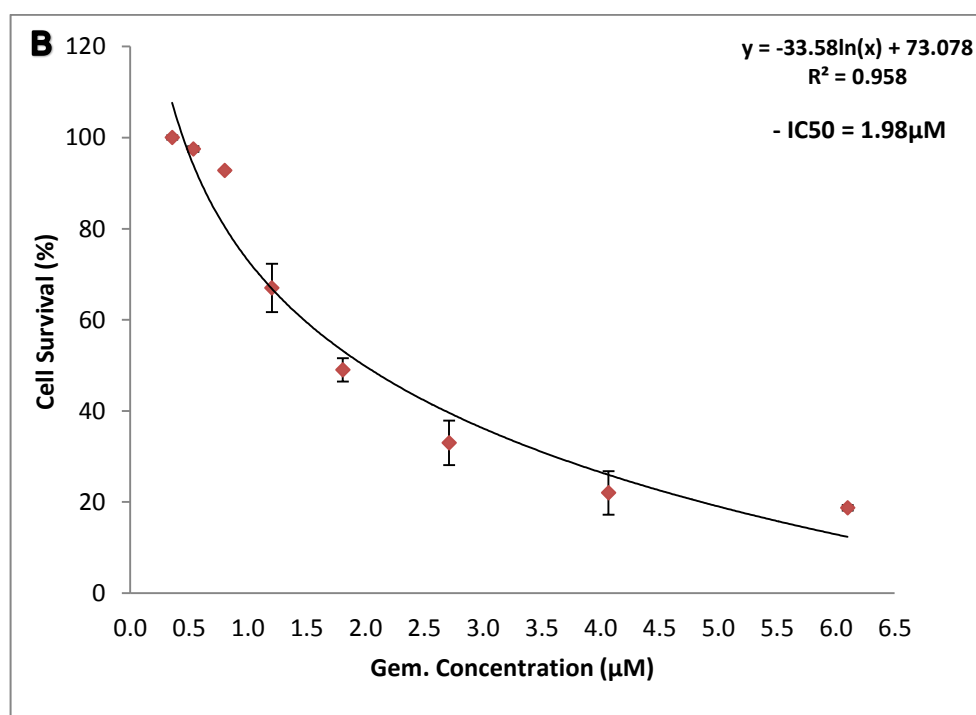
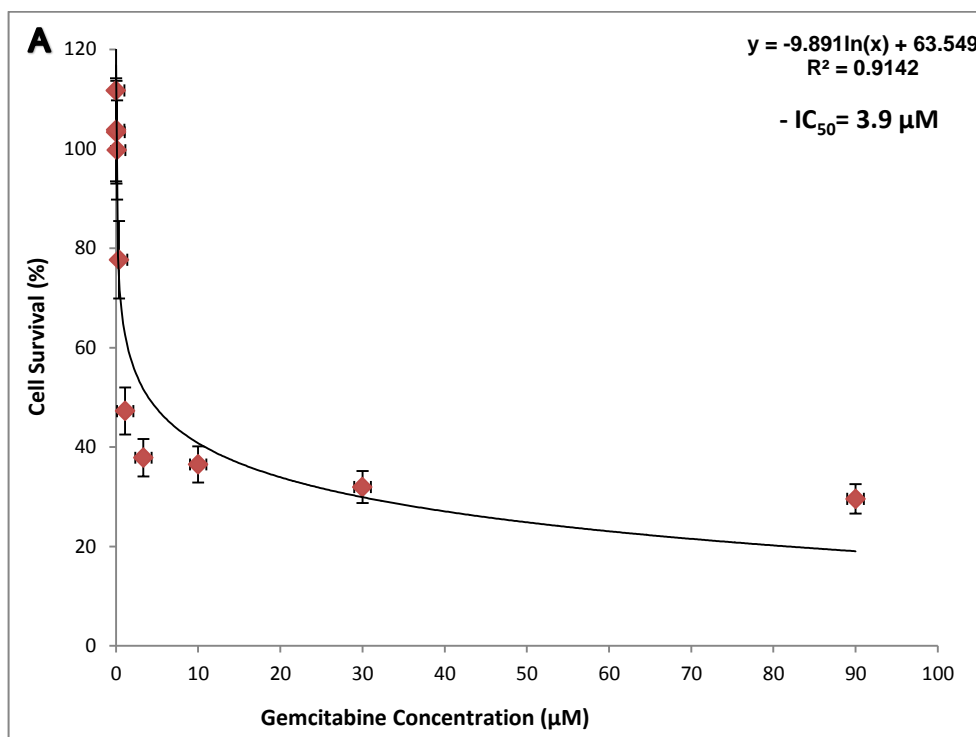


Figure 3.38. XTT cell proliferation assay results (A) Gemcitabine, (B) Gemcitabine loaded PHB-MNPs on MCF-7 cells. The data are presented as the mean \pm SEM (n = 3)

3.5 Summary

		PAMAM magnetic nanoparticles (DcMNPs)		Chitosan magnetic nanoparticles (CSMNPs)		PHB magnetic nanoparticles (PHB-MNPs)	
		Bare DcMNPs	Gem-DcMNPs	Bare CSMNPs	Gem-CSMNPs	Bare PHB-MNPs	Gem-PHB-MNPs
TEM results		12 nm	12-14 nm	4 nm	4 nm	13 nm	13-15 nm
XPS results	Nitrogen atom%	8.2%	10.2%	2.1%	2.3%	0%	0%
	Fluorine atom	-	+	-	+	-	+
Zeta Potential results		-10.2	-4.85	-19.8	-8.66	19.9 mV	24.5 mV

		pH	Gem-G5.5DcMNPs	Gem-CSMNPs	Gem-PHB-MNPs
Loading amount	24h	7.2	7.2 µg	8.8 µg	6.5 µg
Release & Stability	24h	4.2	100%	65%	49%
		5.2	100%	33%	-
	36h	7.2	<5%	<8%	19%

	Bare-G5.5 DcMNPs	Gem-G5.5 DcMNPs	Bare CSMNPs	Gem-CSMNPs	Bare PHB-MNPs	Gem-PHB-MNPs
MCF-7 (IC ₅₀ =3.9 µM)	Nontoxic up to 800 µg/ml	3 fold decrease in IC ₅₀ value	Nontoxic up to 560 µg/ml	2.6 fold decrease in IC ₅₀ value	Nontoxic up to 500 µg/ml	2 fold decrease in IC ₅₀ value
SKBR-3 (IC ₅₀ =6.5 µM)	Nontoxic up to 1670 µg/ml	6 fold decrease in IC ₅₀ value	Nontoxic up to 1110 µg/ml	1.4 fold decrease in IC ₅₀ value	Nontoxic up to 1670 µg/ml	2 fold decrease in IC ₅₀ value

CHAPTER 4

CONCLUSION

Magnetic Nanoparticles were synthesized to be used for targeting of tumor cells in the presence of magnetic field. PAMAM, Chitosan and PHB coating around the magnetic nanoparticles reduce the agglomeration, and provide surface functional groups and internal cavities for conjugation or loading of therapeutics drugs.

The terminal amine group of full generation DcMNP with a Cationic bar reduces the binding and encapsulating efficiency of PAMAM with cationic dCdF. Therefore, in this study, the various half generation of PAMAM synthesized for achieving the anionic PAMAM dendrimers. The supplementary tests confirmed the differences between surface structure of half generations and full generation of PAMAM DCMNPs.

Electrostatic interaction could be occurred between the carboxyl groups of weakly acidic Gemcitabine and the amine groups of the half-generation synthesized dendrimers. The chitosan and PHB magnetic nanoparticles loading amount were nearly the same amount with half generation PAMAM dendrimer.

TEM images of Gemcitabine loaded MNPs showed the uniform shape and same size with bare nanoparticles. The FT-IR and XPS analyses supported the drug loading results of nanoparticles. The zeta-potential analysis indicated a decreased surface charge in drug bounded anionic PAMAM and Chitosan nanoparticles and increased surface charge in cationic PHB magnetic nanoparticles.

It was shown Gemcitabine release from magnetic nanoparticles were higher at pH 4.2 compared to pH 5.2. Then, the drug is expected to be released at the targeted

cancer cells, because the pH of tumor tissue and endosomes are acidic. Burst release of Gemcitabine was resulted from DcMNPs at initial stage. Nearly the whole drug was released within first 15h from DcMNPs in pH 4.2. At the same condition Gemcitabine release from CSMNPs and PHB-MNPs showed the different release pattern. Only 65% of drug from CSMNPs and 49% from PHB-MNPs at pH 4.2 were released during 24h. These difference burst release were due to conjugation of drug to the surface of DcMNPs which release whole drug in acidic condition, but in the case of CSMNPs and PHB-MNPs it needs more time for released from interior cavities.

The stability results indicated that Gemcitabine conjugated DcMNPs were highly stable up to 6 weeks in PBS buffer. During 24h just around 4% of drug was released from DcMNPs, but it showed nearly 2 and 5 fold more release in CSMNPs and PHB-MNPs than DcMNPs. DcMNPs and PHB-MNPs were shown stable release after 15h, while at CSMNPs burst release could be seen after 12h.

The bare half generation PAMAM dendrimers have no cytotoxicity on both cell lines at high concentration. But high concentration of bare CSMNPs and PHB-MNPs were shown negligible cytotoxic effect on the MCF-7 cell line. In addition, the IC_{50} values of SKBR-3 and MCF-7 cells lines decreased nearly 6 and 3 fold on Gemcitabine conjugated DcMNPs, While the Gem-CSMNPs just decreased 1.4 and 2.6 fold and Gem-PHB-MNPs 2 fold. These results showed that Gemcitabine conjugated MNPs were more effective over breast cancer cell lines.

As a conclusion, Gemcitabine was more effectively loaded on half-generations of PAMAM DcMNPs when compared to full-generation and also the loaded nanoparticles were found more toxic compared to free form of the drug. The results of this study can provide new insights to the development of targeted drug delivery systems in cancer therapy.

REFERENCES

- A.K. Gupta, M. Gupta. 2005. "Synthesis and Surface Engineering of Iron Oxide Nano- Particles for Biomedical Applications."
- Ahmed, M., and M. Douek. 2013. "The Role of Magnetic Nanoparticles in the Localization and Treatment of Breast Cancer." *BioMed Research International* 2013:281230. Retrieved June 19, 2014 (<http://www.pubmedcentral.nih.gov/articlerender.fcgi?artid=3722907&tool=pmcentrez&rendertype=abstract>).
- Alexander, RL, and BT Greene. 2005. "A Novel Phospholipid Gemcitabine Conjugate Is Able to Bypass Three Drug-Resistance Mechanisms." *Cancer Chemotherapy and Pharmacology* 15–21. Retrieved July 17, 2013 (<http://link.springer.com/article/10.1007/s00280-004-0949-0>).
- Althuri, Avanthi et al. 2013. "Microbial Synthesis of Poly-3-Hydroxybutyrate and Its Application as Targeted Drug Delivery Vehicle." *Bioresource Technology* 145:290–96. Retrieved September 25, 2014 (<http://www.ncbi.nlm.nih.gov/pubmed/23415943>).
- American Cancer Society. 2013. "No Title." Retrieved (<http://www.cancer.org/treatment/treatmentsandsideeffects/guidetocancerdrugs/gemcitabine>). Last accessed date: August 06,2014.
- Arias, José L., L. Harivardhan Reddy, and Patrick Couvreur. 2011. "Superior Preclinical Efficacy of Gemcitabine Developed as Chitosan Nanoparticulate System." *Biomacromolecules* 12(1):97–104. Retrieved July 21, 2012 (<http://www.ncbi.nlm.nih.gov/pubmed/21117615>).
- Arruebo, Manuel, Rodrigo Fernández-pacheco, M. Ricardo Ibarra, and Jesús Santamaría. 2007. "Magnetic Nanoparticles for Drug Delivery." 2(3):22–32.
- Arya, Geetanjali, Mallareddy Vandana, Sarbari Acharya, and Sanjeeb K. Sahoo. 2011. "Enhanced Antiproliferative Activity of Herceptin (HER2)-Conjugated Gemcitabine-Loaded Chitosan Nanoparticle in Pancreatic Cancer Therapy." *Nanomedicine : Nanotechnology, Biology, and Medicine* 7(6):859–70. Retrieved November 12, 2013 (<http://www.ncbi.nlm.nih.gov/pubmed/21550422>).
- Bharali, Dhruva J., Marianne Khalil, Mujgan Gurbuz, Tessa M. Simone, and Shaker a Mousa. 2009. "Nanoparticles and Cancer Therapy: A Concise Review with

- Emphasis on Dendrimers.” *International Journal of Nanomedicine* 4:1–7.
Retrieved July 17, 2012
(<http://www.pubmedcentral.nih.gov/articlerender.fcgi?artid=2720735&tool=pmcentrez&rendertype=abstract>).
- Bildstein, L. Dubernet, C. Marsaud, V. Chacun, H. Nicolas, V. Gueutin, C. Sarasin, A.Bénech, H. Lepêtre-Mouelhi, S. Desmaële, D. Couvreur, P. 2010b.
“Transmembrane Diffusion of Gemcitabine by a Nanoparticulate Squalenoyl Prodrug: An Original Drug Delivery Pathway.” *Journal of Controlled Release : Official Journal of the Controlled Release Society* 147(2):163–70. Retrieved November 12, 2013 (<http://www.ncbi.nlm.nih.gov/pubmed/20691740>).
- Bildstein, L., C. Dubernet, and P. Couvreur. 2011. “Prodrug-Based Intracellular Delivery of Anticancer Agents.” *Advanced Drug Delivery Reviews* 63(1-2):3–23. Retrieved May 30, 2013 (<http://www.ncbi.nlm.nih.gov/pubmed/21237228>).
- Boas, u ; Christensen, J.B; Heegaard, P. M. .. 2006. “Dendrimers : Design , Synthesis.” *Dendrimers in Medicine and Biotechnology. New Molecular Tools* (978-0-85404-852-6):28. Retrieved May 20, 2011
(<http://www.springer.com/978-0-85404-852-6>).
- Cancer.gov. 2014a. “Defining Cancer.” Retrieved
(<http://www.cancer.gov/cancertopics/cancerlibrary/what-is-cancer>). Last accessed date March 07, 2014
- Cancer.gov. 2014b. “Definition of Breast Cancer.” Retrieved
(<http://www.cancer.gov/cancertopics/types/breast>). Last accessed date: March 07, 2014.
- cancer.gov. n.d. “www.cancer.gov/cancertopics/cancerlibrary/what-Is-Cancer.” Last accessed date: March 07, 2014.
- Cancerquest. 2014. “How Cancer Begins.” Retrieved
(<http://www.cancerquest.org/how-cancer-begins-introduction.html>). Last accessed date: August 09, 2012.
- Chaijamrus, S., and N. Udpuay. 2008. “Production and Characterization of Polyhydroxybutyrate from Molasses and Corn Steep Liquor Produced by *Bacillus Megaterium* ATCC 6748.” *Agricultural Engineering International: ...* X:1–12. Retrieved September 25, 2014
(<http://www.cigrjournal.org/index.php/Ejournal/article/view/1216>).
- Chitkara, Deepak, Anupama Mittal, Stephan W. Behrman, Neeraj Kumar, and Ram I. Mahato. 2013. “Self-Assembling, Amphiphilic Polymer-Gemcitabine Conjugate Shows Enhanced Antitumor Efficacy against Human Pancreatic

- Adenocarcinoma.” *Bioconjugate Chemistry* 24(7):1161–73. Retrieved May 30, 2014 (<http://www.ncbi.nlm.nih.gov/pubmed/23758084>).
- Cho, Y. W., J. Jang, C. R. Park, and S. W. Ko. 2000. “Preparation and Solubility in Acid and Water of Partially Deacetylated Chitins.” *Biomacromolecules* 1(4):609–14. Retrieved May 30, 2010 (<http://www.ncbi.nlm.nih.gov/pubmed/11710189>).
- Choi, Jong-il, and Sang Yup Lee. 1999. “High-Level Production of Te) by Fed-Batch Culture of Recombinant Escherichia Coli High-Level Production of Poly (3-Hydroxybutyrate-Co-3- Hydroxyvalerate) by Fed-Batch Culture of Recombinant Escherichia Coli.”
- Crosta, Peter. 2014. “Cancer.” *Medical News Today*. Retrieved November 30, 2014 (<http://www.medicalnewstoday.com/info/cancer-oncology/>).
- Danhier, Fabienne, Olivier Feron, and Véronique Préat. 2010. “To Exploit the Tumor Microenvironment: Passive and Active Tumor Targeting of Nanocarriers for Anti-Cancer Drug Delivery.” *Journal of Controlled Release : official journal of the Controlled Release Society* 148(2):135–46. Retrieved May 26, 2014 (<http://www.ncbi.nlm.nih.gov/pubmed/20797419>).
- DeSantis, Carol, Rebecca Siegel, and Ahmedin Jemal. 2012. “Breast Cancer Facts & Figures Is a Publication of the American Cancer Society, Atlanta, Georgia.” *American Cancer Society*.
- Dobrovolskaia, Marina A. et al. 2013. “Nanoparticle Size and Surface Charge Determine Effects of PAMAM Dendrimers on Human Platelets *in Vitro*.” *NIH Public Access* 9(3):382–93.
- Douziech-Eyrolles, Laurence et al. 2007. “Nanovectors for Anticancer Agents Based on Superparamagnetic Iron Oxide Nanoparticles.” *International Journal of Nanomedicine* 2(4):541–50. Retrieved November 12, 2011 (<http://www.pubmedcentral.nih.gov/articlerender.fcgi?artid=2676819&tool=pmcentrez&rendertype=abstract>).
- Egusquiaguirre, Susana Patricia, Manuela Igartua, Rosa María Hernández, and José Luis Pedraz. 2012. “Nanoparticle Delivery Systems for Cancer Therapy: Advances in Clinical and Preclinical Research.” *Clinical & Translational Oncology : official publication of the Federation of Spanish Oncology Societies and of the National Cancer Institute of Mexico* 14(2):83–93. Retrieved November 12, 2013 (<http://www.ncbi.nlm.nih.gov/pubmed/22301396>).
- Gao, Jinhao, Hongwei Gu, and Bing Xu. 2009. “Multifunctional Magnetic Nanoparticles: Design, Synthesis, and Biomedical Applications.” *Accounts of Chemical Research* 42(8):1097–1107.

- Garg, Neeraj K., Priya Dwivedi, Christopher Campbell, and Rajeev K. Tyagi. 2012. "Site Specific/targeted Delivery of Gemcitabine through Anisamide Anchored Chitosan/poly Ethylene Glycol Nanoparticles: An Improved Understanding of Lung Cancer Therapeutic Intervention." *European Journal of Pharmaceutical Sciences : official journal of the European Federation for Pharmaceutical Sciences* 47(5):1006–14. Retrieved August 6, 2014 (<http://www.ncbi.nlm.nih.gov/pubmed/23041219>).
- Garg, Tarun, and Onkar Singh. 2011. "Dendrimer: A Novel Scaffold for Drug Delivery." *International Journal of Pharmaceutical Sciences Review and Research* 7(2). Retrieved September 25, 2014 (www.globalresearchonline.net).
- Gillies, Elizabeth R., and Jean M. J. Fréchet. 2005. "Dendrimers and Dendritic Polymers in Drug Delivery Well as Agents for Both Boron Neutron Capture Therapy and Photodynamic Therapy . REVIEWS." *Drug Discovery Today* 10(1). Retrieved November 12, 2011 (www.drugdiscoverytoday.com).
- Gomez, M. Victoria, Javier Guerra, V. Sue Myers, Richard M. Crooks, and Aldrik H. Velders. 2009. "Nanoparticle Size Determination by (1)H NMR Spectroscopy." *Journal of the American Chemical Society* 131(41):14634–35. Retrieved November 12, 2013 (<http://www.ncbi.nlm.nih.gov/pubmed/19785420>).
- Gu, FX, R. Karnik, and AZ Wang. 2007. "Targeted Nanoparticles for Cancer Therapy." *Nano today*. Retrieved September 25, 2014 (<http://www.sciencedirect.com/science/article/pii/S174801320770083X>).
- Holliday, Deborah L., and Valerie Speirs. 2011. "Choosing the Right Cell Line for Breast Cancer Research." *Breast Cancer Research : BCR* 13(4):215. Retrieved (<http://www.pubmedcentral.nih.gov/articlerender.fcgi?artid=3236329&tool=pmcentrez&rendertype=abstract>).
- Hu, Che-Ming Jack, Santosh Aryal, and Liangfang Zhang. 2010. "Nanoparticle-Assisted Combination Therapies for Effective Cancer Treatment." *Therapeutic Delivery* 1(2):323–34. Retrieved September 25, 2014 (<http://www.ncbi.nlm.nih.gov/pubmed/22816135>).
- Ibezim, Emmanuel Chinedum, Cristina Tristao Andrade, Cristina Marcia, Bianca Barretto, and Damian Chukwu Odimegwu. 2011. "Ionically Cross-Linked Chitosan / Tripolyphosphate Microparticles for the Controlled Delivery of Pyrimethamine." *Ibnosina Journal of Medicine and Biomedical Sciences* 77–88. Retrieved September 15, 2013 (<http://www.ijmbs.org>).
- Inkyo, Mitsugi et al. 2006. "Experimental Investigation of Nanoparticle Dispersion by Beads Milling with Centrifugal Bead Separation." *Journal of Colloid and Interface Science* 304(2):535–40. Retrieved November 12, 2013 (<http://www.ncbi.nlm.nih.gov/pubmed/17022990>).

- Ito, Akira, Masashige Shinkai, Hiroyuki Honda, and Takeshi Kobayashi. 2005. "Medical Application of Functionalized Magnetic Nanoparticles." *Journal of Bioscience and Bioengineering* 100(1):1–11. Retrieved November 7, 2013 (<http://www.ncbi.nlm.nih.gov/pubmed/16233845>).
- Jain, Amit, Subodh Dubey, Atul Kaushik, and A. Tyagi. 2010. "Dendrimer: A Complete Drug Carrier." *International Journal of Pharmaceutical Sciences and Research* 1(4):38–52. Retrieved September 25, 2014 (www.ijpsr.com).
- Jin, Geun Woo et al. 2011. "PAMAM Dendrimer with a 1,2-Diaminoethane Surface Facilitates Endosomal Escape for Enhanced pDNA Delivery." *Polymer* 52(2):339–46. Retrieved September 25, 2014 (<http://www.sciencedirect.com/science/article/pii/S0032386110010104>).
- Kamaly, N., and Z. Xiao. 2012. "Targeted Polymeric Therapeutic Nanoparticles: Design, Development and Clinical Translation." *Chemical Society ...* 41(7):2971–3010. Retrieved September 25, 2014 (<http://pubs.rsc.org/en/content/articlehtml/2012/cs/c2cs15344k>).
- Khaira, Rekha, Jyoti Sharma, and Vinay Saini. 2014. "Development and Characterization of Nanoparticles for the Delivery of Gemcitabine Hydrochloride." *The Scientific World Journal* 2014:560962. Retrieved October 25, 2014 (<http://www.pubmedcentral.nih.gov/articlerender.fcgi?artid=3925564&tool=pmcentrez&rendertype=abstract>).
- Khodadust, Rouhollah, Gozde Unsoy, Serap Yalcın, Gungor Gunduz, and Ufuk Gunduz. 2013. "PAMAM Dendrimer-Coated Iron Oxide Nanoparticles: Synthesis and Characterization of Different Generations." *Journal of Nanoparticle Research* 15(3):1488. Retrieved May 31, 2014 (<http://link.springer.com/10.1007/s11051-013-1488-6>).
- Kievit, Forrest M. et al. 2009. "PEI-PEG-Chitosan Copolymer Coated Iron Oxide Nanoparticles for Safe Gene Delivery: Synthesis, Complexation, and Transfection." *Advanced Functional Materials* 19(14):2244–51. Retrieved May 31, 2014 (<http://www.pubmedcentral.nih.gov/articlerender.fcgi?artid=2756666&tool=pmcentrez&rendertype=abstract>).
- Lansakara-P, Dharmika S. P., B. Leticia Rodriguez, and Zhengrong Cui. 2012. "Synthesis and *in Vitro* Evaluation of Novel Lipophilic Monophosphorylated Gemcitabine Derivatives and Their Nanoparticles." *International Journal of Pharmaceutics* 429(1-2):123–34. Retrieved July 17, 2013 (<http://www.pubmedcentral.nih.gov/articlerender.fcgi?artid=3335205&tool=pmcentrez&rendertype=abstract>).

- Larsson, Mikael, Anna Bergstrand, Lilyan Mesiah, Celine Van Vooren, and Anette Larsson. 2014. "Nanocomposites of Polyacrylic Acid Nanogels and Biodegradable Polyhydroxybutyrate for Bone Regeneration and Drug Delivery." *Journal of Nanomaterials* 2014:1–9. Retrieved September 25, 2014 (<http://www.hindawi.com/journals/jnm/2014/371307/>).
- Liu Dechun, Chen Yanbin, Feng Xiaoshan, DengMiao, Xie Gangqiang, Wang Jianguang, Zhang Like, Liu Qipeng, Yuan Pengfei. 2014. "Micellar Nanoparticles Loaded with Gemcitabine and Doxorubicin Showed Synergistic Effect." *Colloids and Surfaces. B, Biointerfaces* 113:158–68. Retrieved May 15, 2014 (<http://www.ncbi.nlm.nih.gov/pubmed/24077114>).
- Majoros, István J., Balázs Keszler, Scott Woehler, Tricia Bull, and James R. Baker. 2003. "Acetylation of Poly(amidoamine) Dendrimers." *Macromolecules* 36(15):5526–29. Retrieved September 12, 2012 (<http://pubs.acs.org/doi/abs/10.1021/ma021540e>).
- Maksimenko, Andrei et al. 2013. "Polyisoprenoyl Gemcitabine Conjugates Self Assemble as Nanoparticles, Useful for Cancer Therapy." *Cancer Letters* 334(2):346–53. Retrieved November 6, 2013 (<http://www.ncbi.nlm.nih.gov/pubmed/22935679>).
- Martín-Banderas, Lucía et al. 2013. "Biocompatible Gemcitabine-Based Nanomedicine Engineered by Flow Focusing for Efficient Antitumor Activity." *International Journal of Pharmaceutics* 443(1-2):103–9. Retrieved November 12, 2013 (<http://www.ncbi.nlm.nih.gov/pubmed/23299085>).
- medscape.com. 2014. "712338-fig3." Retrieved September 25, 2014 (http://www.medscape.com/viewarticle/712338_7). Last accessed date: September 25, 2014
- Mini, E., S. Nobili, B. Caciagli, I. Landini, and T. Mazzei. 2006. "Cellular Pharmacology of Gemcitabine." *Annals of Oncology : official journal of the European Society for Medical Oncology / ESMO* 17 Suppl 5(Supplement 5):v7–12. Retrieved November 12, 2013 (<http://www.ncbi.nlm.nih.gov/pubmed/16807468>).
- Mohamed, Ali, Kenneth Krajewski, Burcu Cakar, and Cynthia X. Ma. 2013. "Targeted Therapy for Breast Cancer." *The American Journal of Pathology* 183(4):1096–1112. Retrieved November 12, 2013 (<http://www.ncbi.nlm.nih.gov/pubmed/23988612>).
- National Cancer, Institute. 2014. "National Cancer Institute." Retrieved September 25, 2014 (http://www.cancer.gov/cancertopics/understandingcancer/targetedtherapies/breastcancer_htmlcourse#a). Last accessed date: September 25, 2014

- Nune, SK, and Padmaja Gunda. 2009. "Nanoparticles for Biomedical Imaging." *NIH Public Access* 6(11):1175–94. Retrieved September 25, 2014 (<http://informahealthcare.com/doi/abs/10.1517/17425240903229031>).
- Pan, G. 2005. "Studies on PEGylated and Drug-Loaded PAMAM Dendrimers." *Journal of Bioactive and Compatible Polymers* 20(1):113–28. Retrieved May 31, 2014 (<http://jbc.sagepub.com/cgi/doi/10.1177/0883911505049656>).
- Piddubnyak, Valeria et al. 2004. "Oligo-3-Hydroxybutyrates as Potential Carriers for Drug Delivery." *Biomaterials* 25(22):5271–79. Retrieved September 25, 2014 (<http://www.ncbi.nlm.nih.gov/pubmed/15110478>).
- Robinson, Blaine W. et al. 2001. "Radiosensitization by Gemcitabine in p53 Wild-Type and Mutant MCF-7 Breast Carcinoma Cell Lines Radiosensitization by Gemcitabine in p53 Wild-Type and Mutant." *American Association for Cancer Research* 2581–89. Retrieved September 12, 2012 (<http://clincancerres.aacrjournals.org/content/7/8/2581>).
- Rodrigues, Susana, Marita Dionísio, Carmen Remuñán López, and Ana Grenha. 2012. "Biocompatibility of Chitosan Carriers with Application in Drug Delivery." *Journal of Functional Biomaterials* 3(4):615–41. Retrieved January 12, 2014 (<http://www.mdpi.com/2079-4983/3/3/615/>).
- Rouhollah, Khodadust, and Mutlu Pelin. 2013. "Doxorubicin Loading, Release, and Stability of Polyamidoamine Dendrimer- coated Magnetic Nanoparticles." *Journal of ...* 102(6):1825–35. Retrieved September 25, 2014 (<http://onlinelibrary.wiley.com/doi/10.1002/jps.23524/full>).
- Sawyers, Charles. 2004. "Targeted Cancer Therapy." *Nature* 432(7015):294–97. Retrieved September 25, 2013 (<http://www.ncbi.nlm.nih.gov/pubmed/15549090>).
- Shcharbin, D. G., B. Klajnert, and M. Bryszewska. 2009. "Dendrimers in Gene Transfection." *Biochemistry* 74(10):1070–79. Retrieved May 31, 2014 (<http://www.ncbi.nlm.nih.gov/pubmed/19916919>).
- Sloata Brian R., Sandovala Michael A, Lib Dong, Chunga Woon-Gye , Lansakara-Pa Dharmika S.P., Proteaub Philip J., Kiguchic Kaoru, DiGiovannic John, Cui Zhengrong. 2011. "In Vitro and in Vivo Anti-Tumor Activities of a Gemcitabine Derivative Carried by Nanoparticles." *International Journal of Pharmaceutics* 409(1-2):278–88. Retrieved November 12, 2013 (<http://www.pubmedcentral.nih.gov/articlerender.fcgi?artid=3079786&tool=pmcentrez&rendertype=abstract>).

- Sun, Conroy, Jerry S. H. Lee, and Miqin Zhang. 2008. "Magnetic Nanoparticles in MR Imaging and Drug Delivery." *Advanced Drug Delivery Reviews* 60(11):1252–65. Retrieved November 12, 2013 (<http://www.pubmedcentral.nih.gov/articlerender.fcgi?artid=2702670&tool=pmcentrez&rendertype=abstract>).
- Svenson, Sönke, and Donald a Tomalia. 2005. "Dendrimers in Biomedical Applications--Reflections on the Field." *Advanced Drug Delivery Reviews* 57(15):2106–29. Retrieved December 12, 2013 (<http://www.ncbi.nlm.nih.gov/pubmed/16305813>).
- Taghavi Pourianazar, Negar, Pelin Mutlu, and Ufuk Gunduz. 2014. "Bioapplications of Poly(amidoamine) (PAMAM) Dendrimers in Nanomedicine." *Journal of Nanoparticle Research* 16(4):2342. Retrieved May 15, 2014 (<http://link.springer.com/10.1007/s11051-014-2342-1>).
- Unsoy, Gozde, Serap Yalcin, Rouhollah Khodadust, Gungor Gunduz, and Ufuk Gunduz. 2012. "Synthesis Optimization and Characterization of Chitosan-Coated Iron Oxide Nanoparticles Produced for Biomedical Applications." *Journal of Nanoparticle Research* 14(11):964. Retrieved January 12, 2014 (<http://link.springer.com/10.1007/s11051-012-0964-8>).
- Vasumathi, V., and Prabal K. Maiti. 2010. "Complexation of siRNA with Dendrimer: A Molecular Modeling Approach." *Macromolecules* 43(19):8264–74. Retrieved November 12, 2013 (<http://pubs.acs.org/doi/abs/10.1021/ma1012495>).
- Viota, J L, Carazo, A., Munoz-Gamez, J a, Rudzka, K., Gómez-Sotomayor, R., Ruiz-Extremera, A., Salmerón, J., Delgado, a V. 2013. "Functionalized Magnetic Nanoparticles as Vehicles for the Delivery of the Antitumor Drug Gemcitabine to Tumor Cells. Physicochemical *in Vitro* Evaluation." *Materials Science & Engineering. C, Materials for Biological Applications* 33(3):1183–92. Retrieved November 12, 2013 (<http://www.ncbi.nlm.nih.gov/pubmed/23827558>).
- Walter, Marie V, and Michael Malkoch. 2012. "Simplifying the Synthesis of Dendrimers: Accelerated Approaches." *Chemical Society Reviews* 41(13):4593–4609. Retrieved May 31, 2014 (<http://www.ncbi.nlm.nih.gov/pubmed/22592560>).
- Wilczewska, Agnieszka Z., Katarzyna Niemirowicz, Karolina H. Markiewicz, and Halina Car. 2012. "Nanoparticles as Drug Delivery Systems." *Pharmacological reports : PR* 64(5):1020–37. Retrieved May 31, 2014 (<http://www.ncbi.nlm.nih.gov/pubmed/24124007>).
- Xiong, Yu-Cui, Yong-Chao Yao, Xiao-Yong Zhan, and Guo-Qiang Chen. 2010. "Application of Polyhydroxyalkanoates Nanoparticles as Intracellular Sustained

Drug-Release Vectors.” *Journal of Biomaterials Science. Polymer Edition* 21(1):127–40. Retrieved September 25, 2014 (<http://www.ncbi.nlm.nih.gov/pubmed/20040158>).

Yalcin, Serap. n.d. “Synthesis and Characterization of Poly-Hydroxybutyrate (PHB) Coated Magnetic Nanoparticles as Biodegradable Drug Delivery Agent.”

Yalcin, Serap, Gozde Unsoy, Pelin Mutlu, Rouhollah Khodadust, and Ufuk Gunduz. 2014. “Polyhydroxybutyrate-Coated Magnetic Nanoparticles for Doxorubicin Delivery: Cytotoxic Effect Against Doxorubicin-Resistant Breast Cancer Cell Line.” *American journal of therapeutics* (1):2–11. Retrieved (<http://www.ncbi.nlm.nih.gov/pubmed/25137407>).

Yalçın, S. ; Khodadust, R. ; Ünsoy, G.; Garip, I.C. ; Mumcuoğlu, Z.D. ; Gündüz, U. 2014. “Synthesis and Characterization of Poly-Hydroxybutyrate (PHB) Coated Magnetic Nanoparticles: Toxicity Analyses on Different Cell Lines.” *Synthesis and Reactivity in Inorganic, Metal-Organic, and Nano-Metal Chemistry S*.

Yang Yang, Suhair Sunoqrot, Chelsea Stowell, Jingli Ji, Chan-Woo Lee, Jin Woong Kim, Seema A. Khan, and Seungpyo Hong. 2012. “Effect of Size, Surface Charge, and Hydrophobicity of Poly(amidoamine) Dendrimers on Their Skin Penetration.” *Biomacromolecules* 13(7):2154–62.

APPENDIX A

Additional Analysis of PAMAM DcMNPs

A.1. Loading of Gemcitabine on Generation 4 and 7 of DcMNPs

In our initial attempts, we tried to load Gemcitabine (7.5, 15 and 22.5 $\mu\text{g/ml}$) on 2.5 mg/ml of PAMAM dendrimers (G4-DcMNP and G7-DcMNP) at methanol, PBS, water and TPP. However, Gemcitabine binding was not observed on full generations of (G4 and G7)PAMAM dendrimers.

Table A. 1. Effect of initial drug concentration and solvent on encapsulation efficiency of G4 and G7 DcMNPs at various solvents.

Drug Concentration	7.5 $\mu\text{g/ml}$	15 $\mu\text{g/ml}$	22.5 $\mu\text{g/ml}$
Methanol	0	0	0.9 μg
PBS	0	0	1.35 μg
Dis Water	0	0	0

A.2. PAMAM Dendrimer Synthesized with Mechanical Stirrer

The adding of methylacrylate methanol solution and ethylenediamine-methanol solution for coating the DCMNPs, were also done by mechanical stirrer at room temperature. The results of conjugation efficacy of Gemcitabine to these DcMNPs did not shown so much difference with ultrasonic synthesized DcMNPs.

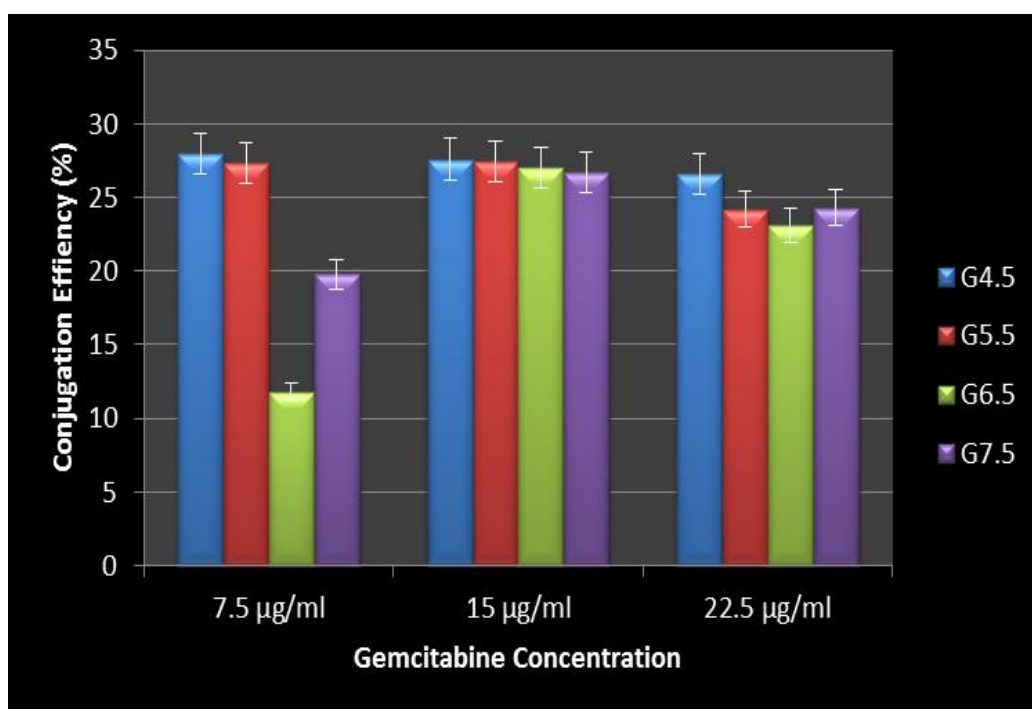


Figure A. 2 Gemcitabine conjugation efficiency of various half – generation of PAMAM dendrimer synthesized with mechanical stirrer.

A.3. Zeta (ζ) Potential Analysis

The zeta potential values for different half-generation of DcMNPs were measured at pH 7.2.

Table A. 2. Zeta potential results for different half generations of PAMAM number.

Generation number of PAMAM	G4.5	G5.5	G6.5	G7.5
	-2.28	-10.2	-6.68	-4.14

A.4. Fourier Transform-Infrared spectroscopy (FT-IR)

FT-IR spectra of Gemcitabine conjugated G4.5 and G7.5 PAMAM dendrimer coated magnetic nanoparticles, band at 2800-3000 cm^{-1} showed the interaction of DcMNPs and NH group of drug molecule.

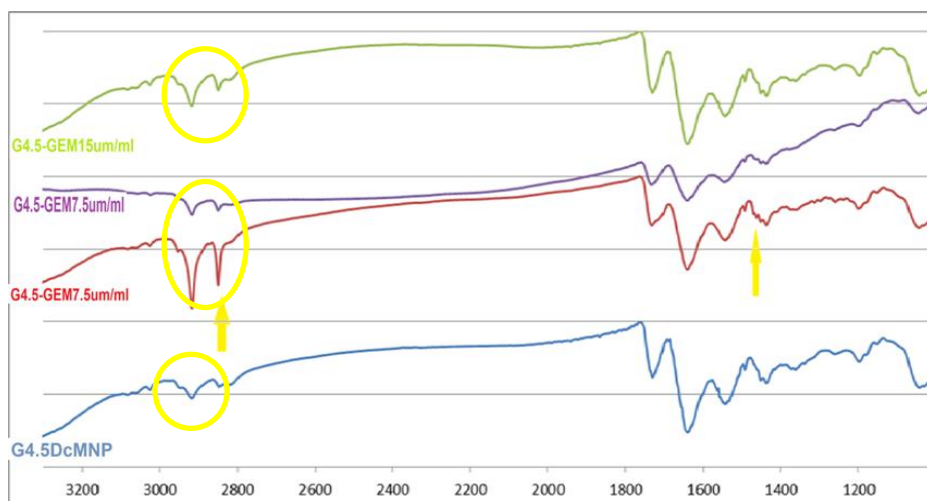


Figure A. 2. FT-IR spectra of Gemcitabine, G4.5MNP and G4.5MNPs conjugated by 7.5, 15 and 22.5 $\mu\text{g}/\text{ml}$ Gemcitabine.

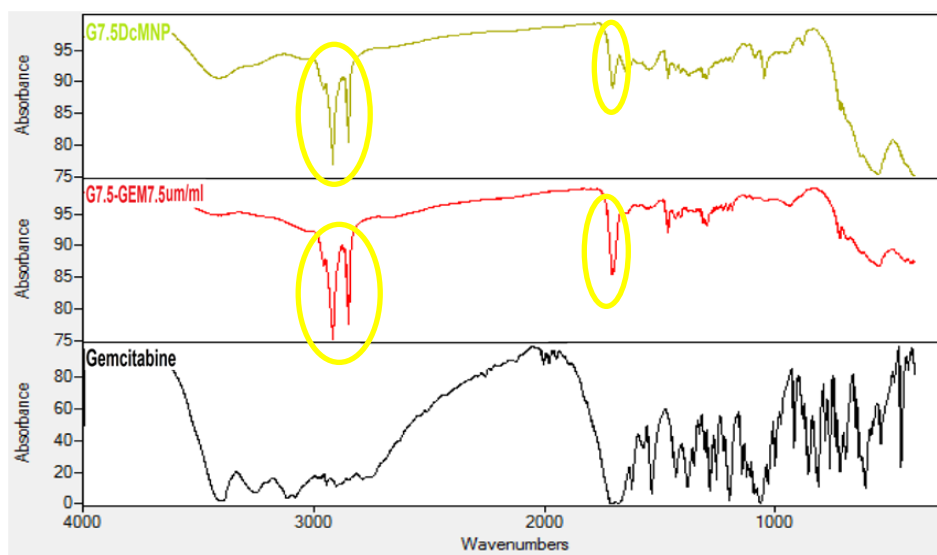


Figure A. 3. FT-IR spectra for GEM-G7.5 DcMNP. Difference between Gemcitabine, DcMNPs and Gem-DcMNPs.

A.5. Standard curves of Gemcitabine

Gemcitabine release profiles showed pH dependent release pattern. Good linearity of the standard curves for Gemcitabine in PBS at pH 7.2 ($R=0.9996$), and acetate buffer at pH 4.2 ($R=0.9993$) and pH 5.2 ($R=0.9999$) can be obtained.

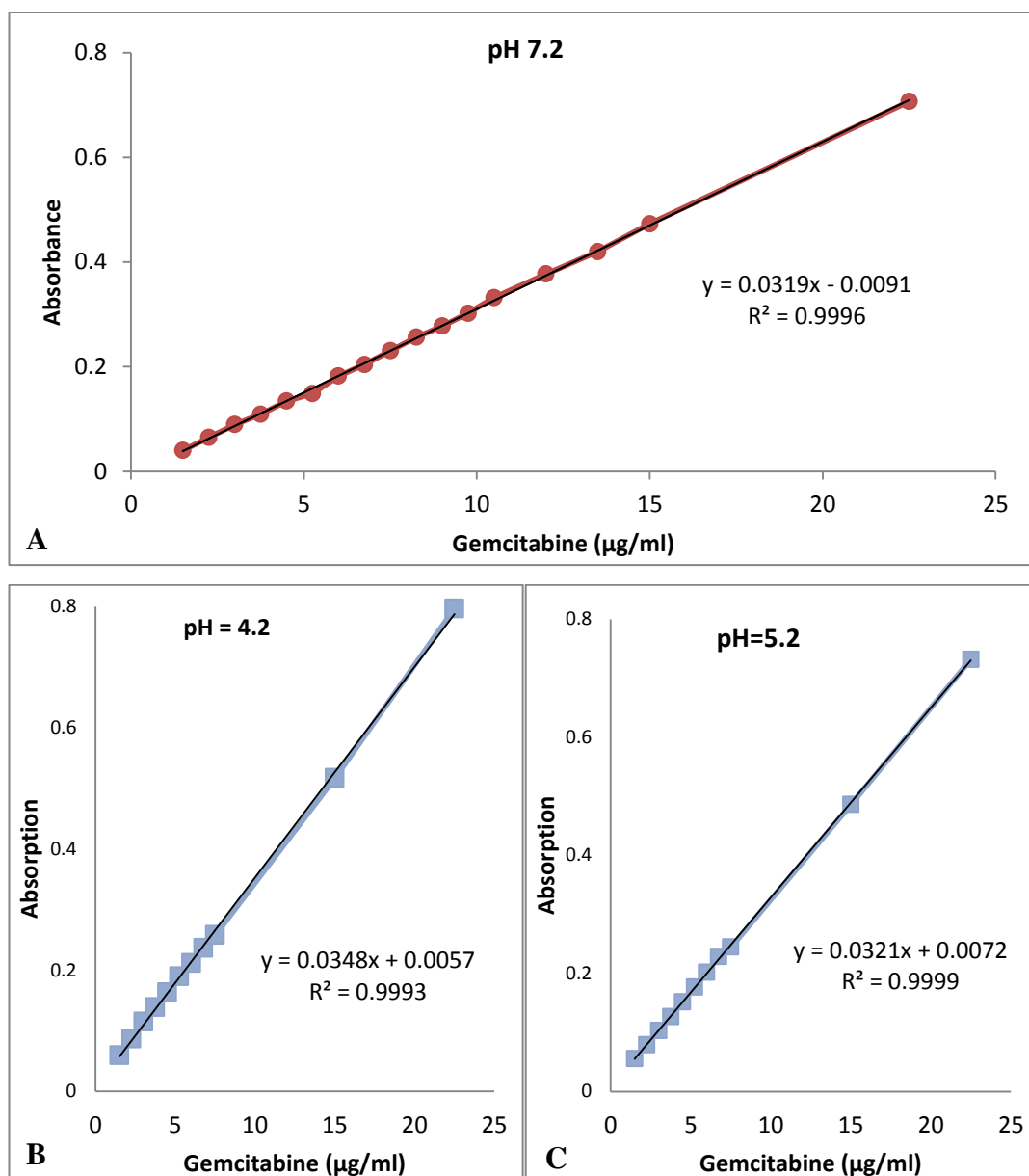


Figure A. 4. Standard curves of Gemcitabine in (A) PBS (pH 7.2), and acetate buffer at (B) pH 4.2 and (C) pH 5.2.

A.6. XTT Cell Proliferation Assay

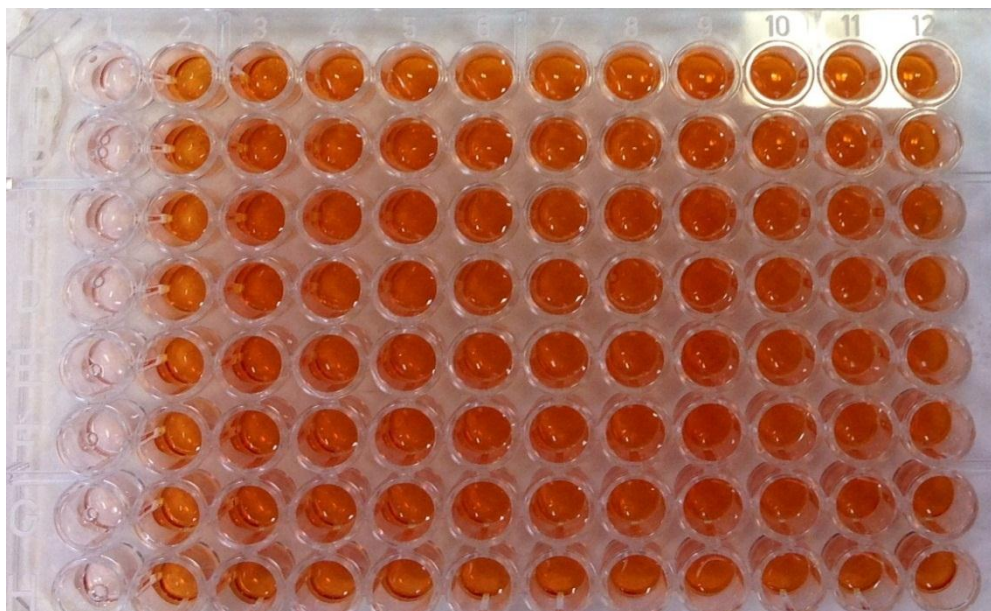


Figure A. 5. Schematic representation of MCF-7 (6×10^3 cells/well) cells seeded to 96 well plates and treated by bare DcMNPs, 4h after XTT reagent addition to plate.



Figure A. 6. Schematic representation of MCF-7 (6×10^3 cells/well) cells seeded to 96 well plates and treated by Gemcitabine conjugated DcMNPs, 4h after XTT reagent addition to plate.

A.7. Light Microscopy Images of MCF-7 Cells

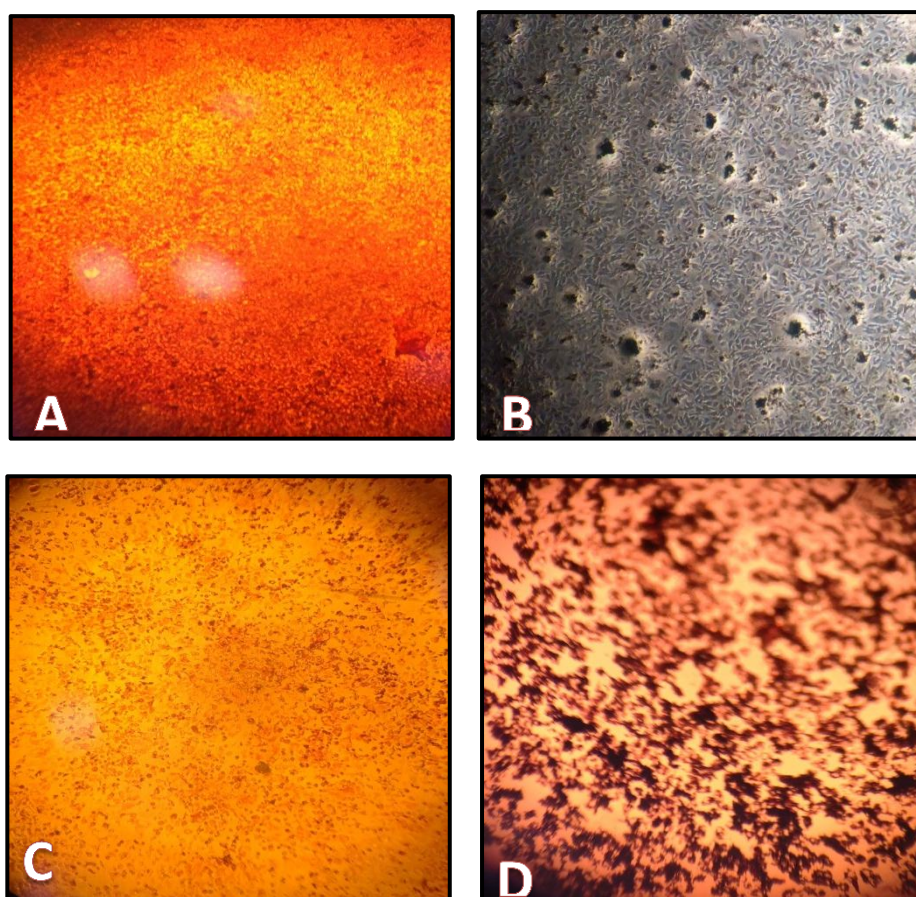


Figure A. 7. Cellular internalization of DcMNPs by light microscopy (A) MCF-7 (6×10^3 cells/well) cells. (B) Bare DcMNPs treated MCF-7 cells. (C) lowest drug dose ($2.5 \mu\text{M}$) treated MCF-7 cells. (D). Highest drug dose ($90 \mu\text{M}$) treated MCF-7 cells

APPENDIX B

Additional Analysis of CSMNPs

B.1. Loading of Gemcitabine on CSMNPs

Gemcitabine loading was investigated at different drug dilutions (7.5, 15 and 22.5 $\mu\text{g/ml}$) using 2.5 mg/ml of CSMNPs in various solvents were done.

Table B. 2. Loading efficiencies of different initial Gemcitabine loading concentrations on 2.5 mg/ml Chitosan magnetic nanoparticles in various solvents.

Drug concentration	7.5 $\mu\text{g/ml}$	15 $\mu\text{g/ml}$	22.5 $\mu\text{g/ml}$
TPP	25%	0	0
PBS (pH 7)	29.4%	17%	6%
PPB (pH 7.2)	20%	10%	6.2%
PPB (pH 6.2)	16%	15%	14.3%
PPB (pH 6)	7.4%	3%	0